AUTOMATED ULTRASONIC INSPECTION

OF HEAT EXCHANGER TUBESHEET WELDS

DISSERTATION HANDED IN TO THE UNIVERSITY OF CAPE TOWN

AUTHOR: IAIN MICHAEL REYNARD
DATE: AUGUST 1996

Synopsis

The objective of this research was to design an automated scanning and signal interpretation system for ensuring the integrity of the welds in a specific heat exchanger presently used in industry.

The First Effect Steam Chest is a shell and tube, one pass type of heat exchanger used in the production of chlorine. A caustic soda/salt mixture is pumped through the bottom channel head through the tubes whilst steam passes through the shell. There are nine hundred and eighty tubes in the tube bundle, welded to the outer surface of the tubesheet.

One such heat exchanger, approximately four years after installation, revealed severe erosion of the steam chest's tubing by the caustic soda, allowing leakage of the steam. With the high cost of replacement, maintenance tasks were performed to prolong the life of the heat exchanger. These included improving the design of tube welds and checking the integrity of these welds before commissioning.

Inspection methods available for the inspection of the welds were limited to manual techniques. This proved to be very labour intensive, leading to operator fatigue. Furthermore, the interpretation of the results from the inspection equipment was subjective. Lastly, no record of the inspection data was kept for future comparisons. It was thought that these problems could be overcome by an automated scanning and signal interpretation system.

A survey of the automated scanning equipment commercially available revealed that most scanning systems were designed for eddie current inspection. Furthermore, most equipment was found to either be designed for a specific heat exchanger configuration, and thus was not suitable for the abovementioned application, or was designed with the nuclear industry in mind, thus being unnecessary complicated and consequently overpriced. Thus, it was concluded that a dedicated scanning system would have to be designed for the application.

Research work was then done into suitable probe manipulation techniques. A multiple-position frame (one that has to be relocated during the scanning process to reach all tube openings)

was chosen rather than a single position frame. Trials in probe manipulation were done on two 'robots': the SCROBOT ERIII and a CNC machine. Firstly, the DA312 ultrasonic probe from Krautkamer was selected for the ultrasonic inspection. Then, a Probe Insertion Mechanism (P.I.M.) was designed for each robot. These were to hold the ultrasonic probe as well as provide the final manipulation of the probe once inside the tube opening. The PIM for SCORBOT ERIII consisted mainly of lever arms and a holding cage, whilst the PIM for the CNC consisted of an entire robot wrist which had separate motors and was controlled by a second computer. A acoustic lens was designed to fit the ultrasonic probe, providing for the flat/round interface between the probe and the tube surface, as well as supplying a constant layer of couplant fluid. Lastly, a test rig representing the heat exchanger, made from sections of PVC piping, was made to carry out tests on.

The software written for each test robot was done in the programming language Turbo C++(TM), versions 1.0 to 3.0. The function of the software in each case was to control the manipulation of the probe in and around the tube openings, collect and interpret data from the ultrasonic inspection equipment and provide interface data to the supervisory operator. The software communicated with SCORBOT ERIII through a dedicated, but problematic, control box. In the case of the CNC setup, electronic circuits had to be built as an interface between the software (run on a 386 PC) and the robotic wrist. A secondary control system operated the CNC itself through software downloaded from a XT PC to the CNC's own on-board computer.

Results from the scans of the test rig showed the main failing of the SCORBOT ERIII setup to be inaccurate probe manipulation. Some of the inaccuracy was due to a faulty motor on the robot arm, but the majority was attributed to the unsuitability of SCORBOT's configuration for the application. Successful probe manipulation results obtained using the CNC showed that a XY scanner configuration (rather than a robot arm configuration) was the most suitable for the scanning of the heat exchanger.

The signal interpretation software was proved to be reliable in detecting the presence of flaws but discrepancies were found in attempts to estimate the size of the flaws. It was thus concluded that the software would be suitable for locating flaws, thereafter relying on further

human interaction if further data on the individual flaws (size, shape, orientation) were needed.

From the results gained from the two robots, a scanning device suitable for the industrial application was designed. It consisted of a 1,1 by 1,1 metre aluminium frame, on which a travelling arm was mounted. The arm was powered on one side by a stepper motor, and had a PIM mounted on itself, which could traverse the horizontal arm. Once over the tube opening, the PIM had the capability of lowering the ultrasonic probe into the hole and orientating the probe to face the weld site. The motion of the probe around the tube circumference was provided by the horizontal arm and the PIM moving together.

Alternative control and ultrasonic inspection hardware setups were investigated for the final scanner and it was concluded that a number of options were available to the manufacturer of the scanner, depending on what ultrasonic interpretation equipment was already acquired. The software written for the two test robots was suggested to be suitable for the final scanner with the exception of the motor control logic. Theoretical operational specifications were calculated for the final scanner using the data from equipment catalogues and the results gained from scans performed using the CNC setup. These were proved sufficient to carry out the scan on the First Effects Steam Chest.

FIGURES **PAGE**

CHAPTER 1

CHAPTER 3

CHAPTER 4

CHAPTER 1

INTRODUCTION

1.1 FOREWORD

When the integrity of fabricated parts is of importance, destructive inspection is usually impractical. This is because of the high cost and the inability of such methods to accurately predict the quality of parts other than those inspected. However, nondestructive testing can be used, where little or no physical damage is done to the part, still yielding an estimate of the part's present state of integrity.

It can be argued that the idea of using nondestructive inspection methods dates back to testing clay artifacts for cracks by noting the sound they gave off when tapped[1]. However, the first modern nondestructive technique was that of eddy current inspection, used by Kranz in the mid-1920's to measure the wall thickness of a testpiece.[2] This was followed by the application of sonic depth finding to thickness measurement by Firestone in 1942, later being developed into ultrasonic inspection. After 1945, with the increased demand for nondestructive testing, techniques such as microwave inspection and the magabsorption inspection were developed, leading to the diversity of the present day industry.

Today, nondestructive inspection techniques are recognised as dependable quality control tools. Codes and standards have been developed to enhance the reliability of the estimates given. Furthermore, the development of microprocessors has meant that, with automation, a lot more information can be rapidly considered to reach a final decision on a part's integrity.

1.2 ULTRASONIC INSPECTION TECHNIQUES

Before describing automated ultrasonic scanning systems, a background knowledge into the fundamentals of ultrasonic inspection techniques is needed. Thus, this section gives a functional view of the inspection technique.

Early investigations into the specific problem of this research revealed that ultrasonic inspection would be used. A detailed study of other NDT methods, including eddy current, radiology, magnetic particle and leak penetration inspection , were carried out. However, for reasons of the shear volume of data, the results have not been included in this text.

1.2.1. Introduction

Ultrasonic inspection is a NDT method which uses beams of high frequency sound introduced into the test piece for detection of surface and subsurface flaws.

Ultrasonic inspection is most commonly used to detect cracks, laminations, shrinkage cavities, bursts, flakes, pores, disbonds and other discontinuities.[3] It is suitable for inspecting materials that do not have an excessively high attenuation of sound energy and is not restricted only to metal test pieces. Due to the high reflection characteristics of typical discontinuities (ie: air in metal), defects in the size range of 10^{-5} metres may be detected.

The method is based on the phenomenon that sound waves travelling through a homogeneous material are reflected or scattered at interfaces within the material. Thus, by causing acoustic energy to enter the part and by either monitoring the energy transmitted through the part or the energy reflected back to the original surface, the size, orientation, shape and position of any interface within the path of the sound may be found.

1.2.2. Physical properties of ultrasonic waves

Ultrasonic waves are mechanical vibrations, the amplitude of which are well below the elastic limits of most test materials.[3] These waves can be reflected from surfaces, refracted when crossing a boundary between two inhomogeneous materials and can be diffracted at the edge of obstacles. Furthermore, the velocity of the wave is dependent on the material characteristics of the transmission medium and not on the wave itself.

Wave modes

Ultrasonic wave propagation can be categorised into four basic modes as longitudinal, transverse, surface or lamb waves. Each mode type is characterised by the pattern of deformation resulting from the wave passing through the material and can be broken down into Longitudinal, Transverse, Surface and Lamb waves. (Further information available in references 1, 4 and 5).

Wave propagation characteristics

Important characteristics particular to each wave mode and dependent on the transmitting medium include:

- velocity
- acoustic impedance
- attenuation

The velocity of a particular mode of wave is determined by the medium in which it propagates and is related to the frequency by:

$$v = f \times l$$

where v = velocity (m/s)
f = frequency (Hz)
l = wavelength (m)

Acoustic impedance of a wave in a material is given by:[6]

$$Z = p * v$$

where p = density g/cm^3
v = cm/s

The attenuation of ultrasonic beams in a material has to be accounted for in some aspects of ultrasonic inspection.[5] Attenuation is the reduction in beam intensity with distance from the source and is a result of transmission losses,[3] interference effects and beam spreading.

Wave interaction with interfaces

Ultrasonic waves arriving at plane interfaces are influenced by the two different mediums present at the interface, the angle of incidence and the thickness of each medium[6]. The wave can undergo one or more of the following changes:

- reflection
- refraction
- mode conversion
- diffraction

At a zero angle of incidence to the normal, only transmission and reflection occur and the extent of each is dependent on the impedance ratio (Z_2 / Z_1), known as the mismatch factor, between the two materials. The percentage reflection of the original beam is given by:[6]

$$R = \frac{Z_2 - Z_1}{Z_2 + Z_1}$$

R = Refraction coefficient
Z_1 = Impedance of material 1
Z_2 = Impedance of material 2

Refraction of ultrasonic waves typically occurs when the angle of incidence is no longer

normal, resulting in a different direction of wave propagation and the possibility of additional wave modes being generated. The refractive angle can be found using Snell's law:[6]

Mode conversion of a sound beam at an interface results in the incident beam of sound energy being propagated in one or more different modes. Whereas Snell's law gives the angles of propagation of the waves in these modes, Knott's equations[7] give the acoustic pressure of each resultant wave form. Knotts' equations can be simplified in the case of solid-air interfaces since transmission is assumed negligible. The resultant ratios of reflected to incident acoustic energy are a function of Poisson's ratio alone.

When the interface is of another form (ie: liquid-liquid or solid-liquid), complicated calculations using the densities and elastic constants of the media are needed. As an example, the power reflected and transmitted for a longitudinal incident wave on a steel-water interface is given by figure 1.1[1].

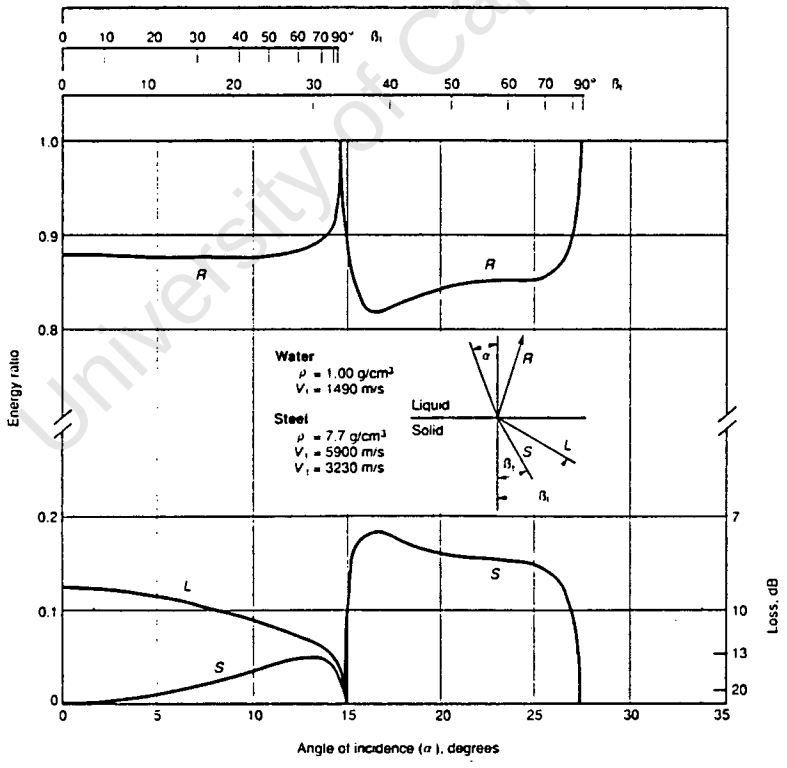

Figure 1.1: Power of reflected and transmitted beams for steel-water interface with a longitudinal incident beam

Diffraction of an ultrasonic wave occurs when it passes through an aperture or over a reflector, resulting in a divergence in the beam path[6]. This causes interference phenomena which has effects on:

- transducer beam spreads
- beam profiles
- defect reflection factors

Near and far field beam characteristics

The characteristics of an ultrasonic sound beam from a flat transducer can be attributed to two separate stages in the sound beam's path, namely the near field and the far field.

The near or Fresnel field of a sound beam extends from the face of the transducer and has a length of N, where:

$$N = \left(\frac{D^2 - L^2}{4L} \right)$$

D = active diam. of transducer
L = wavelength of sound generated

in the case of circular transducer faces. The variation in acoustic pressure in the near field can be analysed using Huygen's principle[6]. Assuming an ideal transducer, plane waves generated by the piston motion of the transducer will form interference patterns with the spherical waves generated by the edges of the transducer. This interference leads to a composite standing wave with characteristic maxima and minima points of acoustic energy.

Calculating the sound intensity at any one point in the near field is a complex process whereby the contribution of every section of the transducer's face to the intensity at that point is summed. Figure 1.2 shows the sound intensity plotted for a portion of a near field with a a/l ratio of 5.0.

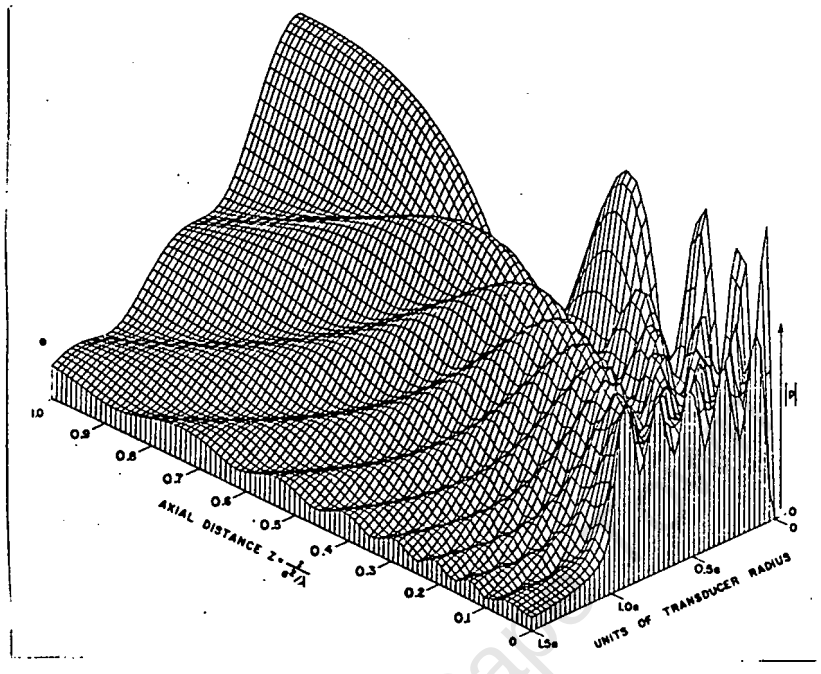

Figure 1.2: Magnitude of sound pressure computed on a grid within the near field of a circular transducer (a/l= 5.0).

As shown in figure 1.2, along the central axis of the sound beam, the series of acoustic pressure maxima becomes more widely spaced[3], until a final maximum at a distance N, whereafter the interchange exponentially decreases. The positioning of these axial maxima and minima in the case of a circular piston is a function of the transducer's diameter and the wavelength of the sound in the material[1].

The importance of the near field sound intensity patterns become apparent when it is necessary to test for defects in a region irradiated by a transducer's near field. When comparing test results to standard test blocks, ambiguous results can arise if the frequency, water path length and flaw depth used in both tests are not identical[1]. In the far field, there are no significant interference effects and there is a gradual transition from a planar to a spherical wave front.

1.2.3. Inspection techniques

The two major techniques of ultrasonic inspection are the transmission method and the pulse echo method.[3] The primary difference between those two methods is that the transmission method measures only the attenuation in the signal whereas the pulse-echo method measures both the attenuation and the time of flight of the signal.

Using the transmission method, flaws are detected by comparing the intensity of ultrasound transmitted through the test piece with the intensity through a reference standard of the same material.[3] Transmission testing requires two probes, one to transmit and the other to receive[3].

The pulse-echo technique involves the detection of echoes reflected from discontinuities or interfaces in the part[3]. Flaw depth can be determined by the time of flight between either the initial pulse and flaw echo or between the flaw echo and the backwall echo. Pulse-echo testing requires short bursts of ultrasonic energy, introduced into the testpiece at regular intervals. Both the intensity and the time of flight of the return signal relative to the initial pulse are monitored.

In most pulse-echo systems, a single transducer is used for both the transmission and the reception of the signal. Whilst a broad band of sound is transmitted, the received signal is generally shown filtered.

Theoretically, the maximum depth of inspection depends on the frequency of the pulse repetition rate. However, in practice, this maximum depth is reduced by the effects such as sound attenuation. Furthermore, it is advantageous to allow the internal reflections from each initial pulse to die down below interference levels before initiating the next pulse. This further reduces the desired pulse repetition rate and the depth of testing possible. However, the internal vibrational effects are less noticeable in large objects and axial inspections of test pieces six metres in length or more are possible.

Other inspection techniques

Alternative techniques that are less commonly used include the frequency modulation method, the spectral analysis method and the sound conduction method. Further details of these are given in references 3, 8, 9 and 10.

1.2.4. Data representation

Data from ultrasonic scans is usually presented in one of three different formats, termed A, B and C scans.

The data presented from a transmission test is limited in that the depth of flaws cannot be determined. Thus, the output signals are normally shown as A-scans on oscilloscope traces, strip chart recorders or meter readings[3]. However, in the case of pulse-echo inspection, A, B and C-scans are used.

An A-scan image provides a one-dimensional description for a given test point.[12] An example of this is the information given on an oscilloscope of the signal amplitudes and time of flight data obtained for a single point on the surface of the testpiece[3].

The output is a plot of amplitude of incoming signals versus time elapsed from the initial pulse. When the horizontal sweep time is calibrated to represent distance, the location of flaws can be measured directly from the screen.

A B-scan presentation is a two-dimensional or cross-sectional view of the testpiece. B-scan images are suitable for long, narrow test pieces, where a third dimension is unimportant.

A C-scan image is similar to that of a B-scan, except it represents a plan view of the testpiece. Discontinuities in the part are shown as a dark region on the plot and, in the case of pulse-echo inspections, the depth of flaws are either shown by a variation in the darkness of the region or by using a different colour. Although instrumentation exists that will produce

a C-scan[1], the most common technique is using computer storage.

1.2.5. Interpretation of ultrasonic signals

Depending on the inspection technique used, interpretation of the data received from ultrasonic scans is necessary to select useful indications from duplicated data (ie: repeated back wall and flaw echoes) and possible spurious indications (caused by surface finish, part geometry etc.).

Transmission inspection techniques provide a shadow picture of flaw presence and is relatively easy to interpret. A drop in the intensity of the beam entering the receiver transducer signals the presence of a flaw. In the case of pitch-catch transmission, spurious signals may be separated from wanted indications by their corresponding transit times[3]. The resolution of a transmission inspection system depends primarily on:[6]

- the ratio of defect area to beam size
- the separation between the defect and the transducers.

However, large discrepancies in the received beam intensity can result by small variations in the coupling conditions, thus giving erroneous results. For instance, a 10% variation in coupling efficiency could lead to a 10% drop in beam intensity, causing the indication of a significant flaw.[3] Another factor which can cause erroneous variations in the received beam intensity is the build-up of standing waves in the testpiece. As mentioned previously, this is overcome by using a modulated frequency for transmission of the initial pulse.

Pulse-echo techniques require more interpretation due to the increased amount of information available. Both conventional (ie: time of flight indications) and spectrometry techniques can be used to detect flaws.

Two basic variables are measured by the conventional pulse-echo techniques: time-of-flight and echo amplitude[11]. These two, along with the variations in amplitude of the signal relative

to probe movement, provide the necessary information for defect location and characterisation.

The time of flight of the return of the initial signal gives the depth of an interface existing in the part. This can be compared to the distance to the backwall or other geometric features to detect the presence of flaws.

The height of the defect echo is proportional to the reflected energy but does not always give an indication of the defect size. This is because the reflected energy is affected by the orientation of the defect, it's shape and it's distance from the probe[11]. Defect echo heights compared to reference standards usually indicate a minimum flaw size.

The variation of signal amplitude with probe movement can help distinguish the shape of the defect. Planar defects give very localised reflection signals whereas spherical and cylindrical defects give scattered signals, resulting in a relatively constant echo amplitude over a wide region of receiver probe movement.

A-scan time of flight interpretation

An example of a conventional time of flight A-scan output is shown in figure 1.3[3]. It shows a basic A-scan immersion setup with a diagram of both the full video display and the section of the display normally used for flaw detection.[3] The flaw indicated was at a depth of 45% plate thickness and was planar in nature.

As illustrated by figure 1.3 (b), the reverberations of the echoes have all been included in the trace. Indications labelled 1-6 are reverberations of the backwall reflection, those labelled A-K are reverberations of the primary flaw echo and those labelled X-Z are reverberations of a subordinate flaw echo induced by re-reflection of the first back reflection.

Figure 1.3 (c) shows a section of the full video that is needed for interpretation purposes. The correct adjustment of the display instrumentation provides only this information which then simplifies the identification of flaws.

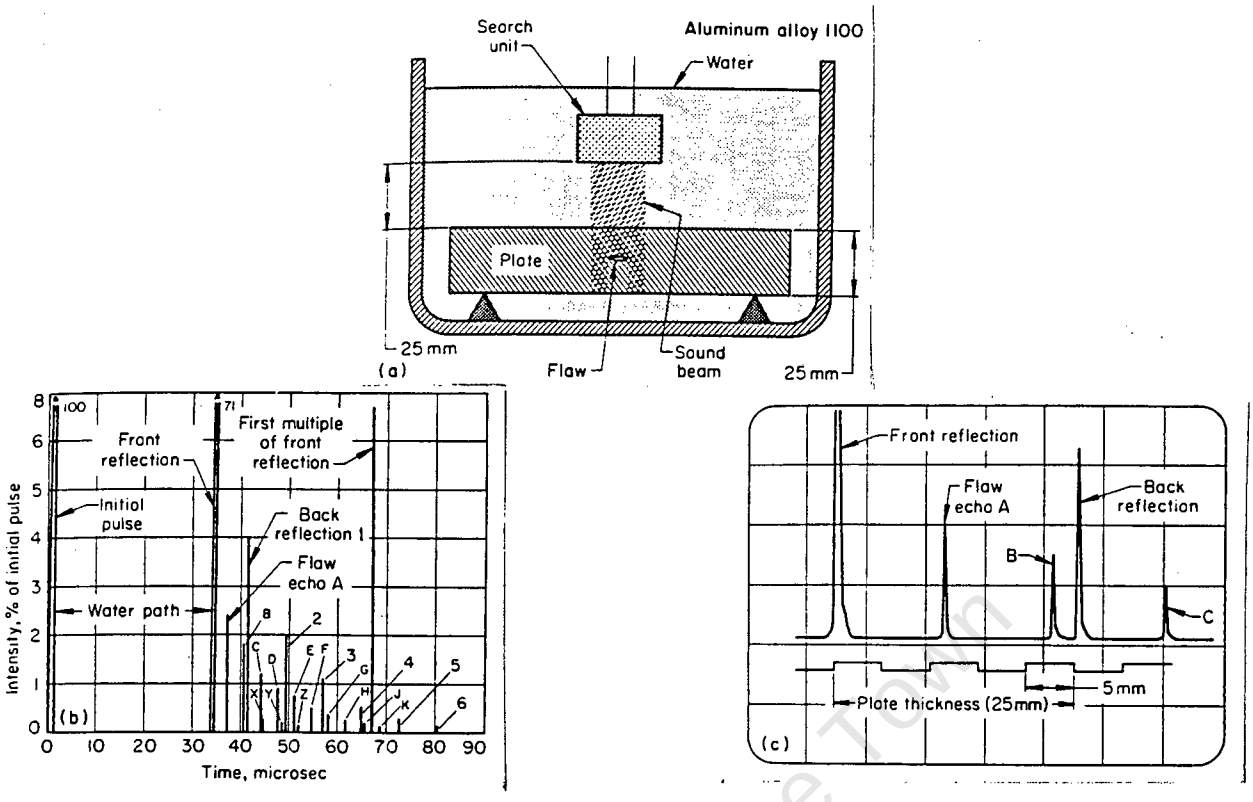

Figure 1.3: **(a) Typical A-scan immersion test setup**
(b) Full video mode output from a scan
(c) Section of video mode output

Flaw size estimation:

The echo amplitude from a flaw is directly proportional to the projected area of the flaw reflecting the sound. If a flaw is not planar or is not parallel to the surface, the echo amplitude will be less than for one that is parallel. As flaw sizes are often estimated by comparing the echo amplitudes of the flaw to those of reference holes, the operator must be familiar with the variations in echo amplitude with flaw shape and orientation variations.

Partial or complete loss of backwall indications are as a result of a 'shadow' caused by the presence of a flaw in the sound beam being cast on the backwall. The reduction in echo amplitude does not correspond directly to the area of the shadow cast by the flaw but can be used as a secondary estimate of flaw size[3]. When flaws scatter the sound from the beam in such a way that it does not reach the receiver probe, and, hence a flaw is not indicated, the reduction in backwall echo can indicate the presence of the flaw.

1.3. WELD INSPECTION USING ULTRASONICS

The ultrasonic technique used for the inspection of welds depends on the type of weld (butt, spot, T-joint etc.), the method by which the weld is formed (resistance, arc), the form of defect expected and the configuration of the workpiece.

1.3.1. Reflection characteristics of weld discontinuities

The types of flaws most commonly found in welds are:[3]

- Porosity
- Entrapped slag
- Incomplete penetration (LOP)
- Incomplete fusion (LOF)
- Cracks
- Overlaps and underfills
- Undercuts
- Laminar tearing
- Weld mismatch

Some defects such as porosity, slag inclusions, cracks, LOP and LOF occur more frequently than others in all five of the most common welding techniques[12]. All of these defect types are identifiable by the reflection pattern of the ultrasonic signal.

Porosity defects

Porosity, in the form of gas bubbles or pores, are defects formed during solidification of the weld. These pores are normally rounded or elongated teardrop shapes without sharp points[12].

The reflected ultrasonic signals from porosity defects are usually small and narrow[12]. The returned signal amplitude will vary if the transducer is moved around the defects or the weld

is scanned from the opposite side.

Slag defects

Slag inclusions are caused by nonmetallic solid material becoming entrapped in the weld. These defects are normally found near the surface and in the root of the weld, between the weld beads and at the side of the weld near the root[12].

The returned signal from a slag inclusion has a high amplitude and the scattered nature of the ultrasonic energy produces a relatively wide signal. As the transducer is manipulated around the slag inclusion, the signal height does not decrease significantly but the position of the edges of the signal vary. Slag discontinuities can be distinguished from cracks and LOF defects by the width of the returned signal.

Lack of fusion defects

Lack of fusion (LOF) discontinuities, a condition where the fusion between weld and base material is incomplete, are found on the sidewalls of a joint.

LOF discontinuities act as flat reflectors to the ultrasonic beam[12]. Thus, if orientated perpendicular to the beam, a narrow, high amplitude indication will result. If orientated at an angle to the beam, a much reduced indication will result.

Crack defects

Cracks in the weld are discontinuities characterised by their high length and width to opening ratio. They can occur both in the weld and base metal, in longitudinal and transverse directions. Since LOF and crack defects are similar in shape, both produce similar indications. However, LOF defects can be distinguished from cracks in welds by estimating the orientation of the discontinuity by scanning both sides of the weld.

LOF discontinuities are located on the sidewall of the joint and thus normally inclined. The

echo amplitudes of scans from one side of the wall will be considerably lower than from the other due to the reflective nature of the inclined flaw. However, cracks, which are usually vertical, will give rise to echo amplitudes of equal size of both sides of the weld. This is the factor which is used to distinguish between the two defects.

Weld mismatch

Weld mismatch occurs when two misaligned parts are joined. The indication from a mismatch is narrow and easily confused with one from a root crack. However, scanning from the other side of the weld will not give rise to any indication, distinguishing it from a mismatch defect.

1.3.2 Defect characterisation techniques in welds

Defect characterisation involves determining the location, orientation and shape of a flaw in the test material.

The location or depth of defects within a weld can be determined by the time-of flight of the reflected energy from a pulse-echo test. Furthermore, an estimate of the orientation of the defect can be obtained by various techniques of moving the probe relative to the defect [refs 1, 13 and 14].

The sizing of flaws relies mostly on pulse-echo detection techniques. Three of the most common methods are:[1]

[1] Observing the change in the reflection echoes as the probe is moved across the flaw

[2] The DGS method, where the maximum reflection amplitude from the flaw is evaluated.

[3] Spectroscopy methods, where the frequency spectrum of the reflected pulse is analysed.

[4] Comparing returned ultrasonic signals with known signature traces.

Defect sizing by method [1] was reported to be the most accurate when the crack length exceeded the width of the ultrasonic beam[1]. This method involves observing when the maximum received defect echo decreases by half its amplitude, thus indicating an edge of the crack. From this, an estimate of the crack length can be made using information concerning the location of the defect and the type of probe used.

Where the defect size is smaller than the beam width, method [2] is normally used. This is because the reflection indicated by a small flaw is dependent on factors such as the characteristics and the relative positions of the transmitter, reflector and receiver[1] making method [1] inaccurate. Thus, DGS scales have been developed which relate the size of the flaw to the height of the echo amplitude received from the different probe frequencies and diameters. The scales correspond to the maximum amplitude of the reflection echo and the size determined represents the size of an ideal planar defect that would give the same reflection amplitude. Alternative forms of the DGS scales are available, such as the slide rule type developed by Dianov[15].

Crack size and shape determination using method [3] is still in the development stages. In Doyle et al[16], it was suggested that spectroscopy could be used effectively in the study of extremely small cracks.

The comparison of returned ultrasonic signals with known signature traces relies on the accumulation of data from test pieces. Expected defect types are manufactured into test pieces and then inspected. The returned traces are stored for comparison with signals from inspection sites and a correlation between the defects on the site and those on the test piece are made from the similarity between their respective traces.

Further documentation on flaw characterisation is available in [refs 1, 17 and 18].

1.4 AUTOMATION OF ULTRASONIC INSPECTION

From the literature studied, it was concluded that the automation of ultrasonic inspections is presently concentrated in four main areas:

[1] Inspection of nuclear power stations. The risk of exposure of personnel to radiation requires remote control of the inspection equipment.

[2] Inspection of large volumes or throughput of product that requires comprehensive inspection, (example: piping industry).

[3] Inspection of large articles, requiring a large number of samples to be taken (10^4 - 10^6) .

[4] Inspection of parts with complicated contours, requiring precision probe positioning (example: aerospace industry).

Each of the above were originally a niche market in the inspection industry. However, with the increase in computational power and the advances made in robotics, these niche markets are expanding such that most industrial inspection applications in the near future will use some form of automation.

Section 1.4.1 gives a brief overview of some of the main developments in each of the above four areas. Section 1.4.2 then discusses the field of automated heat exchanger inspection and section 1.4.3 presents a specific heat exchanger inspection problem that was addressed by this research.

1.4.1. Past and present automated ultrasonic systems

One of the major uses of automated ultrasonic systems in the nuclear industry is to carry out the Pre-service (PSI) and In-service (INI) inspections on the radioactive circuit of the steam generation plant.

Examples are the automated systems used on the primary circuit of a pressurised water reactor in 1976[19], and on the butt welds around the gas circulator mounting structure in 1978[20]. More recently, in February 1993, the first ISI of Koeberg's Unit 2 reactor Pressure Vessel, using automated techniques was performed.[21]

Another major use for automated ultrasonic systems is in the inspection of tubular products. The requirement that the entire tube must be inspected, along with the large volumes of throughput, make this an ideal application for automation.

An example of the automated ultrasonic inspection of tubular products is the system developed by the VNIIK, Russia, in 1977 for the inspection of tubes with an inside diameter of between 20 and 120 mm[22]. Another system, the ATLAT-1, developed in 1984, was specifically designed for the automatic inspection of thin-walled tubing[23].

Systems developed for the inspection of large articles (ie:submarines) include the AFDS equipment, developed by Russian researchers and operational by 1986[24]. These systems were designed to overcome the reduction in reliability and productivity found when large numbers of sampling points resulted in operator fatigue.

Lastly, systems have been developed for the low-volume inspection of parts with complicated geometries. One example is the system developed by Shorts Brothers Ltd, England, to inspect composite cowl panels using a Cincinnati T3-566 robot driven by a CAD-derived scanning pattern.[25] Another example is the computerised shear wave technique developed to detect flaws in helicopter parts.[26]

1.4.2. Automated inspection of heat exchanger welds

Presently, almost all of the automated systems developed for heat exchanger tube inspections use one form or another of eddy current inspection.[2][28][31][33] This is because most inspections require the entire length of tube to be inspected, for which eddy current techniques are most suited.

Few references to the use of ultrasound techniques were found. Furthermore, those that did exist were limited to the automation of the signal interpretation whilst still relying on manual probe movement. However, some systems were capable of both ultrasonic and visual inspections as secondary techniques after eddy current techniques.

Present inspection systems

The development of the present automated systems used for heat exchanger inspections resulted mainly from maintenance needs in the nuclear power industry. These automated systems were developed in order to inspect heat exchangers on the active circuit of nuclear power stations without long-time radiation exposure of personnel.

In the present automated systems, the transducers and interpretation software used for such systems are similar to manual set ups. However, the automation of the process involves some form of manipulation that controls the position of the search unit. These manipulators have been developed with the criteria of nuclear inspections in mind and thus are not optimally designed for inspection of non-radioactive heat exchangers with exposed end plates.

Thus, an assessment of the suitability of present manipulator models on the market to the inspection of a normal heat exchanger was conducted. Present models of manipulator's used for nuclear inspection applications include:

[1] Laborelec's polar manipulator

[2] Westinghouse's Rosa arm

[3] Babcock & Wilcox's Roger manipulation

[4] Brown Boveri's Vermaak manipulator

[5] B & W's Cobra arm

[6] Intercontrole's Bikinic "fingerwalker" manipulator

[1] Laborelec's polar manipulator[27]

The manipulator consists of two distinct parts:

- The pole, capable of angular rotation in directions "a" and "d" (see figure 1.4)
- The rail carrier, which carries the trolley

The rotational movement of the arm and the radial movement of the trolley along the arm are automatically controlled using digital position encoders. The final position of the probe is determined by the position of the small arm mounted on the trolley. This arm was a necessary addition to ensure that almost all the holes in the tube sheet were reachable and is manually adjusted to one of four possible positions prior to scanning a particular section of the tubesheet.

Inspections are done using either eddy current probes or a small camera for visual inspection. Scanning is initialized by defining the heat exchanger model to be inspected, the starting positions of the arm, and trolley and the tubes to be inspected. The motion of the trolley, as well as the signals received from the eddy current unit, are completely controlled by computer software. The time taken between tubes averages 1 to 2 seconds, resulting in scanning speeds of up to 250 holes per hour.

This equipment has shown a high positioning reliability (error-free positioning over 50 000 holes test), is simple in construction and allows access to 99,5 percent of a typical tube bundle.

Laborelec's automated polar manipulator is shown in figure 1.4 and 1.5.

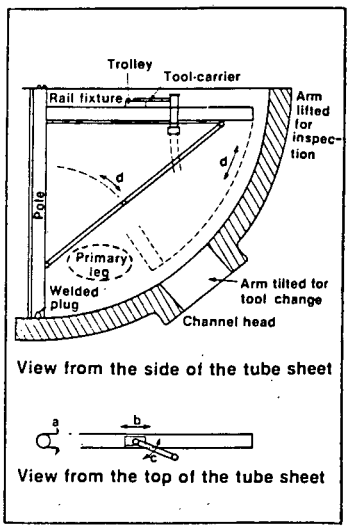

Figure 1.4: Schematic view of Laborelec's polar manipulator. Letters a-d show the various ways in which the manipulator can move.

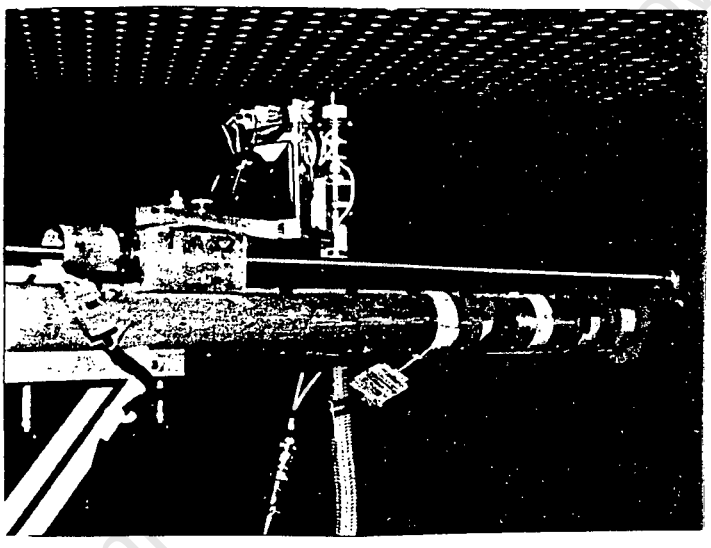

Figure 1.5: Close-up photograph of the polar manipulator in use.

The disadvantages of this equipment however, for the inspection of conventional heat exchanger are:

- It is designed to operate inside the head of the heat exchanger and thus is dependent on the support of the head.
- It is designed for a particular size of heat exchanger.

[2] Rosa (Westinghouse)[28]

The Rosa (remotely operated service arm), developed by Westinghouse, is shown in figure 1.6 . It is a all-electric robotic arm with six degrees of freedom, designed for the inspection and repair of tube sheets.

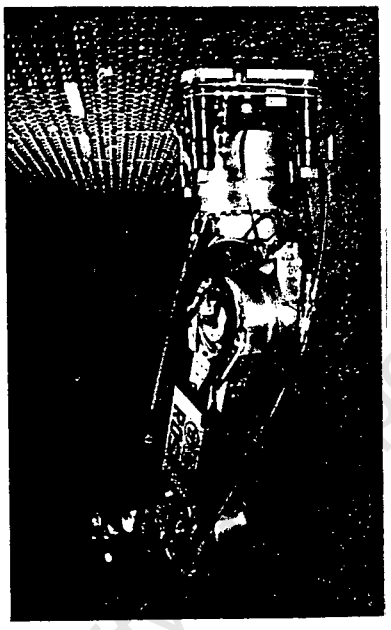

Figure 1.6: Rosa in position inside the channel head of the steam generator tube.

ROSA consists of four subsystems: the remotely operated service arm, a supervisory control computer, a base unit and an end-effector subsystem. The arm is capable of lifting 23 kg at its full 2.1 metre extension and its position is either controlled by a joystick or a preprogrammed scanning pattern.

It was mentioned that simple ultrasonic inspections using a contact probe were possible with ROSA although no applications to date were reported. Furthermore, it was unclear as to how the probe was manipulated inside the tubes, if at all, and what type of search unit (i.e.: probe angle, couplant etc) was used.

The disadvantage of Rosa is that it is designed specifically for safety in a nuclear environment. It locates itself outside the manhole of the head of the heat exchanger so as not to require a "jumper" (person entering cavity of heat exchanger head) to install it. This has the implications that it is very mechanically complicated (to provide the rigidity as well as having complicated motion controls). Whilst these properties of Rosa are necessary for nuclear inspection, it has disadvantages that Rosa is overdesigned and extremely costly for use in a non-radioactive environment.

[3] Roger (Babcock & Wilcox)[29]

The Roger (Remote operated generator examination and repair), developed by Babcock & Wilcox, is a high strength robotic arm. Its capabilities include tube inspection, milling, tube sample removal, remote welding, plugging and sleeving.

The system comprises of a microcomputer and a high strength, lightweight manipulator. The manipulator itself consists of an articulated arm connected to a central mast. The arm can withstand loads of up to 90 kg and is equipped with, among other tools, cameras mounted on each of the repair heads to allow the operator to have visual coverage of the repair operations.

However, as with Rosa, Roger is specifically designed for a nuclear environment. Its method of location inside the head of the heat exchanger limits it to certain designs of heat exchangers and prohibits it from inspecting a heat exchanger with an exposed endplate.

[4] Cobra (Babcock and Wilcox Ltd and Frametone Ltd)[30]

The Cobra, brought out by Babcock and Wilcox Ltd and Frametone Ltd (France) in 1991, is shown in figure 17.

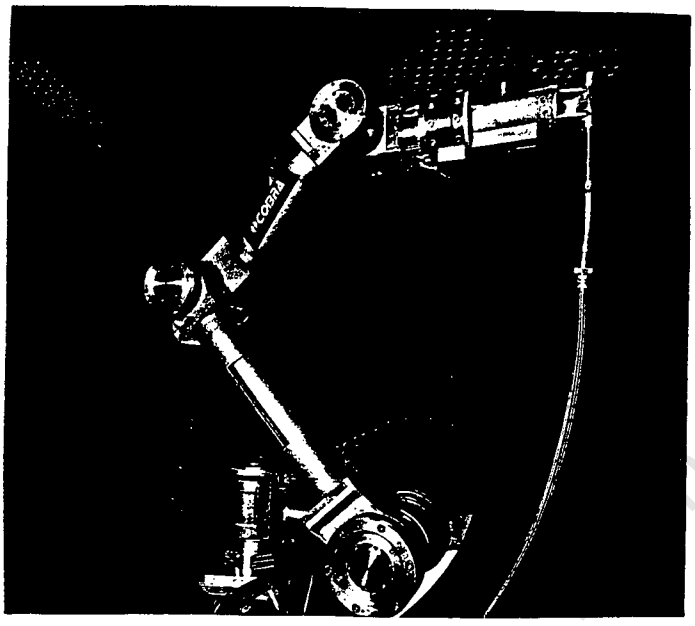

Figure 1.7: **The BWNS-designed Cobra manipulator**

It was designed to perform the following tasks:

- tube inspections
- tube and plug removal
- tube plugging and stabilizing
- tube shot peening
- tube U-bend stress relief

It was reported that Cobra also did not require a "jumper" for installation, tool changes could be made outside the head and that it could reach all the tubes from a single location without a re-positioning move.

One interesting feature of the Cobra is its locating attachment. It requires bolting to the holes of the manhole cover and rests on a single leg on the bottom of the channel. Whilst this

allows the probe to reach every single hole, it does make it dependent on the design of the manhole cover.

[5] Vermaat manipulator[31]

The Vermaat manipulator, developed in 1979, was originally designed for eddy current and ultrasonic testing (no applications mentioned) of tubes, visual inspection of the tubesheet and profilometry measurements.

The manipulator, shown in figure 1.8, consists of two parts: the "leg" and the "arm". The leg consists of a central shaft with a coupling device for the manipulator arm and a vertical movement drive. The arm is designed to carry probes and tooling equipment.

Installation consists of using a pulley to lift the leg section into the heat exchanger channel head. The leg is located by three pins in the tubesheet and by a pneumatic clamp at the lower end. The arm is then moved into the chamber using slides and secured to the leg with a locating pin.

The inspection of a heat exchanger is controlled by a microcomputer which has the configuration of the heat exchanger pre-programmed in memory.

One interesting feature was that, although it was designed to require the use of a "jumper", the mounting mechanism is independent of the head's manhole configuration. However, the nature of the "leg" support made the unit dependent of the head being in place

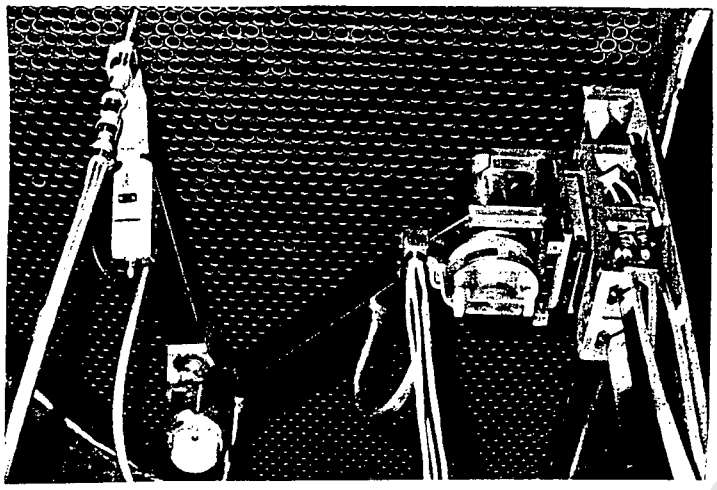

Figure 1.8: The Vermaat Manipulator in its working positions in a steam generator. An eddy current test probe and a television camera are installed on the manipulator arm.

[6] <u>Bikinic Manipulator</u> (Intercontrole Ltd)[32]

Another probe manipulator is the Bikinic Manipulator, one of several 'Fingerwalker' designs produced by Intercontrôle Ltd.

Figure 1.9 and 1.10 show the Bikinic Manipulator. The system is primarily designed for eddy current inspections using axial and rotating probes but can also perform helium leak tests. It is pneumatically operated except for the carriage ring which is electrically driven.

The manipulator is installed onto the tubesheet manually and locks into the holes, its only support, with two pairs of positively locking expandable grippers. To move from hole to hole, one of the grippers is released and moved at a time, whilst the other three remain stationary.

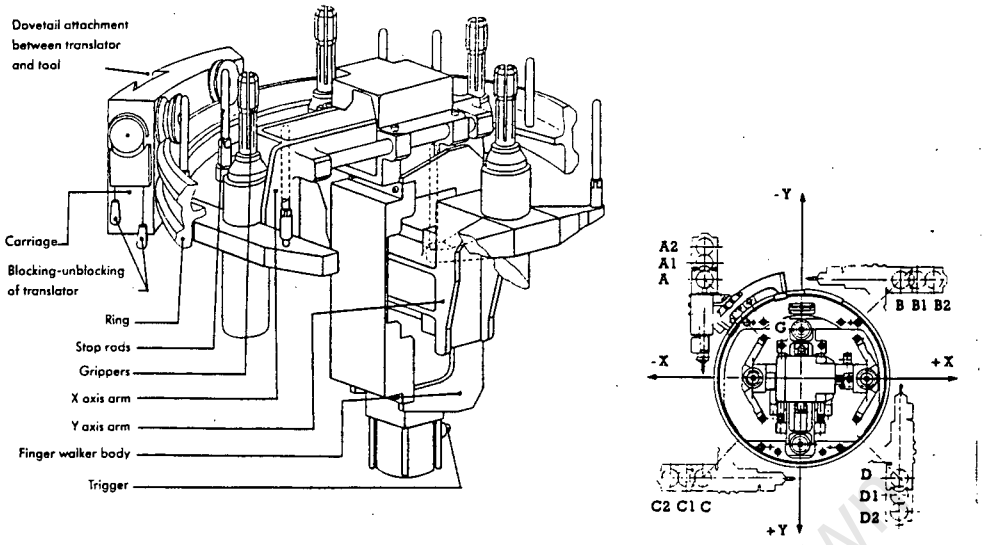

Figure 1.9: Schematic view of the Bikinic Manipulator

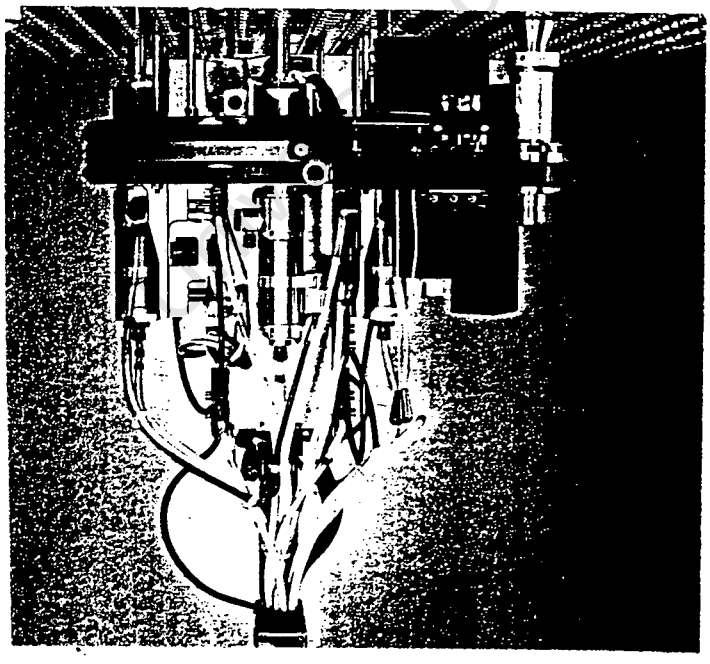

Figure 1.10: Side view of the Bikinic manipulator

The eddy current probes are fed into each tube via a holder located on the carriage ring. This ring allows the maximum number of holes to be inspected without having to relocate the manipulator.

The system is controlled by Supervisor™ software which allows full automated motion of the manipulator from hole to hole. The monitoring of the signals from the eddy current probes and the control of the manipulator can be up to 300 metres away via a linking cable.

Another form of 'fingerwalker' by Intercontrôle[33] is the Ritmic manipulator, shown in figure 1.11.

The Ritmic manipulator works on a similar principle as the Bikinic manipulator. However, it is capable of moving one entire inspection head whilst the other holds the equipment in place.

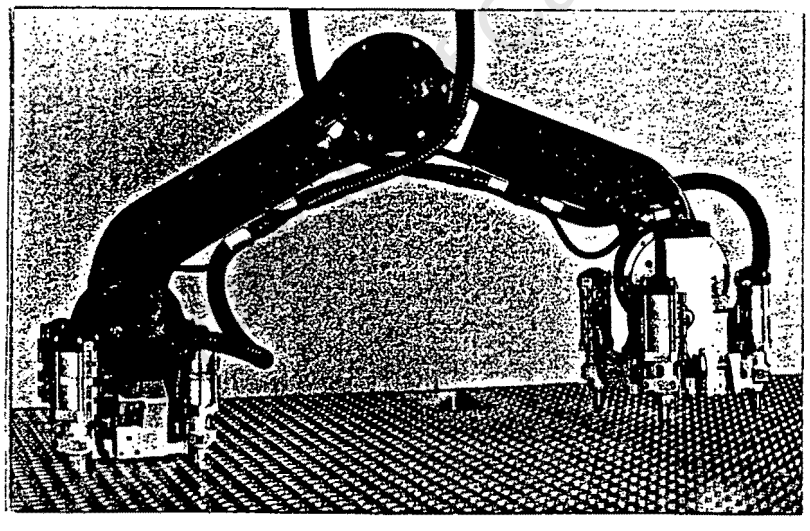

Figure 1.11: Ritmic manipulator

The Bikinic and Ritmic manipulators are most suited for adaptation from nuclear applications

to the inspection of a conventional heat exchanger. They do not rely on the head of the heat exchanger being in place during inspection. Furthermore, they are suited to any shape and size of endplate. Also, little modification is needed to allow ultrasonic inspection to take place. These manipulators are impartial to the inclination of the end plates.

However, one disadvantage was that the "fingerwalker" units were designed for total remote operation once installed, hence the complicated nature of the design. It was felt that a simpler model could be designed if the size restriction was eliminated. This would reduce the costs of the final model.

1.4.3 Specific inspection problem faced by industry

Background

One phase of the production of chlorine involves heating a mixture of caustic soda and salt by steam in the First Effect Steam Chest.

This heat exchanger is typically a vertically standing, one-pass type with the caustic soda being pumped from the bottom channel head up through the tubes.

Due to the corrosive nature of caustic soda, the tubes, tubesheet and channel head are made from pure nickel. There is a total of 980 tubes in the tube bundle, each tube having been welded to the outer surface of the tubesheet. For this, a tungsten inert gas welding technique is used with an 75%-25% Argon-Helium gas cover. The weld configuration is shown in figure 1.12.

Approximately four years after the installation of one such heat exchanger, it became apparent that severe erosion by the caustic soda of certain sections of the steam chest's tubing had taken place, allowing leakage of the steam into the caustic soda - salt mixture.

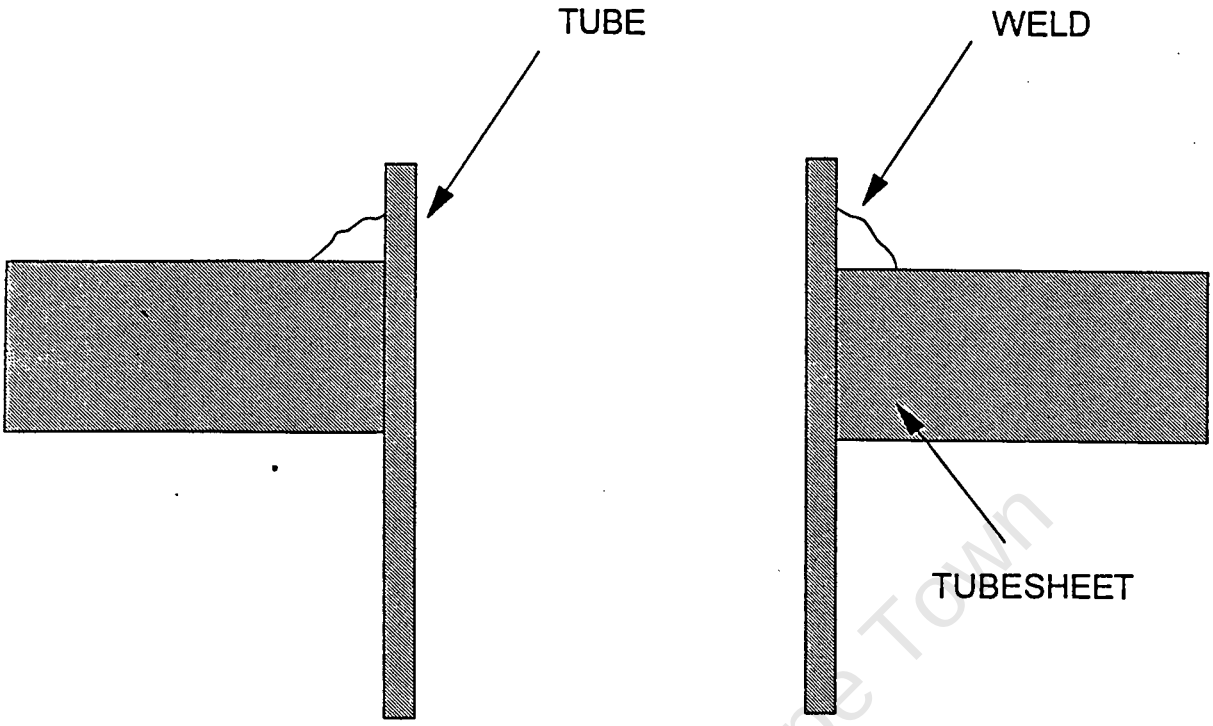

Figure 1.12: Weld configuration between the tubes and the tube sheet.

A maintenance inspection revealed that erosion had taken place in the bottom 200 mm of the tubes. The leakage had first occurred where there had been insufficient penetration of the weld between the tube at the lower tubesheet.

Present solutions to the problem

With the immanent replacement of the vessel, it was decided to investigate methods for further prolonging the life of the vessel. Three strategies were decided upon:

[1] Improving the design of the weld between the tubes and the tubesheet.

[2] Checking the integrity of the welds before commissioning.

[3] Inserting a 150 mm-long ferrule into the beginning of each tube on the lower tubesheet.

Firstly, by improving the quality of the weld and, more specifically, the length of the penetrated section of the weld in the vertical direction, the time the tube remained intact before allowing a leak to form would be increased.

Secondly, by ensuring the integrity of these welds, the chances of a lack of penetration, and thus a premature leakage, could be reduced. Thus, the integrity of the welds were manually checked using ultrasonic techniques before installation of the present vessel.

To increase the length of the penetrated zone, the production of new tube bundles included milling a chamfer on the tube hole on the upper surface of the tubesheet. Thus, when the tube was welded, a greater height of weld was achieved, effectively increasing the joint area between the tubes and the tubesheet. This weld configuration is shown in figure 1.13.

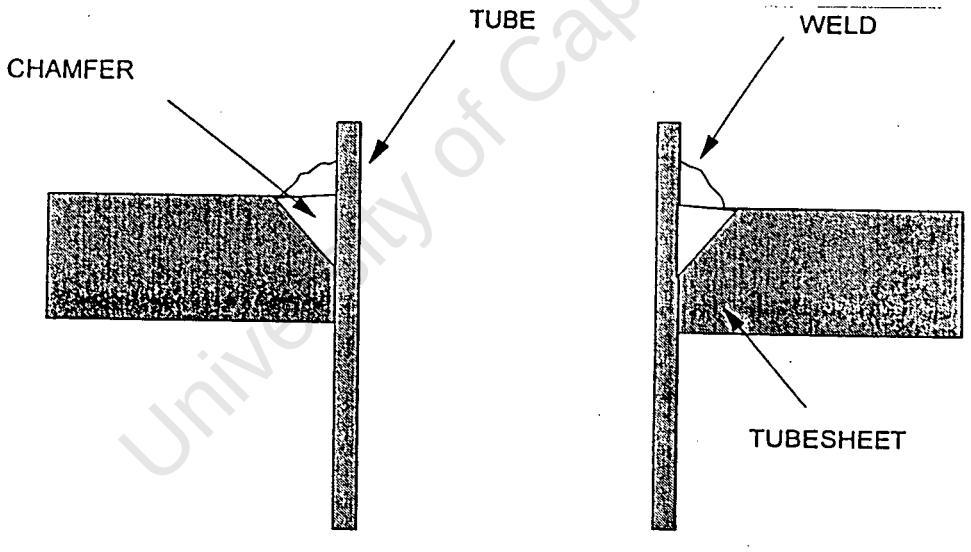

Figure 1.13: Weld configuration using chamfered hole technique.

The third strategy involved inserting ferrules, tubes with a flared end, into the beginning of each tube once the tube ends had worn sufficiently. These effectively increased the wall thickness of the tubes over the weld area and acted as a wear surface. The disadvantages of

this strategy are the cost of the ferrules (R 200 000 for machining and installation alone) and the fact that the wall thickness of the tube in this area could no longer be measured.

One possible solution that has not been implemented in the design of the new tube bundle is that of explosion or pressure expansion welding. This involves pressure-fitting the tube ends into the tubesheet, using either a ultra-high pressure hydraulic system or a small explosive charge to supply the pressure needed for deformation. The advantage of this welding technique is that the weld effectively extends right throughout the entire depth of the tubesheet and hence increase the life of the tube bundle dramatically.

Remaining problems

The primary problem was that the ultrasonic inspection of the welds between the tubes and both endplates was done totally manually. This had the following disadvantages:

[1] The inspection was very labour intensive. This resulted in high man-hours costs as well as a long plant down-time period.

[2] Both the number and repeatability of the samples could lead to operator fatigue,resulting in an inadequate weld being overlooked and a premature leak forming.

[3] No record of the integrity of each weld for comparison in future inspections.

[4] The quality of the assessment of welds is largely dependant on the skills of the operator and the training he has received.

1.5 CONCLUSIONS

1.5.1 All frequently occurring defects to be found in welds, namely porosity , slag, lack of fusion, cracks and weld mismatch can be positively identified using ultrasonic scanning techniques.

1.5.2 The existing problems with the present techniques used to inspect the welds on the First Effects Steam Chest are:

- High number of man-hours needed to complete an inspection (high plant downtime and thus cost).
- Operator fatigue (affecting quality of the inspection and the analysis of the results).
- No records of welds for future inspections.
- Analysis of weld information is dependent on operator's competency.

1.5.3 All of the above problems can be overcome by an automated inspection system. However, existing equipment on the market has the following disadvantages for use in this scanning application, because these systems:

- Predominately were designed for using eddy current equipment
- Are dependent on the heat exchanger head being in place and thus are also dependent on the design of the head interior.
- Are designed for quick installation, remote operation and high stand-alone reliability, specifically for the nuclear industry. This makes them expensive and unnecessarily complicated.

1.5.4 Thus, the optimum solution to the present scanning problems was to design a dedicated scanning system for the application.

CHAPTER 2

PROBE MANIPULATION

2.1 INTRODUCTION

Initial design work was undertaken to develop a suitable mechanism to move the ultrasonic inspection probe (UIP) around on the tubesheet. Such a mechanism would typically consist of a frame with a Probe Insertion mechanism (PIM), and would provide probe manipulation between tubes as well as inside tube openings.

The design was done in two stages. Firstly, a number of frame concepts were theoretically analysed and the advantages/disadvantages of each evaluated. This included analysing the benefits of a "single-position" frame versus a "multi-position" frame.

Secondly, two working models were set up. These two models enabled detailed analysis of the effects of the rigidity and accuracy of the frame on the scanning results. Furthermore, the benefits of a "cartesian plane" frame versus an "articulated arm" frame were analysed. Also, a suitable PIM was constructed and tested on the two models.

2.2 FRAME DESIGN: THEORETICAL WORK

The frame designs analysed can be divided into two categories: single position and multi-position frames. Further defined, these are:

- "Single position" frame:

  Frame providing movement to the probe across the entire tubesheet, without necessitating the relocation of the frame on the tubesheet during the scan.

- "Multiple position" frame:

  Frame requiring relocation on the tube sheet during a scan in order to allow the probe to reach all tube openings on the tubesheet.

[1] Single position frame designs

The first single-position frame conceptualised is shown in figure 2.1. The frame consisted of one arm which pivoted around the central tube in the tube sheet (row 18, tube 6). The probe unit was driven along the arm on guide rails by a lead screw, powered by stepper motor # 1 on the pivot point. The angular position of the arm was changed by stepper motor # 2, which powered a spring-clamped wheel mechanism running on the outer rim of the heat exchanger.

The problem with this design was the potential error that could arise from slippage of the outer wheel mechanism. One alternative was to have stepper motor # 2 power a rack and pinion mechanism. However, to manufacture a circular rack would be impracticable.

The second single-position frame conceptualised is shown in figure 2.2(a) and (b). The frame consisted of four arms, each one secured by a pivot unit that was clamped (bolted into) the edge of the heat exchanger. Each arm could rotate about the pivot point as well as extend or contract its radius. One of the arms was powered by two stepper motors - one driving the rotational

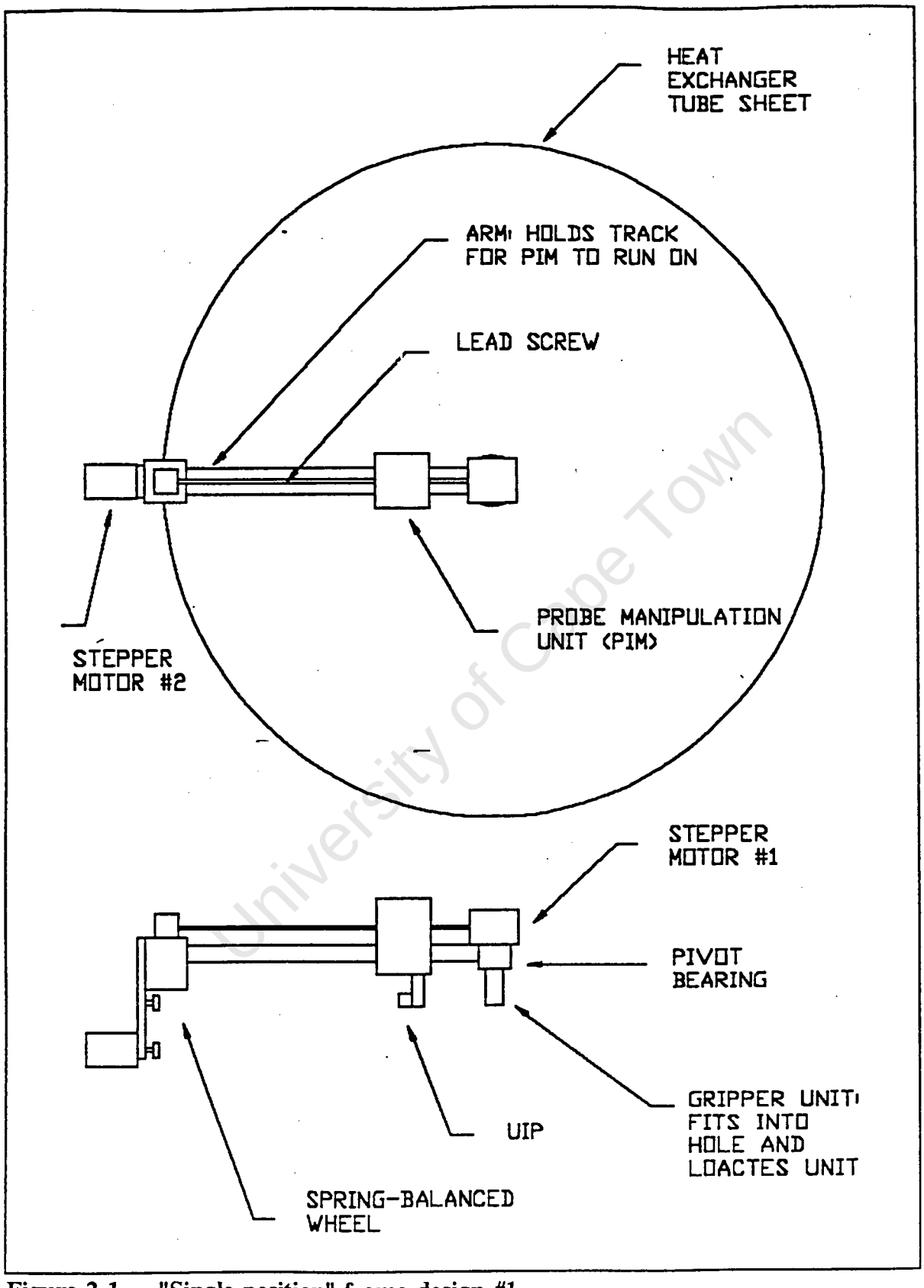

Figure 2.1 **"Single position" frame design #1**

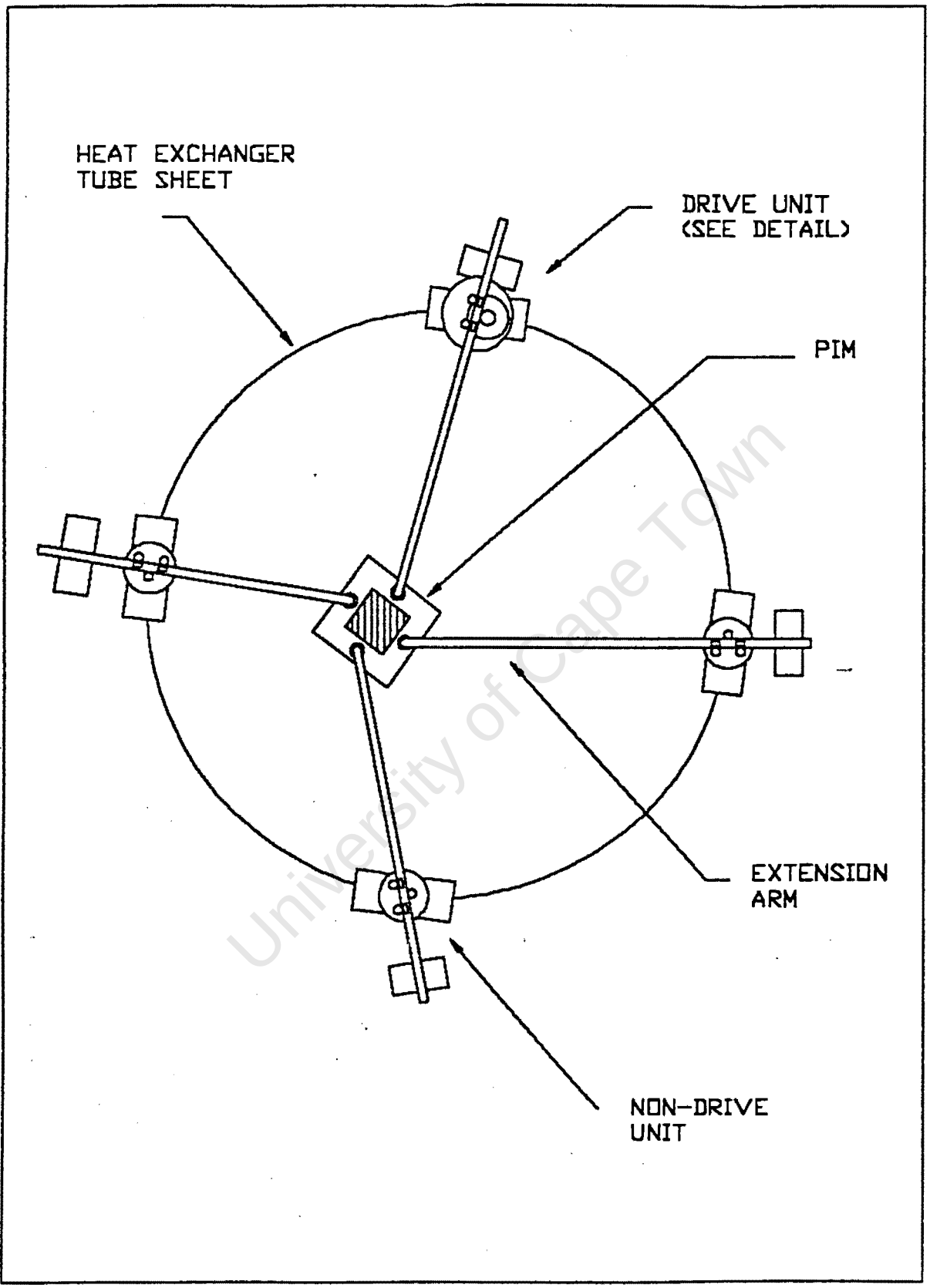

Figure 2.2(a) **"Single postion" frame design #2, overall plane view**

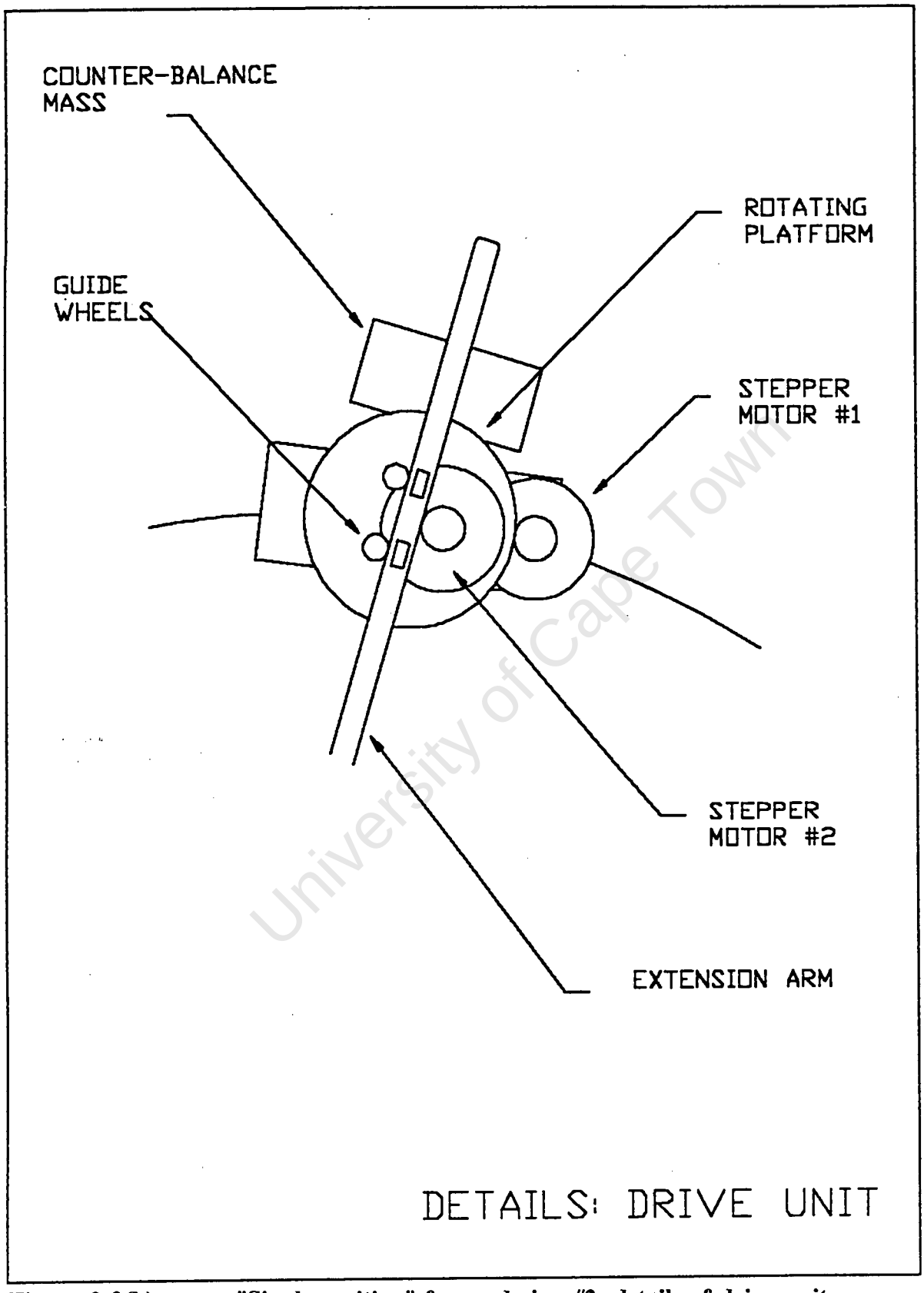

Figure 2.2(b) **"Single position" frame design #2, details of drive unit**

movement and the other driving the extension/contraction of the arm. All four arms were pivoting linked to a central platform which carried the probe insertion mechanism. Thus, the one arm was able to direct the central platform whilst the other three were just pulled along - their function being to give Z axis stability.

The reasons for not accepting this design was because of the following:

[1] *The rigidity of arms required to span the heat exchanger.*

It was estimated that the central platform would weigh about 10 kg (includes a stepper motor) and that the allowable z-axis deflection was approximately 1,5mm. Even with a counter-balance mechanism that could adjust to the length of arm extended, it was questioned whether such rigidity would be achieved.

(2) *Lack of operating space.*

In whatever position the central platform was in, one or more of the arms would be contracted at least half its length. This could cause problems if the heat exchanger was rested with the open tubesheet on the ground as the arms would be unable to contract. This might be overcome by having the arms arranged in a fashion as shown, but will result in a loss of Z directional stability.

An alternative would be to have one or two of the arms to consist of a telescopic design but this would further complicate the design and reduce the overall rigidity.

The third design is shown in figure 2.3(a) and (b). The frame design was an adaptation of Laborelec's poler manipulator[32]. It consisted of two main parts - a vertical mast and a horizontal arm that spanned the radius of the tube sheet. The mast was supported by cable ties that were tightened bo the outer edge of the tubesheet and lifted above the arm's operating plain by pole pulleys. The horizontal arm was supported from the mast by two rods as well as a central

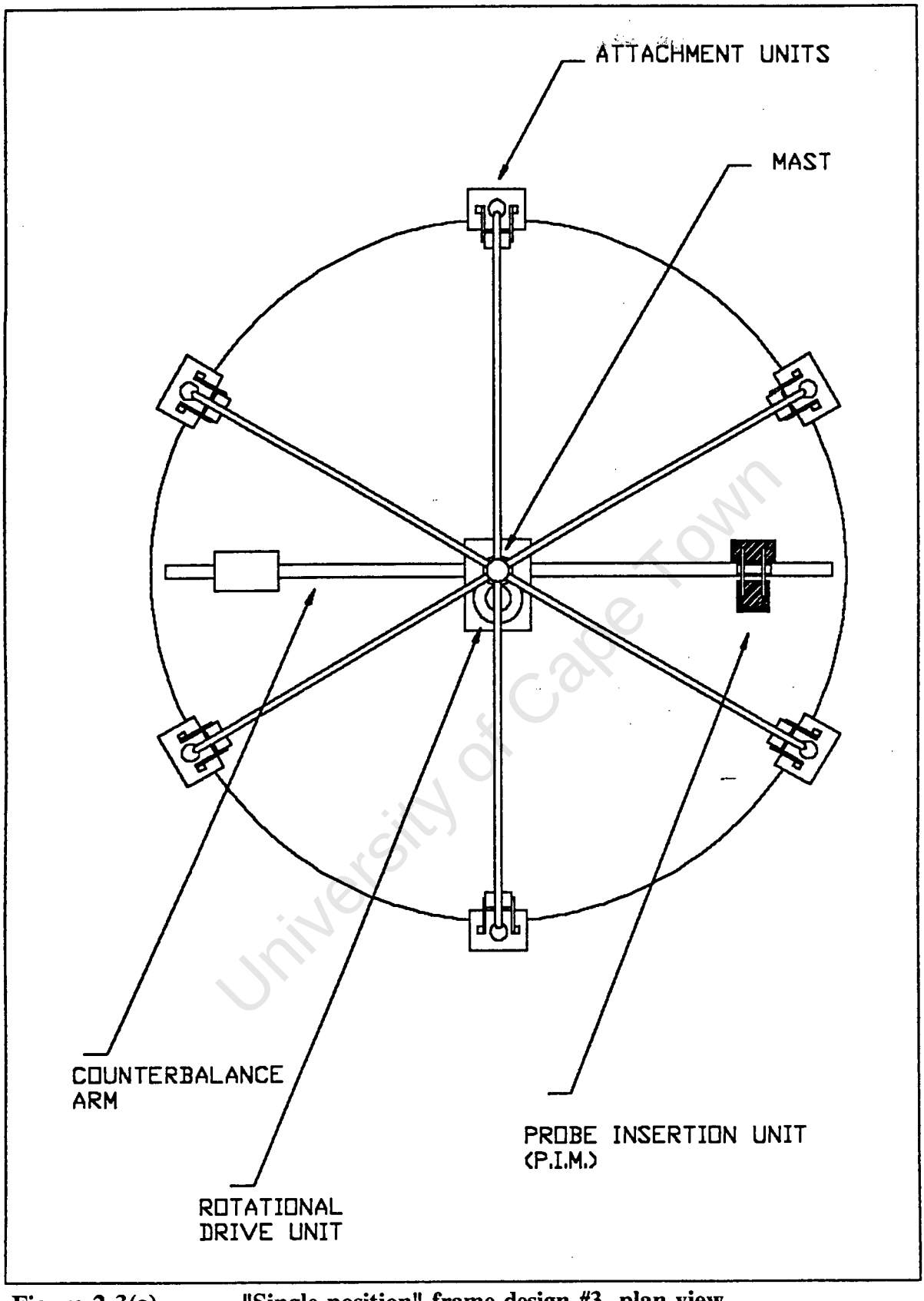

Figure 2.3(a) **"Single position" frame design #3, plan view**

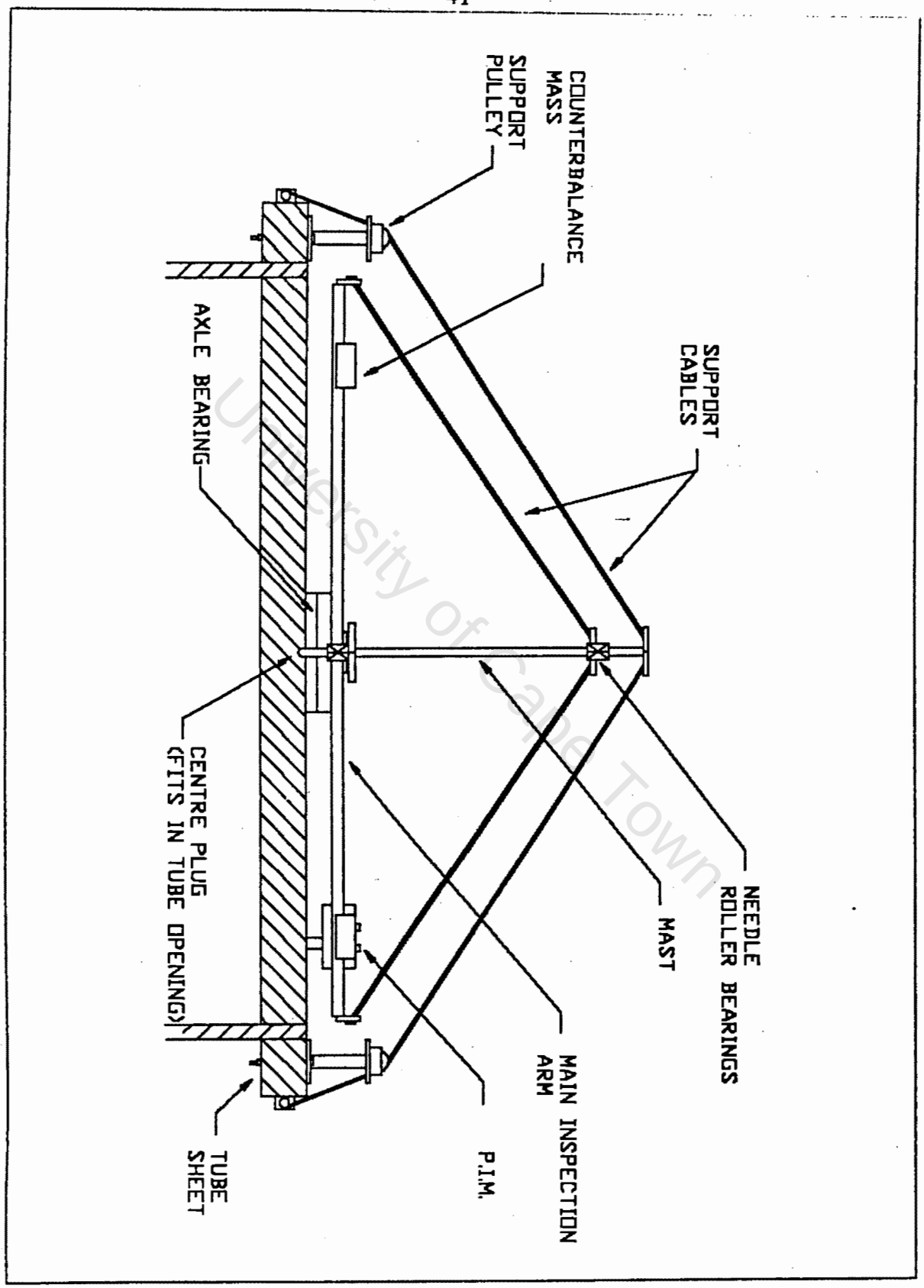

Figure 2.3(b) **"Single position" frame design #3, front view**

platform located on the mast beneath the arm.

The arm was rotated by a stepper motor mounted on a the central platform (off the arm for inertial reasons). The probe insertion mechanism (PIM) was driven along the horizontal arm by stepper motor # 2. Stepper motor # 2 was mounted on the horizontal arm near the mast and drove a lead screw (the nut remaining stationary on the PIM) - this was preferable to the motor being mounted on the PIM. A counter-balance mechanism on the other half of the arm was possible - its position could be controlled by a simple pulley mechanism connected to the PIM.

Although a lot of design work went into this concept, it was rejected for the following reasons:

(1) *Poor lateral positioning.*

If the tube sheet was at a 90 degree angle to the ground, the mast would experience a turning moment of approximately 60 Nm. A deviation in position of 1 mm by the top of the mast can be expected under such torque loading. However, this would lead to the outer reach of the horizontal arm being 3 mm closer to the tubesheet than predicted - an unacceptable error.

(2) *High set up time.*

The mast and support pulley system would require approximately 2 man-hours to set up and dismantle.

(3) *Not all holes scanned.*

With the central platform being necessary, not all of the tubes would be inspected. The remaining holes could be manually inspected after the equipment has been removed but the uniformity in inspection method would suffer.

(2) Multiple position frame designs

A number of shapes of multiple position frames were tested conceptually. Some of the more realistic ones are shown in figure 2.4. Note the extension of the arm beyond the frame - a concept which allows the tubes on the outer edge of the tubesheet to be inspected.

It was assumed that the multiple position frame would not be attached at all to the edge of the heat exchanger but would be located using a number of tube ends as vantage points. Mechanisms considered for locating the frame included magnets, rubber suction cups and tube expanders. Magnets were ruled out because of the non-ferrous nature of the heat exchanger (Nickel). Rubber suction cups were eliminated because of the lack of rigidity provided by the rubber connection. Thus, a mechanism which would expand inside the tube when activated, thus locking into the tube, was chosen.

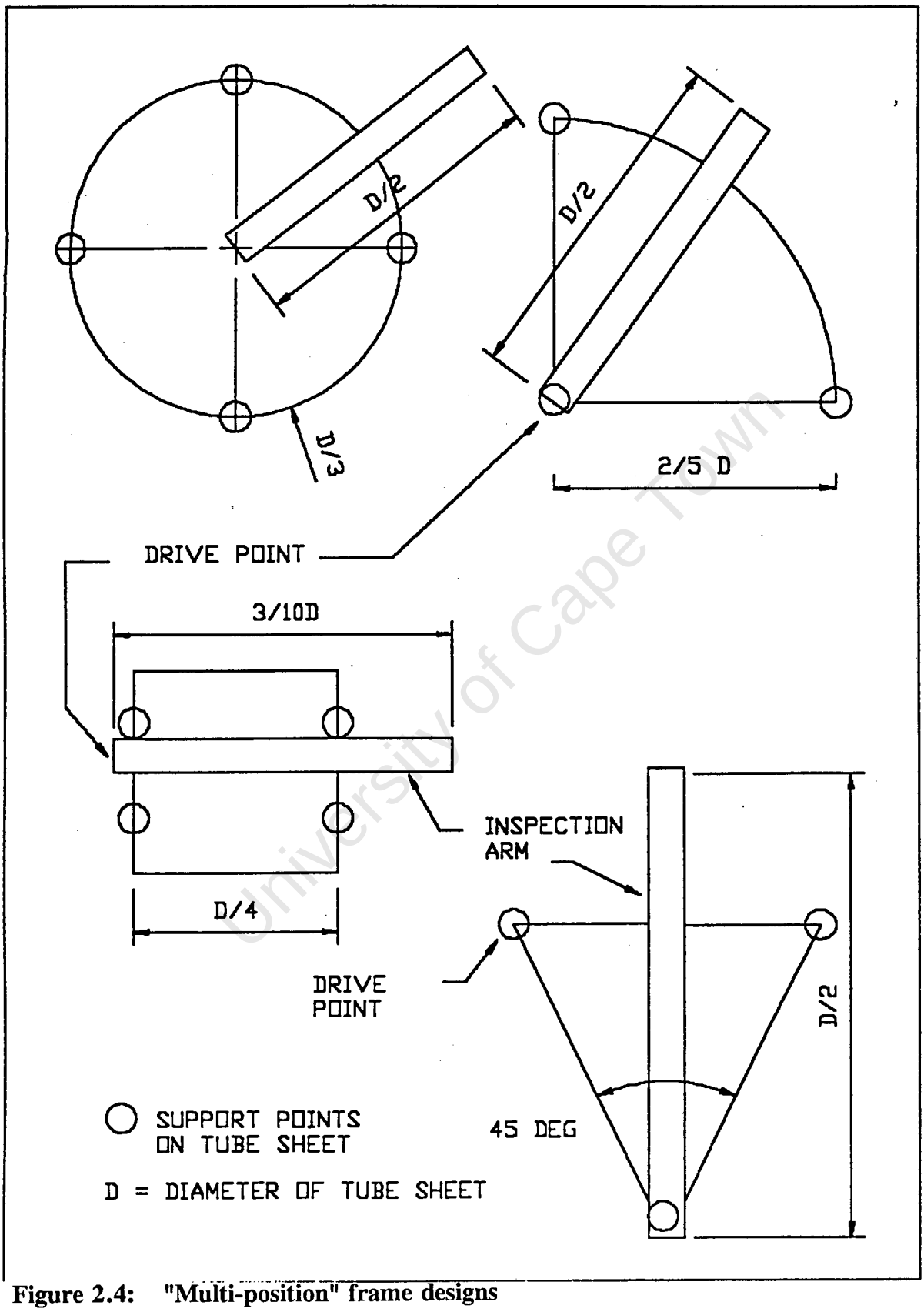

Figure 2.4: "Multi-position" frame designs

2.3 FRAME AND PROBE INSERTION MECHANISM (PIM) DESIGN: MODELS

Further design work was necessary to complete the frame and PIM design. Although the previous theoretical work had indicated that a multi-position frame was preferable, the ideal frame shape had to be found. Furthermore, the probe manipulation software had to be developed.

Two different frame configurations needed to be considered: namely the "rotational arm" frame and the "cartesian plane" frame configuration. A rotational arm frame would typically have five degrees of freedom, consisting of four revolute joints and one prismatic joint. A vertically articulated mechanical arm and gripper would be an example. A cartesian plane frame would provide linear motion in the XY plan and a combination of linear and rotational motion about the Z axis. A common example of this would be a CNC cutting machine.

Thus, two working models were set up to investigate each of the possible frame configurations. The first model used a SCORBOT ERIII robot as the probe manipulator, whereas a programmable CNC was used for the second model. A Probe Insertion Mechanism (PIM) was developed for the SCORBOT ERIII model and later modified for the second model. Furthermore, probe manipulation software was developed to be compatible with both models.

2.3.1 SCORBOT ERIII model

Overall system configuration

The resultant system that was used as a scanning model is shown in figure 2.5. It consisted of the SCORBOT ERIII robot and control box (probe manipulation), a 386PC (controlling software), a DA312 ultrasonic probe (for inspection), a USM2 ultrasonic detector and a HP 54600 oscilloscope (for data transfer). Also, a lubrication system and acoustic lens were designed to enable the ultrasonic scanning of the tube surfaces. The SCORBOT and 386PC communicated bi-directionally via the electronic controller. Likewise, the HP 54600 and 386PC communicated bi-directionally, with the returned ultrasonic signal being transferred

from the detector to the 386PC via the oscilloscope.

Scans done using the DA312 probe were done on a test rig. The probe was moved from tube opening to tube opening by the end-manipulator of the SCORBOT ERIII (modified for movement of probe inside tubes). The information from the DA312 probe was filtered using the USM2 detector and displayed on the HP 54600 oscilloscope. The 386PC controlled the movements of the SCORBOT ERIII and analysed the information coming back from the DA312 probe. Results were displayed during and after the scan on the 386PC.

SCORBOT ERIII robot

The SCORBOT ERIII was an instructional robot with five degrees of freedom. It consisted of a vertically articulated mechanical arm and gripper mounted on a base. The base, shoulder, elbow and wrist were revolute joints whereas the grippers a prismatic joint type performing a linear opening and closing motion.

The working envelope of SCORBOT ERIII is shown in figure 2.6. As shown, SCORBOT has essentially a spherical operating configuration. The arm was driven by sending a sequence of pulses to the relevant joint, resulting in it undergoing a precise angular displacement. Each motor on SCORBOT had a rotary optical encoder, reading directly from the rotor shaft, which enabled the controller to perform closed-loop motion control of the motors.

SCORBOT's end effector (gripper fingers) was modified with the addition of a probe holder mechanism. This mechanism (shown in figures 2.7 and 2.8) held the DA 312 probe, preventing motion of the probe's inspection axis whilst up against the tube wall. Furthermore, it provided the horizontal motion to bring the probe up against the tube wall once the probe had been inserted in the tube opening.

Further information on the specifications of SCORBOT ERIII can be found in appendix A.1.

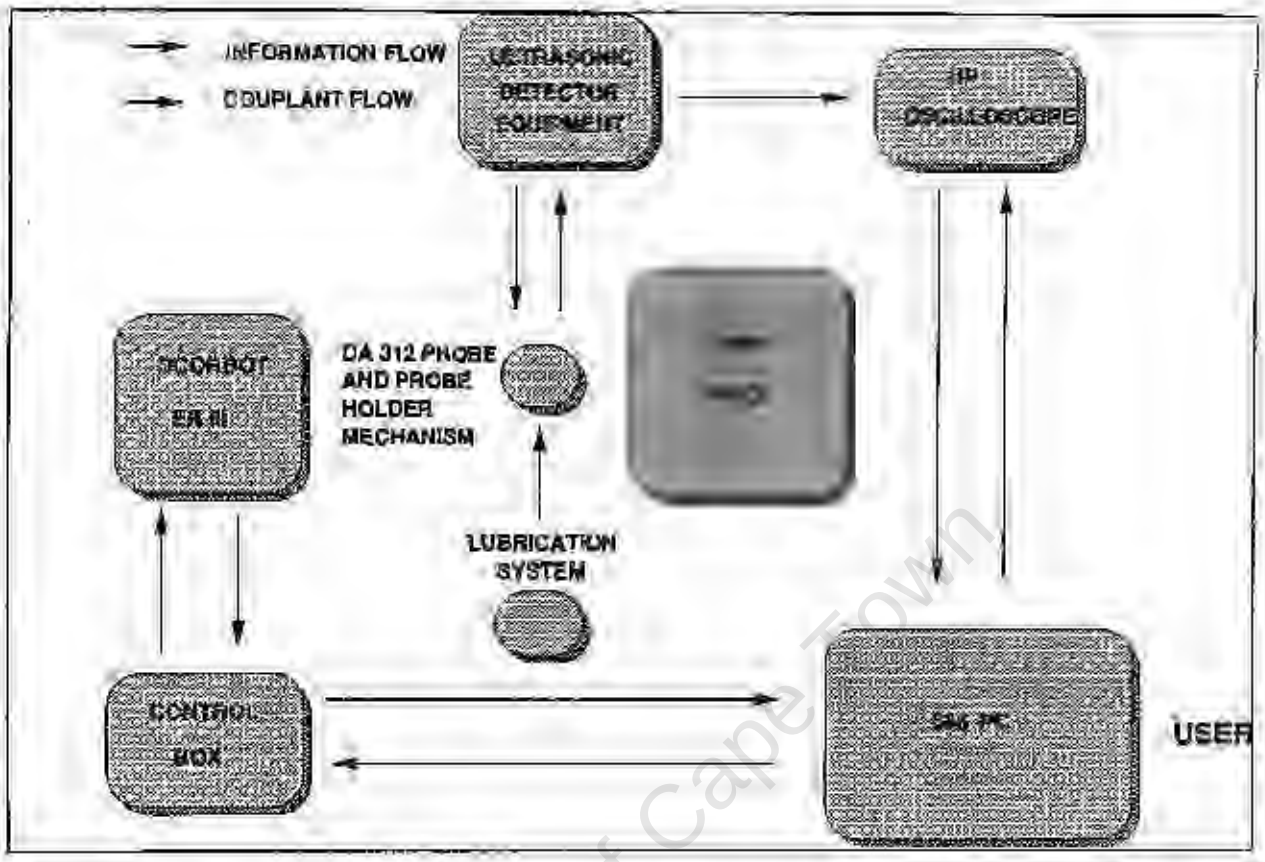

Figure 2.5: Schematic diagram of SCORBOT ERIII model

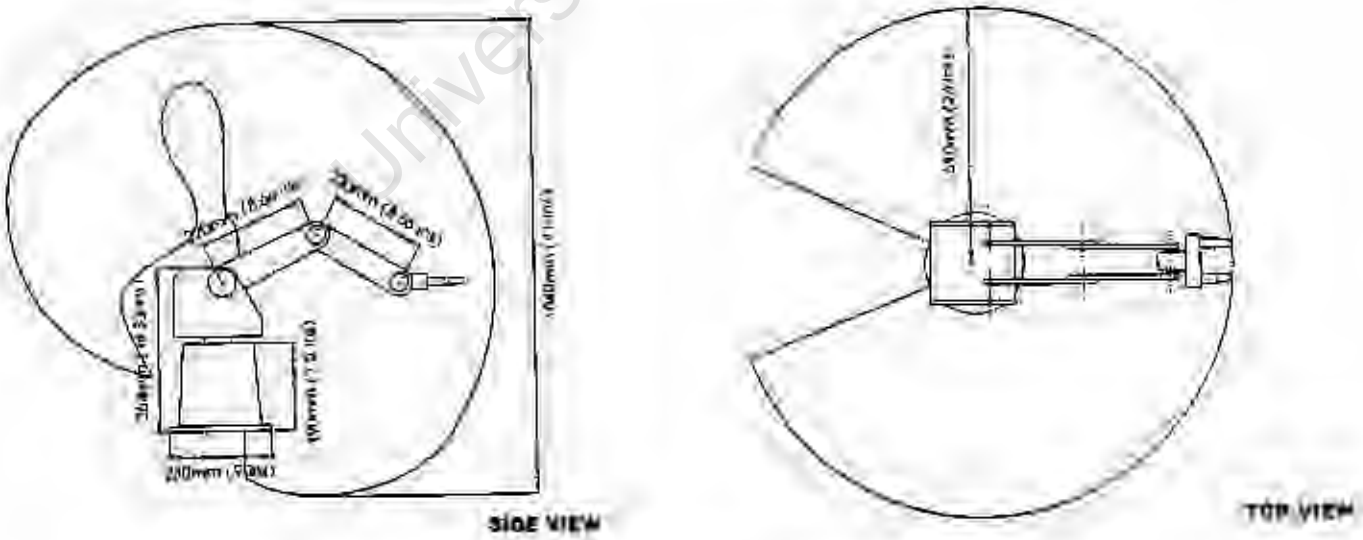

Figure 2.6: Working envelope of SCORBOT ERIII

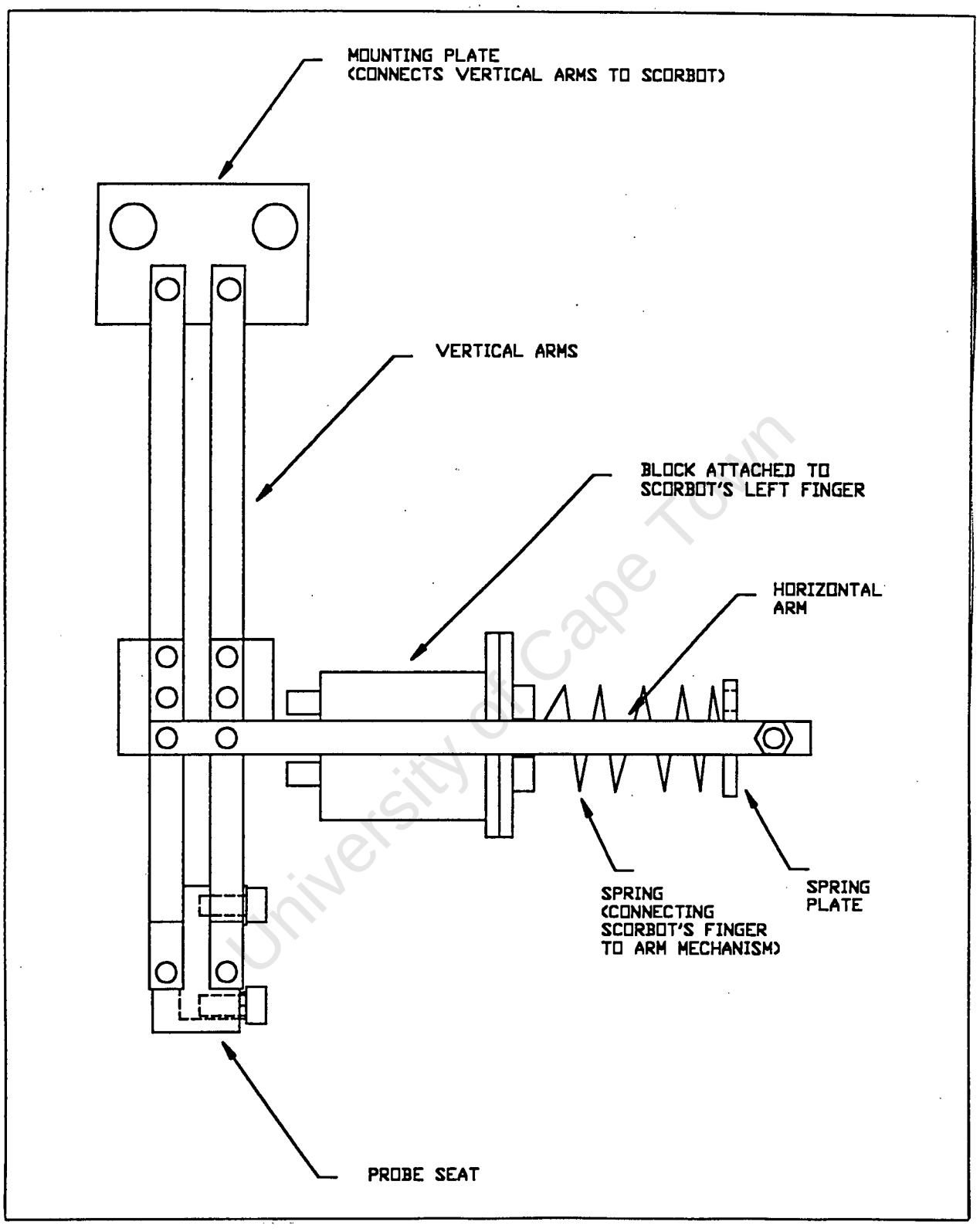

Figure 2.7: Side view of probe holder mechanism

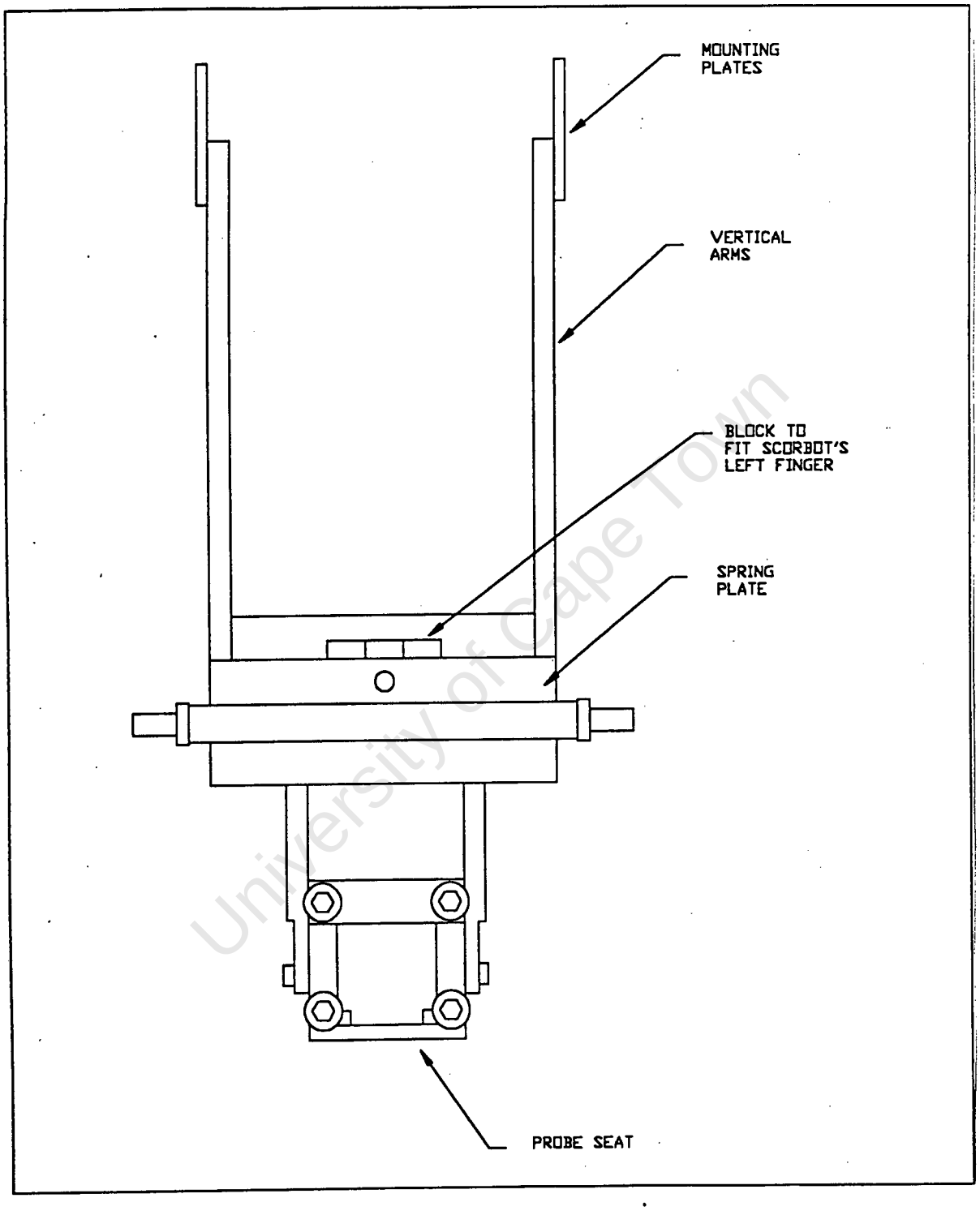

Figure 2.8: Front view of probe holder mechanism

Electronic Controller

The electronic controller was a microprocessor which served as an intelligent interface between the SCORBOT ERIII and the host computer (386 PC). It handled robot operation, memory and logic operations and drivers for the joint's motors.[36]

By serving as an intelligent interface, the main functions of the controller were:

- Translating motor motion commands from the host computer (386 PC) into electrical pulses for the joint motors.
- Follow-up of information received from the motor's encoders, thus ensuring a semi-closed loop control of the motion.
- Acting as interface between the host computer and the robot for
  - (i) Four output relays
  - (ii) Eight input switches
  - (iii) Micro-switches located on the robot body

The 386 PC commands sent to the robot controller were all a continuous serial transmission of ASCII codes. Most responses transmitted back by the controller were the same ASCII format, with the exception of commands requiring high speed data transmission, which were in binary.

The controller was hardwired to SCORBOT ERIII with a dedicated cable. The 386 PC communicated with the controller using its second serial port. Two 25-pin RS232C connectors and a three core wire was used as a cable.

A full wireup diagram of the controller/386 PC interface can be found in appendix C.1.

DA312 probe

A DA 312 dual element Krautkramer probe was chosen for the ultrasonic inspection of the welds. It consisted of two piezoelectric elements, located parallel to each other in a common housing, separated by an acoustic barrier.

The two elements were shaped so as to provide a focused beam, the focal depth in steel being 3 ± 1 mm. At the point of focus, the detection resolution of the probe is at a maximum. As the distance along the main acoustical axis (ie: perpendicular to the face of the probe) is increased or decreased, this resolution decreases. Figure 2.9 shows the characteristic curve of the DA 312 probe, giving the size of discontinuity that may be detected versus the depth of the sound path (data for steel inspection material).

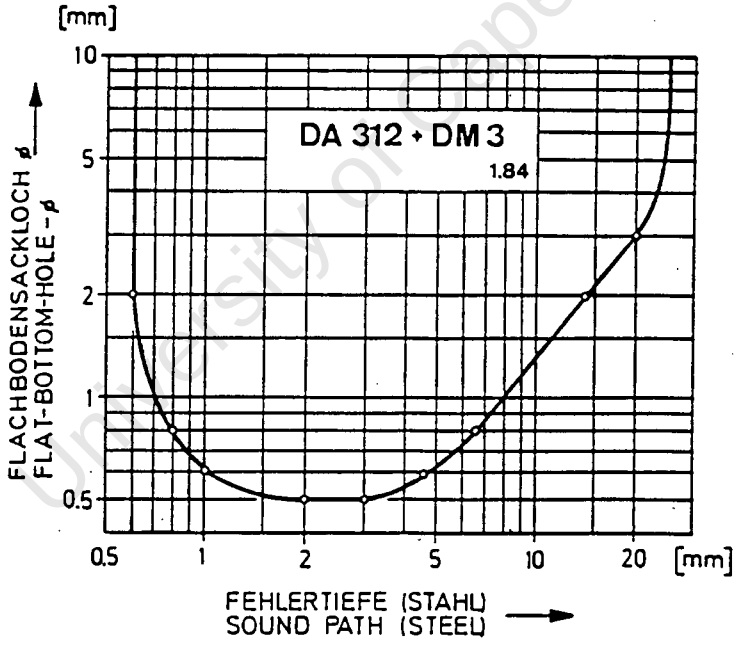

Fig 2.9: Sensitivity curve for the DA 312 probe

The reasons for selecting the DA312 probe were the search unit's small size, good close-range resolution, small probe face and high operational frequency.

One of the disadvantages of the DA312 probe was that it was designed for the inspection of flat surfaces. The transducer crystals were shaped to suit a flat probe/inspection material interface. Thus, when inspecting a tube wall with significant curvature (ie: diameter less than 100 mm), the gap formed between the probe face and the tube wall led to poor acoustic contact and a distortion of the transmitted and received signals.

Another disadvantage was the fact that the probe required a coupling fluid to be applied between the probe face and the inspection surface to improve the acoustic contact. The application of this fluid was to prove difficult under automated operating conditions.

Thus, to overcome these disadvantages, an acoustic lens and coupling fluid system were added to the DA312 probe. These are shown in figures 2.10 and 2.11 respectively. Further design information can be obtained in appendix D.2.

USM2 flaw detector

The USM2 acted as a filter and a primary display unit for the returned signals from the DA312 probe. The USM2 was modified to allow the filtered signal to be displayed on a Hewlett Packard 54600 digital oscilloscope. This was done by installing a cable from the amplifying circuit of the detector to a connecting pin, which was mounted on the back of the instrument. A standard oscilloscope cable then was used to link the oscilloscope and the detector. A complete wire-up diagram of the modifications can be found in appendix C.2.

Test rig

A test rig, consisting of 47 plastic tube ends inserted in wooden board was used to simulate a heat exchanger endplate. The rig was located relative to the robots base using a number of clamps. The rig is shown in figure 2.12.

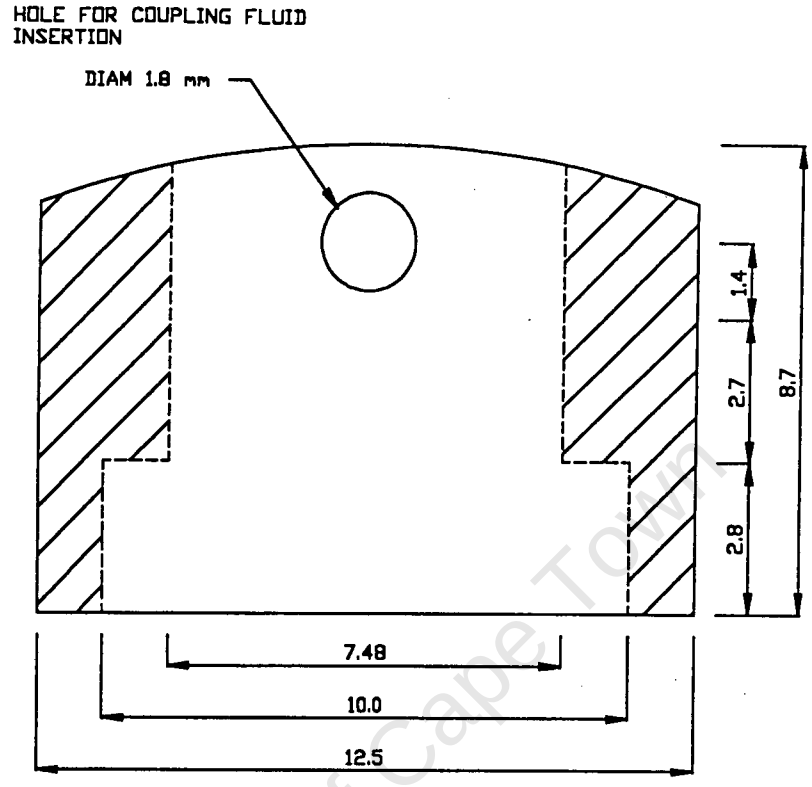

NOTES	REMARKS
1	MATERIAL: PERSPEX
2	RAD. OF CURVE: 18.3 mm
3	TIGHT FIT BETWEEN LENS AND TRANSDUCER

Figure 2.10: **Side view of acoustic lens**

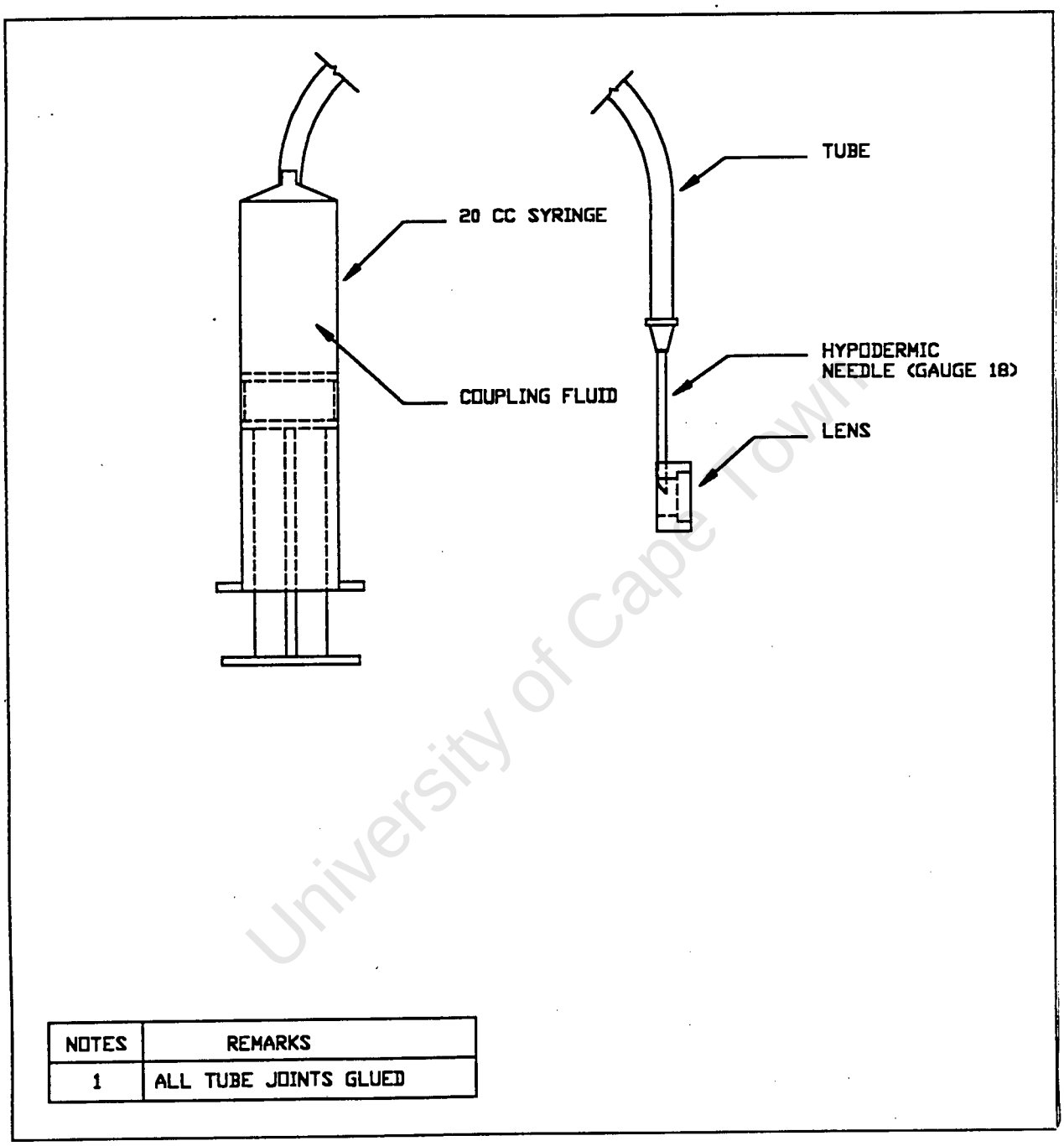

NOTES	REMARKS
1	ALL TUBE JOINTS GLUED

Figure 2.11: **Schematic of the lubrication system**

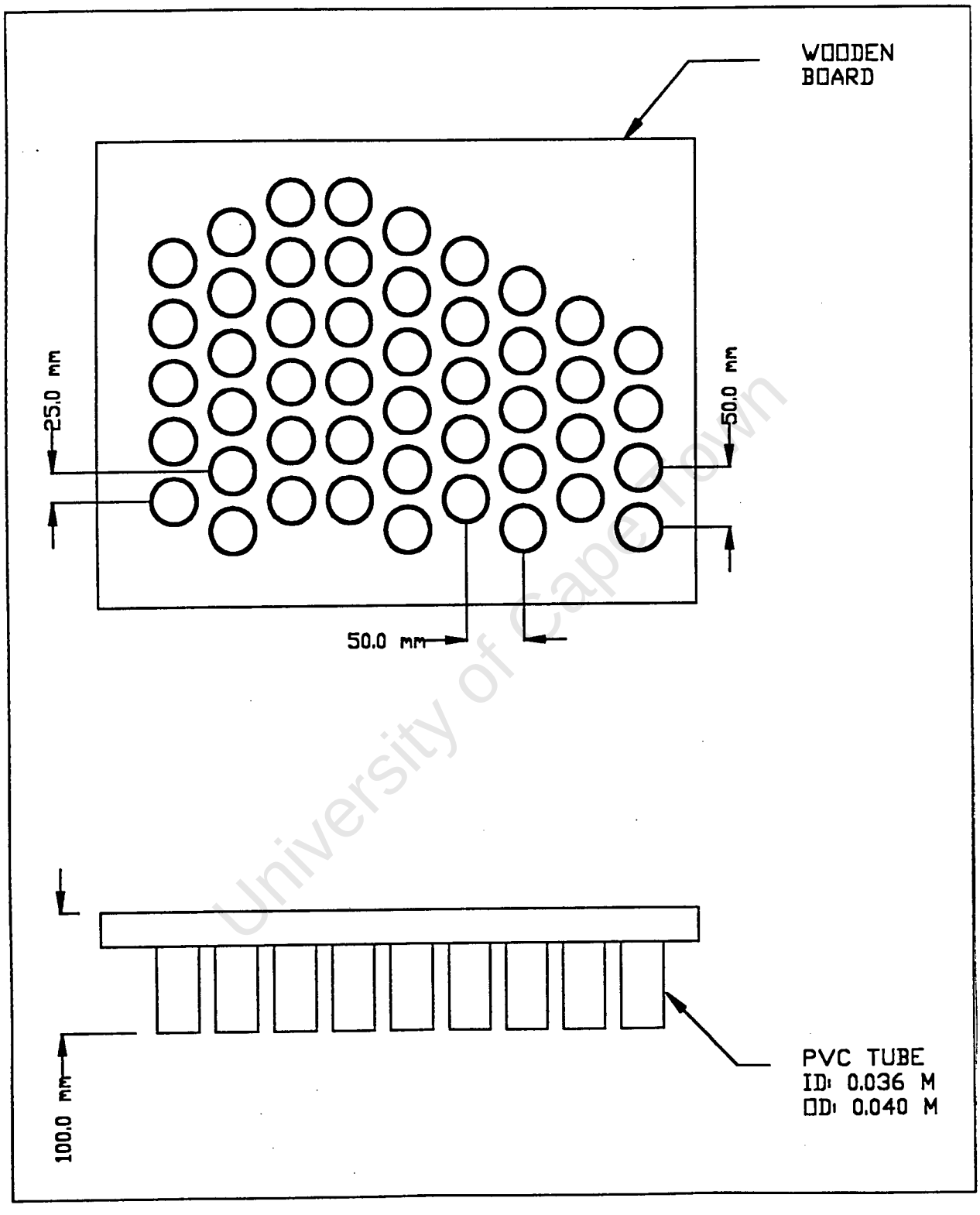

Figure 2.12: Test rig (plan view)

Software for SCORBOT model

The entire inspection system was controlled by dedicated software for the 386 PC. The software was written in the programming language Turbo C++, versions 1.0 and 3.0. Turbo C++ is an object-orientated compiler language. It has a built-in assembler and supports both AT&T C++ and ANSI C applications.

The software developed for the SCORBOT model was programmed to perform five main functions:

[1] Read in heat exchanger configurations
[2] Control the position of SCORBOT prior to the inspection
[3] Collect data from the oscilloscope
[4] Perform the scanning sequence for inspecting the heat exchanger
[5] Analysis of the flaw data collected from the oscilloscope

Heat exchanger configurations could either be entered manually using a standard template or imported from files saved on disc. The entered heat exchanger configuration could then be graphically previewed. Furthermore, the coordinates of the tubes of the heat exchanger could be displayed.

Before a scan was started, the serial ports for the SCORBOT / 386 PC and oscilloscope / 386 PC interfaces were chosen. Also, the oscilloscope display and data capturing settings could be changed through the 386 PC software.

SCORBOT would then be brought into a reference position using the *hardhome* option. Before using this option, SCORBOT was moved manually to a place close to this reference position to avoid any collisions during the routine.

Once in the reference position, the automated scan was initiated. During the scan, the

software displayed information such as the tube being inspected, the location of any flaws detected, and the co-ordinates of each joint of SCORBOT.

After each scan was complete, the software displayed graphic representations of the flaw images captured from the oscilloscope during the scan. The tube number, as well as the exact angular location of the flaw, were also displayed.

Further information on the main software routines can be found in Appendix E.1.

2.3.2. Programmable CNC MODEL

Overall system configuration

The model setup using the programmable CNC is shown in figure 2.13. The heat exchanger test rig was fastened to the bed of the CNC. The probe holder mechanism was mounted on a wrist assembly which, in turn, was inserted in the CNC's 16mm collet.

Probe manipulation from tube opening to tube opening was achieved by moving the CNC's bed relative to the spindle. The probe holder was inserted into the tube openings by hydraulically lowering the CNC's spindle. Movement of the probe towards the tube wall and then around the circumference was achieved using two separate electric motors mounted on the wrist assembly.

The system was controlled by software running on the 386 PC. The co-ordinates for controlling the CNC's movements were downloaded at the beginning of a scan via an XT PC acting as and interface, into the CNC's internal memory. The manual controls of the CNC were electronically linked to the 386 PC's parallel port so that the software could detect any user interaction with the CNC.

The signal sent to and received from the DA 312 ultrasonic probe were again controlled by the USM2 flaw detector. The USM2's signal was displayed on the HP 54600 oscilloscope,

which interfaced directly with the 386 PC via its second serial port.

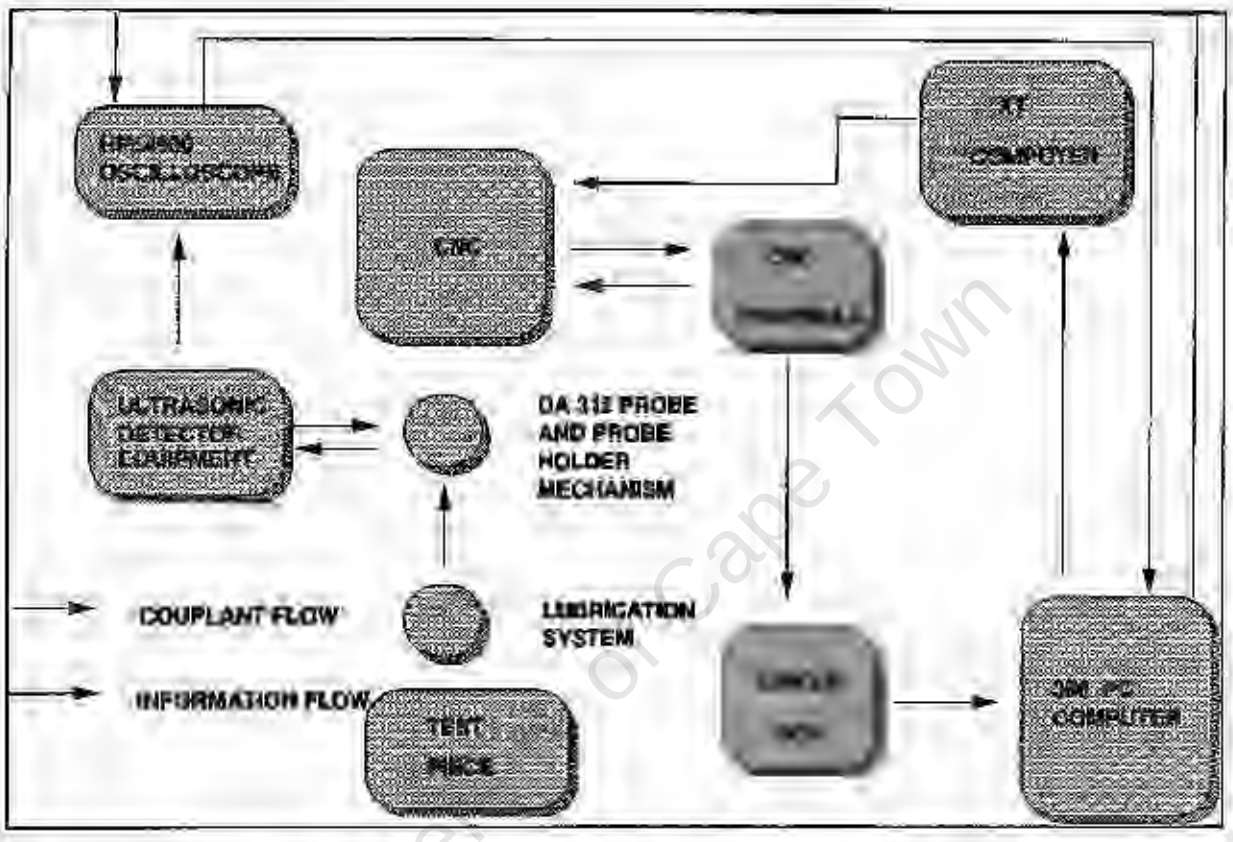

Figure 2.13: Overall system configuration of programmable CNC scanning model.

<u>Hardware specifications</u>

The existing probe and probeholder mechanism, the lens, the lubrication system, the ultrasonic flaw detector, and the test rig remained unchanged from the SCORBOT scanning model.

Thus, the only modifications to the hardware were:

- The CNC and XT interface computer
- The wrist mechanism
- The electronic controlling circuits

XT interface computer

The function of the XT PC was to act as an interface to CNC. The CNC received instructions concerning co-ordinates to move to, travelling speeds and tool change positions in a standard text file format. This file had to be downloaded into the CNC's memory before a scan.

For certain software complications, this text file could not be downloaded from the 386 PC to the CNC. Thus, the solution was to run a CNC interface program on the XT. The data was generated by the software on the 386 PC, transferred to the XT by floppy disc, and then sent to the CNC.

By running the interface software on a separate computer, other pre-scan tasks could take place on the 386 PC whilst the co-ordinate data was downloaded.

The CNC wrist mechanism

A mechanism was needed to, firstly, move the probeholder against the tube wall once inside a tube, and, secondly, to rotate the probeholder around the inner circumference of the tube. These movements had been provided by SCORBOT's finger and wrist joints respectively in the previous model.

An initial idea was to use the rotation of the CNC's spindle (normally used for milling) to move the probeholder around the inner circumference of the tube. However, the slowest spindle speed obtainable by the CNC was 50 rpm. This would have only allowed 27 msec for each sample of the HP54600 oscilloscope during a scan (considerably less time than required).

An alternative would have been to mount a gearbox on the end of the stub shaft, located in the CNC's Collet, to reduce the rotational speed. However, locating the gearbox housing to

the CNC's body to prevent it from spinning would have been difficult. Furthermore, there was no angular positional feedback on the CNC's spindle (thus, the probeholder on tube's circumference was indeterminable).

Thus, it was decided to construct a wrist mechanism to provide the probe's radial and circular motion independently. The mechanism was to be mounted onto a stub axial in the CNC's collet, whilst the CNC's spindle was held stationary.

To provide the radial motion to move the probeholder from the centre to the inner circumference of each tube, three design possibilities were considered. The first was to use a pneumatic cylinder, mounted above the probeholder mechanism. The disadvantage was that this required an air supply, which would not be available on the final scanner design. The second option was to use an electrical solenoid. Whilst this meant simple electronic control, it had the disadvantages that the travel of most solenoids was short, and that the impulse force of the probe hitting the tube wall would cause depolarisation of the ultrasonic transducer crystals.

The third option was to use a small electronic motor to pull the probeholder up against the wall. This options was selected and a 5V DC motor radio-controlled aircraft industry was chosen for its compact size, ease of control (forward/reverse/off) and its slow rotational speed (10rpm).

A SLO SYN M091 stepper motor was selected for the rotational motion of the probe holder. The stepper motor was capable of precise, finite increments of angular motion and could easily be controlled, via a motion translator, by the parallel port of the 386 PC.

The final design of the wrist mechanism is shown in figure 2.14.

The one aspect hampering the design was that the stepper motor only had support holes on the same surface as the drive shaft. Thus, a framework had to be built to provide rigid

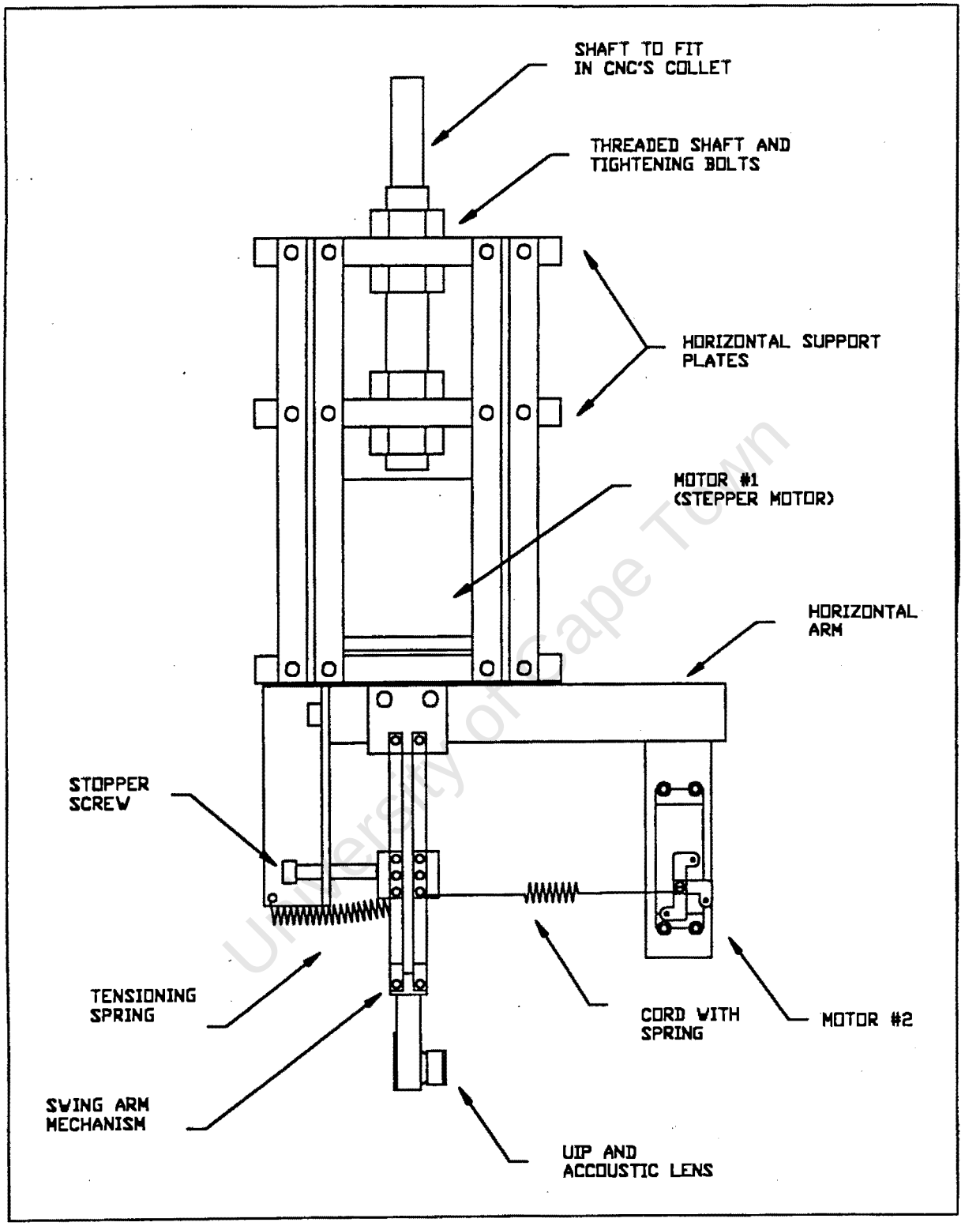

Figure 2.14: **Final wrist mechanism design**

support from the CNC's body, through the stub shaft, to the bottom face of the motor.

The inertial mass rotated by the stepper motor was greatly reduced from the previous design. Furthermore, the horizontal support arm attached to the stepper motor had three 25 mm diameter holes drilled out of it to further reduce the inertial mass.

The small electric motor had a section of nylon wire attached to its output shaft. This was, in turn, attached to a spring which was located at one end to the probe holder's vertical arm. The motor wound up the nylon on its output shaft to bring the probe up against the tube wall and unwound it again to return it to the centre of the tube. There was a second spring attached to the probeholder, to ensure that the probeholder returned to locating bolts before leaving a tube.

Electronic control circuits

The CNC had a number of manual controls operated by push buttons. As there was no software link between the 386 PC and the CNC, a system had to be made where the CNC and 386 PC could be interlocked, thus providing synchronisation between the two machines (CNC and 386 PC).

The two buttons of interest on the CNC were the *edit* and the *hold* buttons. The *edit* button signalled to the CNC to begin its programmed motion whilst the *hold* button acted as an emergency stop button during motion.

An initial idea was to short circuit both push buttons on the CNC control board and have relays, activated by the 386 PC's software, to open and close the circuits. However, the CNC controls were driven by MOSFET transistors which are very sensitive to static, making it impossible to modify the control board.

The solution was to mount small pressure-sensitive pads ontop of each of the push buttons on the control panel. These, in turn were connected to a circuit board. Thus, if the user pressed

movement and the other driving the extension/contraction of the arm. All four arms were pivoting linked to a central platform which carried the probe insertion mechanism. Thus, the one arm was able to direct the central platform whilst the other three were just pulled along - their function being to give Z axis stability.

The reasons for not accepting this design was because of the following:

[1] *The rigidity of arms required to span the heat exchanger.*

It was estimated that the central platform would weigh about 10 kg (includes a stepper motor) and that the allowable z-axis deflection was approximately 1,5mm. Even with a counter-balance mechanism that could adjust to the length of arm extended, it was questioned whether such rigidity would be achieved.

(2) *Lack of operating space.*

In whatever position the central platform was in, one or more of the arms would be contracted at least half its length. This could cause problems if the heat exchanger was rested with the open tubesheet on the ground as the arms would be unable to contract. This might be overcome by having the arms arranged in a fashion as shown, but will result in a loss of Z directional stability.

An alternative would be to have one or two of the arms to consist of a telescopic design but this would further complicate the design and reduce the overall rigidity.

The third design is shown in figure 2.3(a) and (b). The frame design was an adaptation of Laborelec's poler manipulator[32]. It consisted of two main parts - a vertical mast and a horizontal arm that spanned the radius of the tube sheet. The mast was supported by cable ties that were tightened bo the outer edge of the tubesheet and lifted above the arm's operating plain by pole pulleys. The horizontal arm was supported from the mast by two rods as well as a central

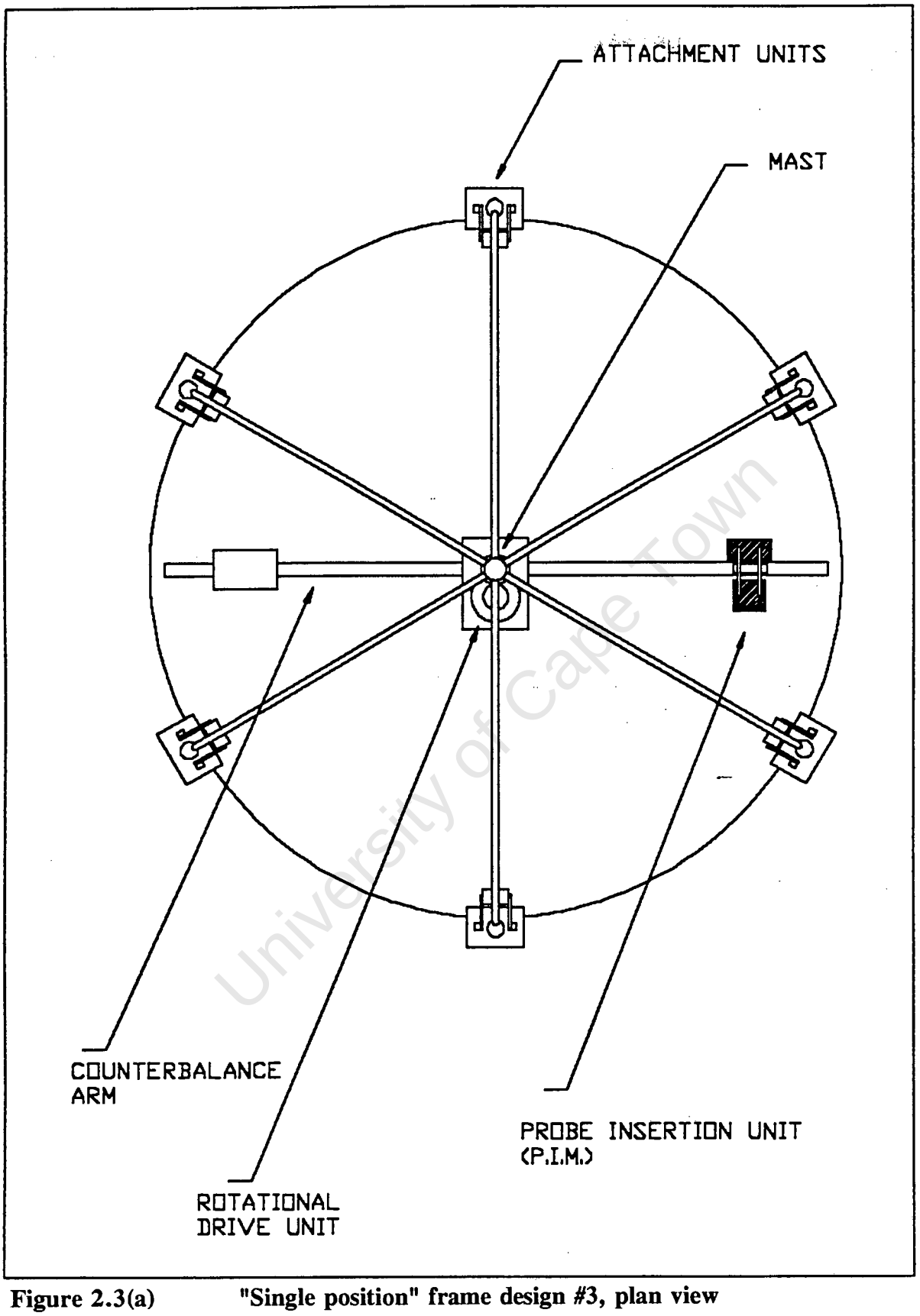

Figure 2.3(a) **"Single position" frame design #3, plan view**

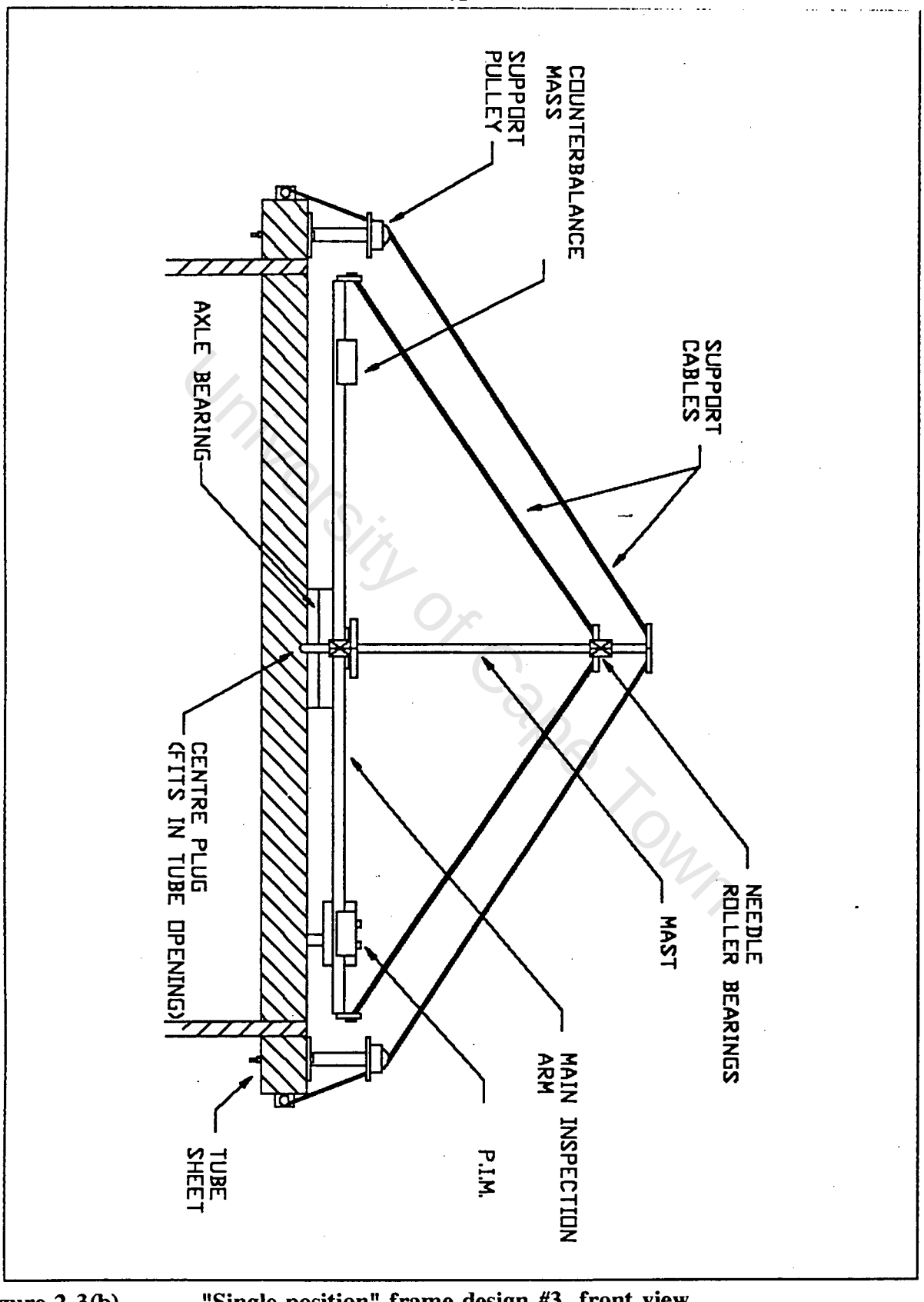

Figure 2.3(b) **"Single position" frame design #3, front view**

platform located on the mast beneath the arm.

The arm was rotated by a stepper motor mounted on a the central platform (off the arm for inertial reasons). The probe insertion mechanism (PIM) was driven along the horizontal arm by stepper motor # 2. Stepper motor # 2 was mounted on the horizontal arm near the mast and drove a lead screw (the nut remaining stationary on the PIM) - this was preferable to the motor being mounted on the PIM. A counter-balance mechanism on the other half of the arm was possible - its position could be controlled by a simple pulley mechanism connected to the PIM.

Although a lot of design work went into this concept, it was rejected for the following reasons:

(1) *Poor lateral positioning.*

If the tube sheet was at a 90 degree angle to the ground, the mast would experience a turning moment of approximately 60 Nm. A deviation in position of 1 mm by the top of the mast can be expected under such torque loading. However, this would lead to the outer reach of the horizontal arm being 3 mm closer to the tubesheet than predicted - an unacceptable error.

(2) *High set up time.*

The mast and support pulley system would require approximately 2 man-hours to set up and dismantle.

(3) *Not all holes scanned.*

With the central platform being necessary, not all of the tubes would be inspected. The remaining holes could be manually inspected after the equipment has been removed but the uniformity in inspection method would suffer.

(2) Multiple position frame designs

A number of shapes of multiple position frames were tested conceptually. Some of the more realistic ones are shown in figure 2.4. Note the extension of the arm beyond the frame - a concept which allows the tubes on the outer edge of the tubesheet to be inspected.

It was assumed that the multiple position frame would not be attached at all to the edge of the heat exchanger but would be located using a number of tube ends as vantage points. Mechanisms considered for locating the frame included magnets, rubber suction cups and tube expanders. Magnets were ruled out because of the non-ferrous nature of the heat exchanger (Nickel). Rubber suction cups were eliminated because of the lack of rigidity provided by the rubber connection. Thus, a mechanism which would expand inside the tube when activated, thus locking into the tube, was chosen.

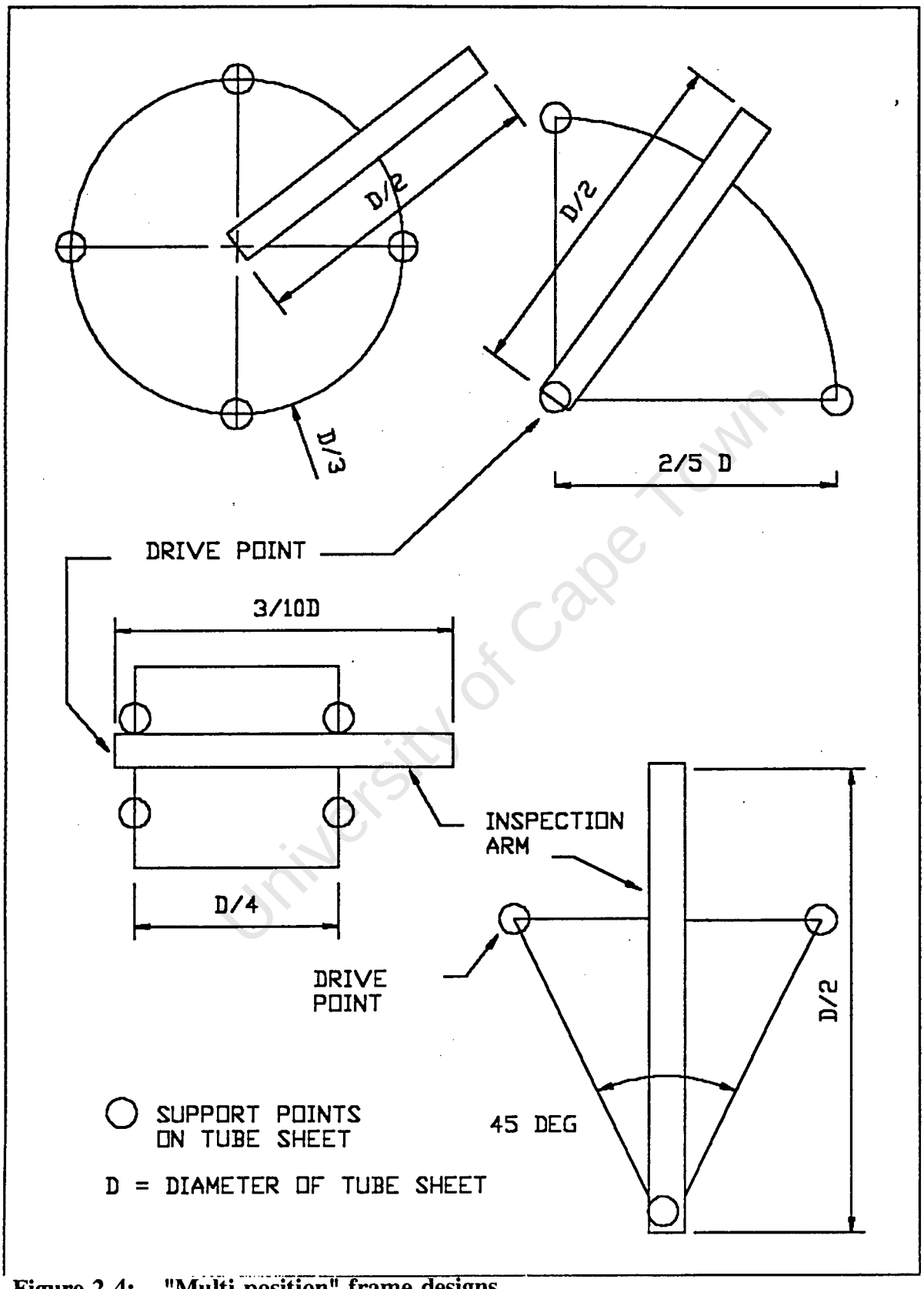

Figure 2.4: "Multi-position" frame designs

2.3 FRAME AND PROBE INSERTION MECHANISM (PIM) DESIGN: MODELS

Further design work was necessary to complete the frame and PIM design. Although the previous theoretical work had indicated that a multi-position frame was preferable, the ideal frame shape had to be found. Furthermore, the probe manipulation software had to be developed.

Two different frame configurations needed to be considered: namely the "rotational arm" frame and the "cartesian plane" frame configuration. A rotational arm frame would typically have five degrees of freedom, consisting of four revolute joints and one prismatic joint. A vertically articulated mechanical arm and gripper would be an example. A cartesian plane frame would provide linear motion in the XY plan and a combination of linear and rotational motion about the Z axis. A common example of this would be a CNC cutting machine.

Thus, two working models were set up to investigate each of the possible frame configurations. The first model used a SCORBOT ERIII robot as the probe manipulator, whereas a programmable CNC was used for the second model. A Probe Insertion Mechanism (PIM) was developed for the SCORBOT ERIII model and later modified for the second model. Furthermore, probe manipulation software was developed to be compatible with both models.

2.3.1 SCORBOT ERIII model

Overall system configuration

The resultant system that was used as a scanning model is shown in figure 2.5. It consisted of the SCORBOT ERIII robot and control box (probe manipulation), a 386PC (controlling software), a DA312 ultrasonic probe (for inspection), a USM2 ultrasonic detector and a HP 54600 oscilloscope (for data transfer). Also, a lubrication system and acoustic lens were designed to enable the ultrasonic scanning of the tube surfaces. The SCORBOT and 386PC communicated bi-directionally via the electronic controller. Likewise, the HP 54600 and 386PC communicated bi-directionally, with the returned ultrasonic signal being transferred

from the detector to the 386PC via the oscilloscope.

Scans done using the DA312 probe were done on a test rig. The probe was moved from tube opening to tube opening by the end-manipulator of the SCORBOT ERIII (modified for movement of probe inside tubes). The information from the DA312 probe was filtered using the USM2 detector and displayed on the HP 54600 oscilloscope. The 386PC controlled the movements of the SCORBOT ERIII and analysed the information coming back from the DA312 probe. Results were displayed during and after the scan on the 386PC.

SCORBOT ERIII robot

The SCORBOT ERIII was an instructional robot with five degrees of freedom. It consisted of a vertically articulated mechanical arm and gripper mounted on a base. The base, shoulder, elbow and wrist were revolute joints whereas the grippers a prismatic joint type performing a linear opening and closing motion.

The working envelope of SCORBOT ERIII is shown in figure 2.6. As shown, SCORBOT has essentially a spherical operating configuration. The arm was driven by sending a sequence of pulses to the relevant joint, resulting in it undergoing a precise angular displacement. Each motor on SCORBOT had a rotary optical encoder, reading directly from the rotor shaft, which enabled the controller to perform closed-loop motion control of the motors.

SCORBOT's end effector (gripper fingers) was modified with the addition of a probe holder mechanism. This mechanism (shown in figures 2.7 and 2.8) held the DA 312 probe, preventing motion of the probe's inspection axis whilst up against the tube wall. Furthermore, it provided the horizontal motion to bring the probe up against the tube wall once the probe had been inserted in the tube opening.

Further information on the specifications of SCORBOT ERIII can be found in appendix A.1.

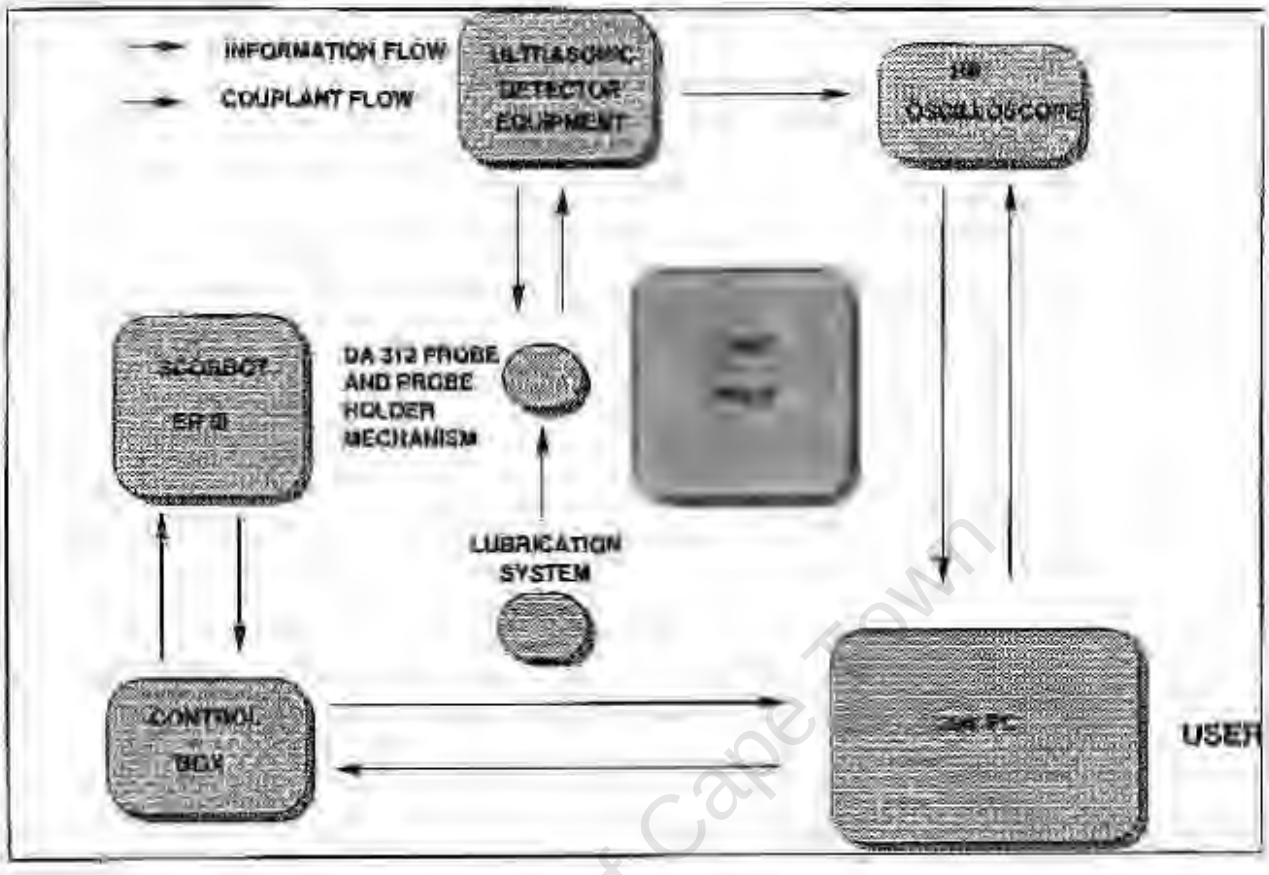

Figure 2.5: Schematic diagram of SCORBOT ERIII model

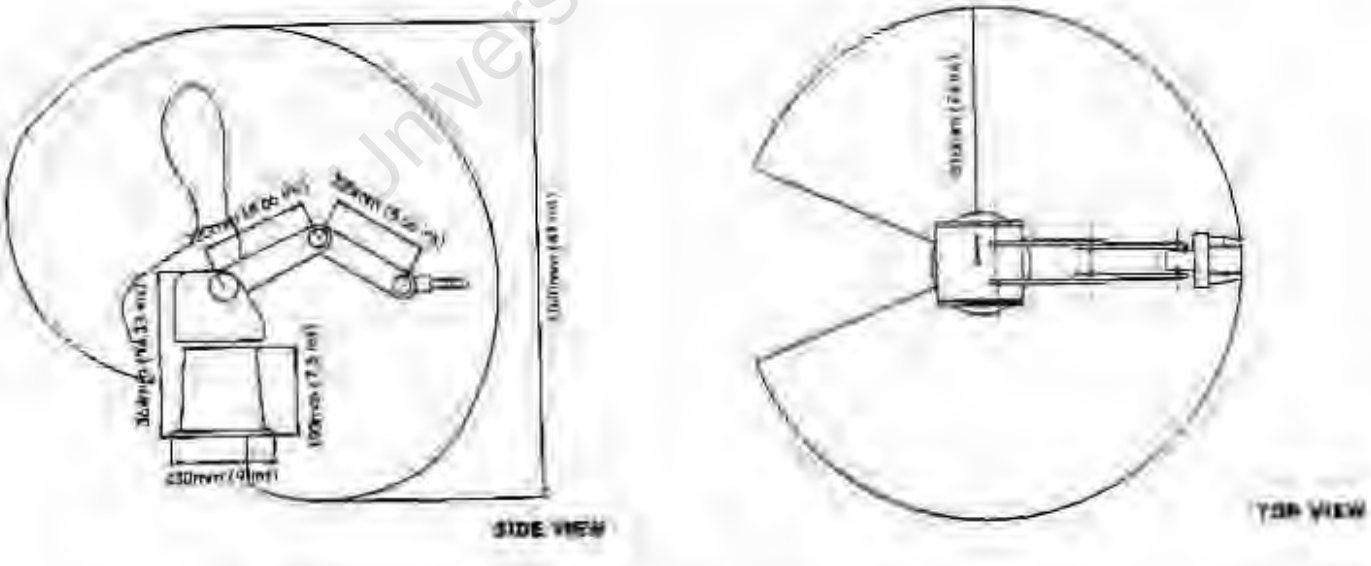

Figure 2.6: Working envelope of SCORBOT ERIII

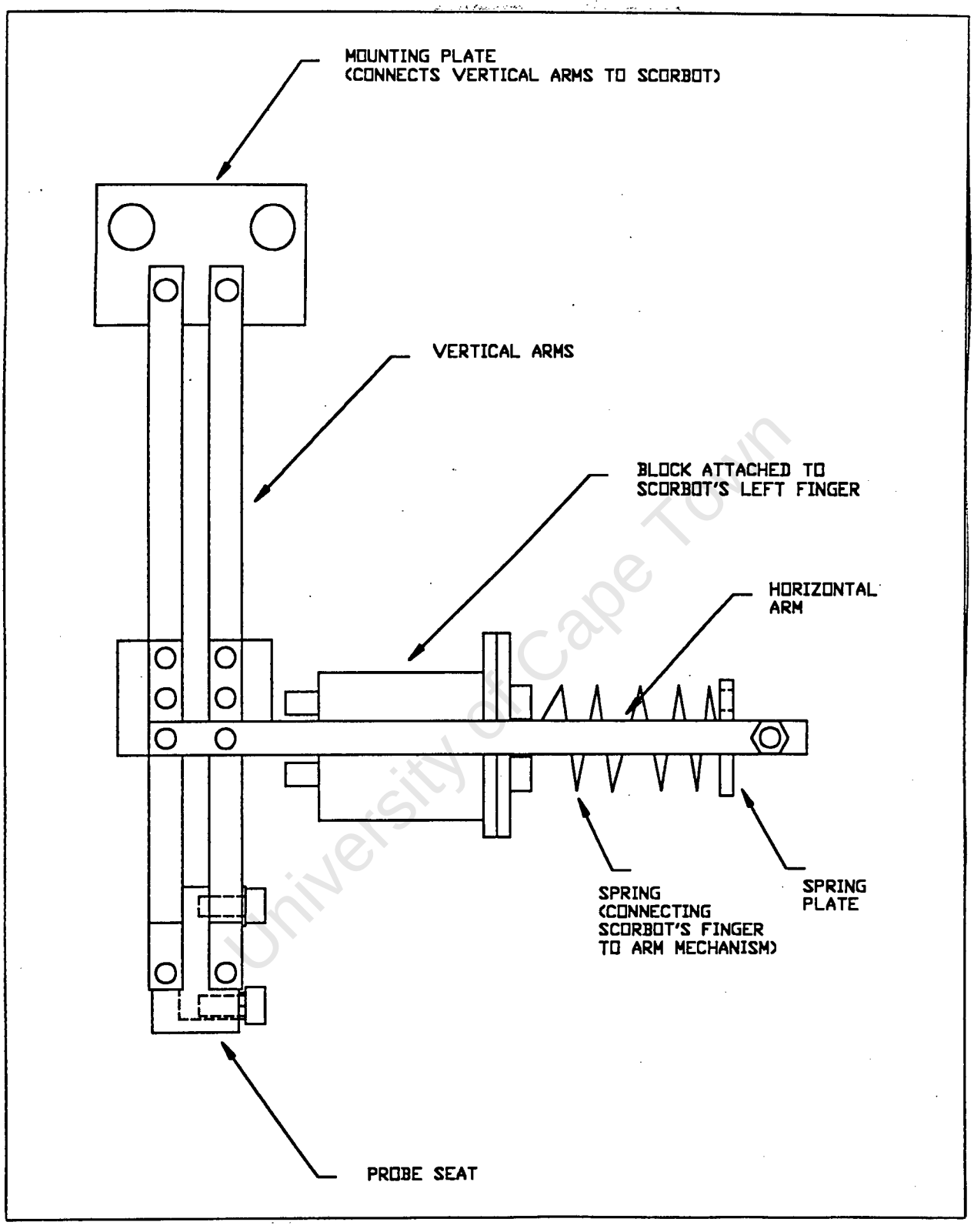

Figure 2.7: Side view of probe holder mechanism

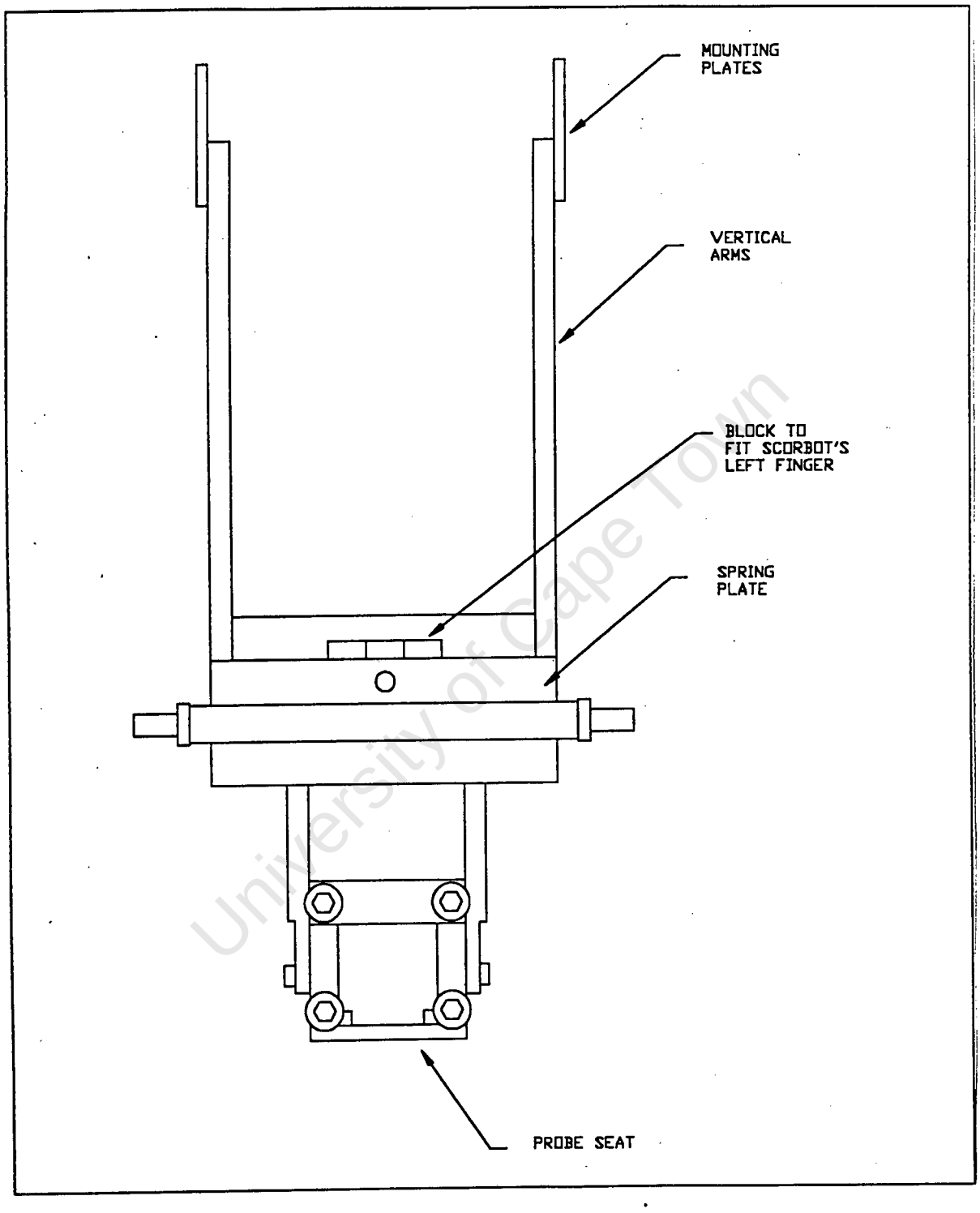

Figure 2.8: Front view of probe holder mechanism

Electronic Controller

The electronic controller was a microprocessor which served as an intelligent interface between the SCORBOT ERIII and the host computer (386 PC). It handled robot operation, memory and logic operations and drivers for the joint's motors.[36]

By serving as an intelligent interface, the main functions of the controller were:

- Translating motor motion commands from the host computer (386 PC) into electrical pulses for the joint motors.
  Follow-up of information received from the motor's encoders, thus ensuring a semi-closed loop control of the motion.
- Acting as interface between the host computer and the robot for
  (i) Four output relays
  (ii) Eight input switches
  (iii) Micro-switches located on the robot body

The 386 PC commands sent to the robot controller were all a continuous serial transmission of ASCII codes. Most responses transmitted back by the controller were the same ASCII format, with the exception of commands requiring high speed data transmission, which were in binary.

The controller was hardwired to SCORBOT ERIII with a dedicated cable. The 386 PC communicated with the controller using its second serial port. Two 25-pin RS232C connectors and a three core wire was used as a cable.

A full wireup diagram of the controller/386 PC interface can be found in appendix C.1.

DA312 probe

A DA 312 dual element Krautkramer probe was chosen for the ultrasonic inspection of the welds. It consisted of two piezoelectric elements, located parallel to each other in a common housing, separated by an acoustic barrier.

The two elements were shaped so as to provide a focused beam, the focal depth in steel being 3 ± 1 mm. At the point of focus, the detection resolution of the probe is at a maximum. As the distance along the main acoustical axis (ie: perpendicular to the face of the probe) is increased or decreased, this resolution decreases. Figure 2.9 shows the characteristic curve of the DA 312 probe, giving the size of discontinuity that may be detected versus the depth of the sound path (data for steel inspection material).

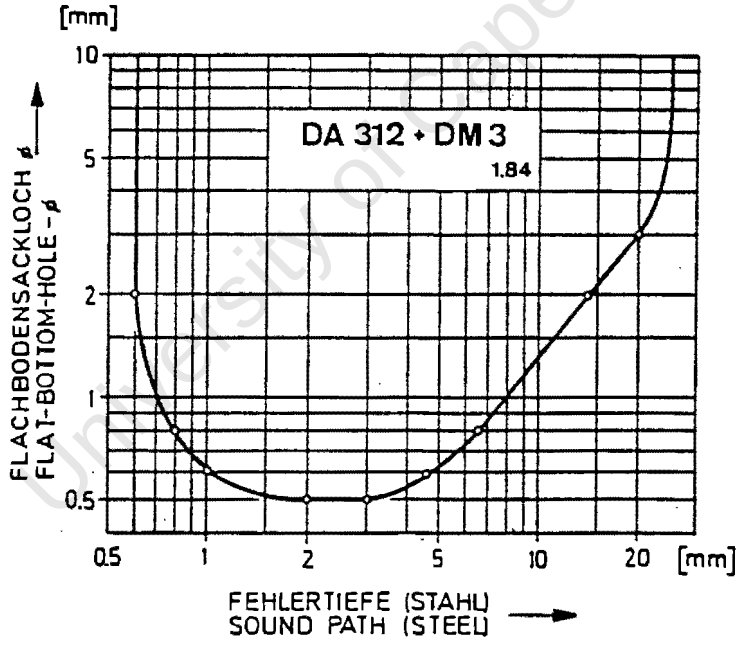

Fig 2.9: Sensitivity curve for the DA 312 probe

The reasons for selecting the DA312 probe were the search unit's small size, good close-range resolution, small probe face and high operational frequency.

One of the disadvantages of the DA312 probe was that it was designed for the inspection of flat surfaces. The transducer crystals were shaped to suit a flat probe/inspection material interface. Thus, when inspecting a tube wall with significant curvature (ie: diameter less than 100 mm), the gap formed between the probe face and the tube wall led to poor acoustic contact and a distortion of the transmitted and received signals.

Another disadvantage was the fact that the probe required a coupling fluid to be applied between the probe face and the inspection surface to improve the acoustic contact. The application of this fluid was to prove difficult under automated operating conditions.

Thus, to overcome these disadvantages, an acoustic lens and coupling fluid system were added to the DA312 probe. These are shown in figures 2.10 and 2.11 respectively. Further design information can be obtained in appendix D.2.

USM2 flaw detector

The USM2 acted as a filter and a primary display unit for the returned signals from the DA312 probe. The USM2 was modified to allow the filtered signal to be displayed on a Hewlett Packard 54600 digital oscilloscope. This was done by installing a cable from the amplifying circuit of the detector to a connecting pin, which was mounted on the back of the instrument. A standard oscilloscope cable then was used to link the oscilloscope and the detector. A complete wire-up diagram of the modifications can be found in appendix C.2.

Test rig

A test rig, consisting of 47 plastic tube ends inserted in wooden board was used to simulate a heat exchanger endplate. The rig was located relative to the robots base using a number of clamps. The rig is shown in figure 2.12.

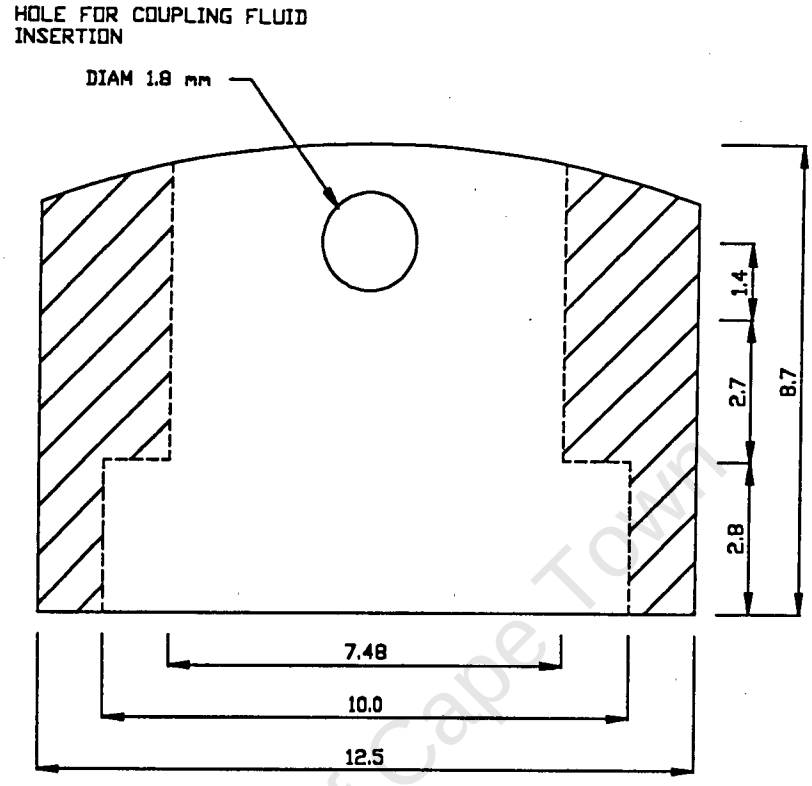

NOTES	REMARKS
1	MATERIAL: PERSPEX
2	RAD. OF CURVE: 18.3 mm
3	TIGHT FIT BETWEEN LENS AND TRANSDUCER

Figure 2.10: **Side view of acoustic lens**

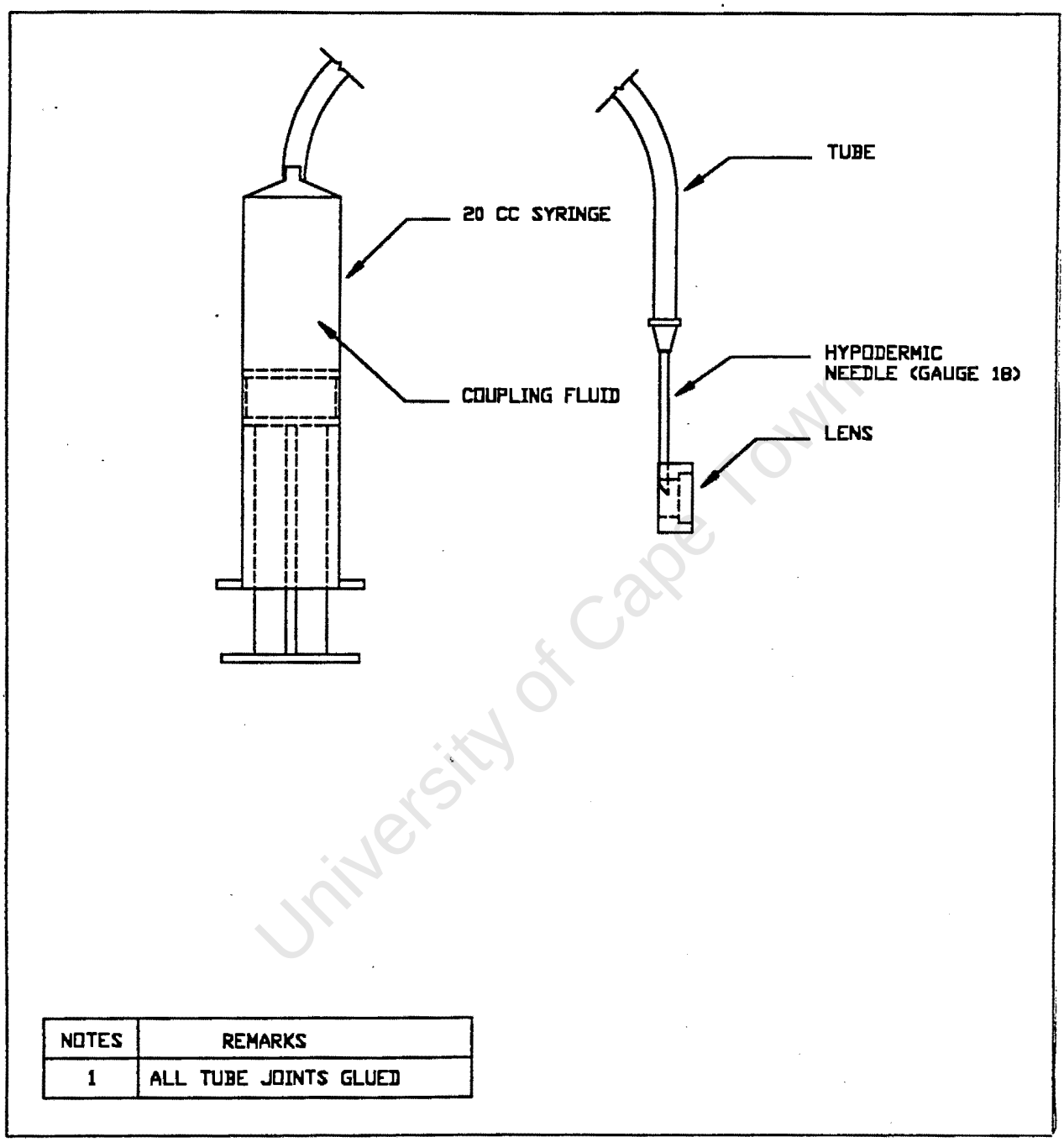

NOTES	REMARKS
1	ALL TUBE JOINTS GLUED

Figure 2.11: **Schematic of the lubrication system**

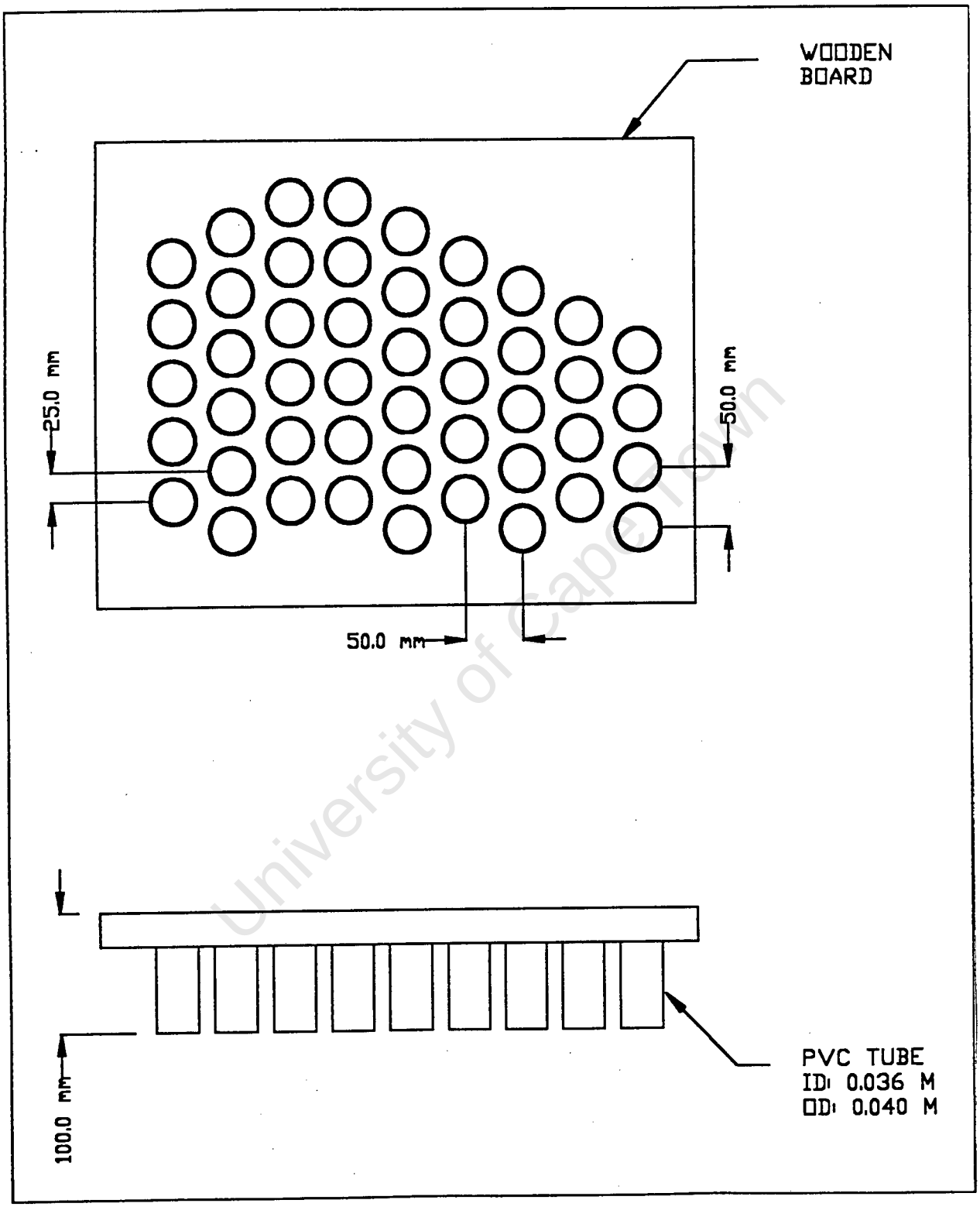

Figure 2.12: Test rig (plan view)

Software for SCORBOT model

The entire inspection system was controlled by dedicated software for the 386 PC. The software was written in the programming language Turbo C++, versions 1.0 and 3.0. Turbo C++ is an object-orientated compiler language. It has a built-in assembler and supports both AT&T C++ and ANSI C applications.

The software developed for the SCORBOT model was programmed to perform five main functions:

[1] Read in heat exchanger configurations
[2] Control the position of SCORBOT prior to the inspection
[3] Collect data from the oscilloscope
[4] Perform the scanning sequence for inspecting the heat exchanger
[5] Analysis of the flaw data collected from the oscilloscope

Heat exchanger configurations could either be entered manually using a standard template or imported from files saved on disc. The entered heat exchanger configuration could then be graphically previewed. Furthermore, the coordinates of the tubes of the heat exchanger could be displayed.

Before a scan was started, the serial ports for the SCORBOT / 386 PC and oscilloscope / 386 PC interfaces were chosen. Also, the oscilloscope display and data capturing settings could be changed through the 386 PC software.

SCORBOT would then be brought into a reference position using the *hardhome* option. Before using this option, SCORBOT was moved manually to a place close to this reference position to avoid any collisions during the routine.

Once in the reference position, the automated scan was initiated. During the scan, the

software displayed information such as the tube being inspected, the location of any flaws detected, and the co-ordinates of each joint of SCORBOT.

After each scan was complete, the software displayed graphic representations of the flaw images captured from the oscilloscope during the scan. The tube number, as well as the exact angular location of the flaw, were also displayed.

Further information on the main software routines can be found in Appendix E.1.

2.3.2. Programmable CNC MODEL

Overall system configuration

The model setup using the programmable CNC is shown in figure 2.13. The heat exchanger test rig was fastened to the bed of the CNC. The probe holder mechanism was mounted on a wrist assembly which, in turn, was inserted in the CNC's 16mm collet.

Probe manipulation from tube opening to tube opening was achieved by moving the CNC's bed relative to the spindle. The probe holder was inserted into the tube openings by hydraulically lowering the CNC's spindle. Movement of the probe towards the tube wall and then around the circumference was achieved using two separate electric motors mounted on the wrist assembly.

The system was controlled by software running on the 386 PC. The co-ordinates for controlling the CNC's movements were downloaded at the beginning of a scan via an XT PC acting as and interface, into the CNC's internal memory. The manual controls of the CNC were electronically linked to the 386 PC's parallel port so that the software could detect any user interaction with the CNC.

The signal sent to and received from the DA 312 ultrasonic probe were again controlled by the USM2 flaw detector. The USM2's signal was displayed on the HP 54600 oscilloscope,

which interfaced directly with the 386 PC via its second serial port.

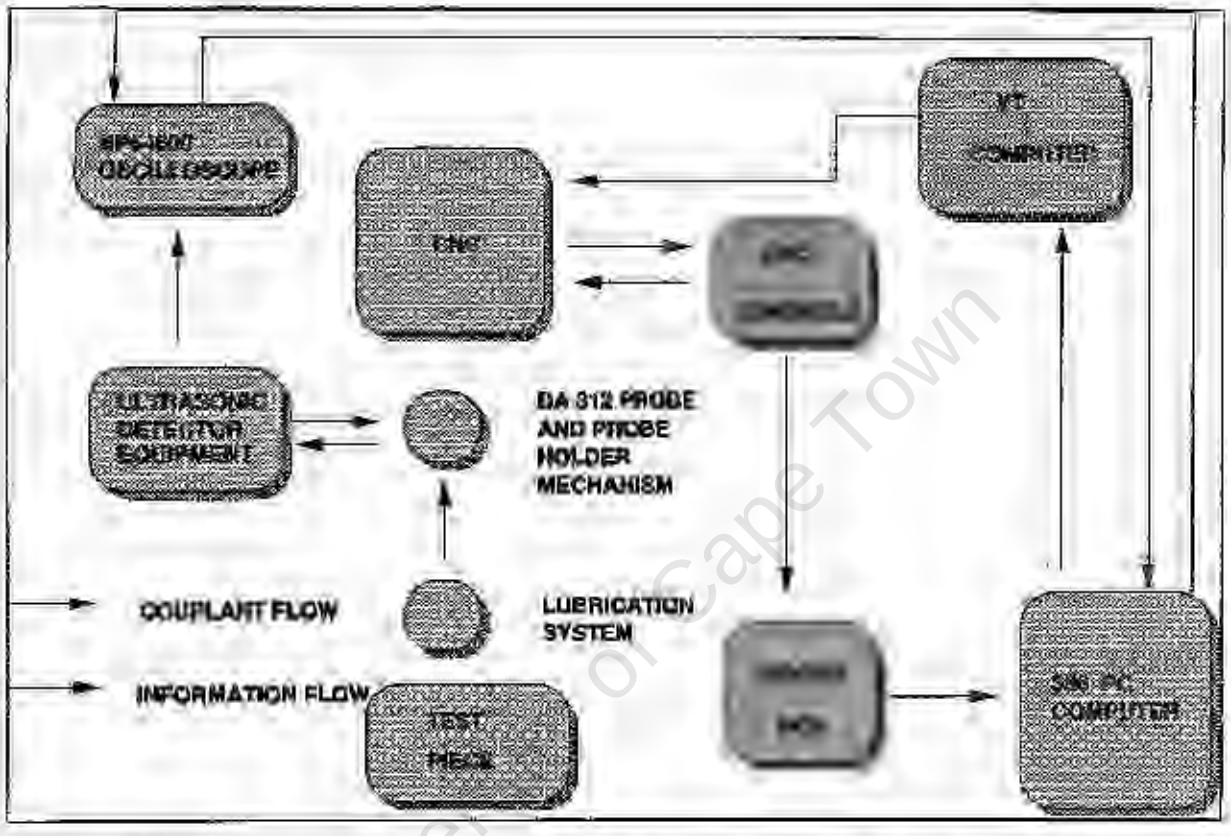

Figure 2.13: Overall system configuration of programmable CNC scanning model.

Hardware specifications

The existing probe and probeholder mechanism, the lens, the lubrication system, the ultrasonic flaw detector, and the test rig remained unchanged from the SCORBOT scanning model.

Thus, the only modifications to the hardware were:

- The CNC and XT interface computer
- The wrist mechanism
- The electronic controlling circuits

XT interface computer

The function of the XT PC was to act as an interface to CNC. The CNC received instructions concerning co-ordinates to move to, travelling speeds and tool change positions in a standard text file format. This file had to be downloaded into the CNC's memory before a scan.

For certain software complications, this text file could not be downloaded from the 386 PC to the CNC. Thus, the solution was to run a CNC interface program on the XT. The data was generated by the software on the 386 PC, transferred to the XT by floppy disc, and then sent to the CNC.

By running the interface software on a separate computer, other pre-scan tasks could take place on the 386 PC whilst the co-ordinate data was downloaded.

The CNC wrist mechanism

A mechanism was needed to, firstly, move the probeholder against the tube wall once inside a tube, and, secondly, to rotate the probeholder around the inner circumference of the tube. These movements had been provided by SCORBOT's finger and wrist joints respectively in the previous model.

An initial idea was to use the rotation of the CNC's spindle (normally used for milling) to move the probeholder around the inner circumference of the tube. However, the slowest spindle speed obtainable by the CNC was 50 rpm. This would have only allowed 27 msec for each sample of the HP54600 oscilloscope during a scan (considerably less time than required).

An alternative would have been to mount a gearbox on the end of the stub shaft, located in the CNC's Collet, to reduce the rotational speed. However, locating the gearbox housing to

the CNC's body to prevent it from spinning would have been difficult. Furthermore, there was no angular positional feedback on the CNC's spindle (thus, the probeholder on tube's circumference was indeterminable).

Thus, it was decided to construct a wrist mechanism to provide the probe's radial and circular motion independently. The mechanism was to be mounted onto a stub axial in the CNC's collet, whilst the CNC's spindle was held stationary.

To provide the radial motion to move the probeholder from the centre to the inner circumference of each tube, three design possibilities were considered. The first was to use a pneumatic cylinder, mounted above the probeholder mechanism. The disadvantage was that this required an air supply, which would not be available on the final scanner design. The second option was to use an electrical solenoid. Whilst this meant simple electronic control, it had the disadvantages that the travel of most solenoids was short, and that the impulse force of the probe hitting the tube wall would cause depolarisation of the ultrasonic transducer crystals.

The third option was to use a small electronic motor to pull the probeholder up against the wall. This options was selected and a 5V DC motor radio-controlled aircraft industry was chosen for its compact size, ease of control (forward/reverse/off) and its slow rotational speed (10rpm).

A SLO SYN M091 stepper motor was selected for the rotational motion of the probe holder. The stepper motor was capable of precise, finite increments of angular motion and could easily be controlled, via a motion translator, by the parallel port of the 386 PC.

The final design of the wrist mechanism is shown in figure 2.14.

The one aspect hampering the design was that the stepper motor only had support holes on the same surface as the drive shaft. Thus, a framework had to be built to provide rigid

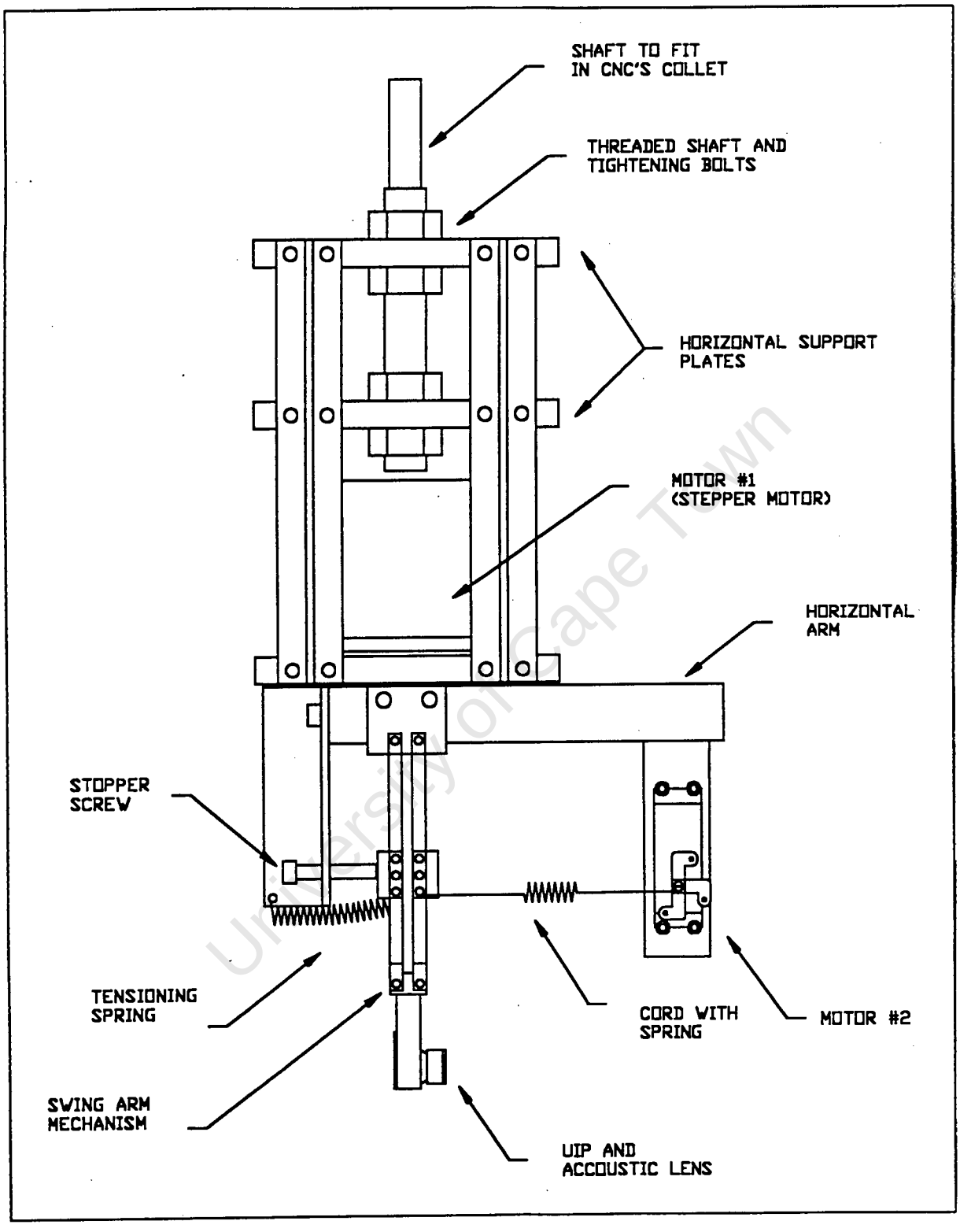

Figure 2.14: **Final wrist mechanism design**

support from the CNC's body, through the stub shaft, to the bottom face of the motor.

The inertial mass rotated by the stepper motor was greatly reduced from the previous design. Furthermore, the horizontal support arm attached to the stepper motor had three 25 mm diameter holes drilled out of it to further reduce the inertial mass.

The small electric motor had a section of nylon wire attached to its output shaft. This was, in turn, attached to a spring which was located at one end to the probe holder's vertical arm. The motor wound up the nylon on its output shaft to bring the probe up against the tube wall and unwound it again to return it to the centre of the tube. There was a second spring attached to the probeholder, to ensure that the probeholder returned to locating bolts before leaving a tube.

Electronic control circuits

The CNC had a number of manual controls operated by push buttons. As there was no software link between the 386 PC and the CNC, a system had to be made where the CNC and 386 PC could be interlocked, thus providing synchronisation between the two machines (CNC and 386 PC).

The two buttons of interest on the CNC were the *edit* and the *hold* buttons. The *edit* button signalled to the CNC to begin its programmed motion whilst the *hold* button acted as an emergency stop button during motion.

An initial idea was to short circuit both push buttons on the CNC control board and have relays, activated by the 386 PC's software, to open and close the circuits. However, the CNC controls were driven by MOSFET transistors which are very sensitive to static, making it impossible to modify the control board.

The solution was to mount small pressure-sensitive pads ontop of each of the push buttons on the control panel. These, in turn were connected to a circuit board. Thus, if the user pressed

the *hold* button on the CNC's panel, a circuit was activated which held a signal 'high' to the input lines of the 386PC parallel port until the software had received the signal. Similarly, when the software on the 386PC was ready to begin a scan, it sent a signal via the output lines or the parallel port which lit up an LED on the board. Once the user had pressed the edit button, the signal was sent to the 386 PC to acknowledge that the CNC had begun its motion.

Thus, a circuit board was built to provide the following functions:

- 'Hold' input signals from CNC to 386 PC
- 'Ready to scan' LED for user
- 'Edit input signal from CNC to 386 PC"
- Stepper motor control from 386 PC
- Small electric motor control from 386 PC

All signals received from and sent to the 386 PC were interfaced through its parallel port. The board was powered by a 6V DC power supply.

A complete diagram of the control circuiting can be found in appendix C.4.

Software Specifications

The controlling software for the CNC scanning model was written entirely in Turbo C++, version 3.0. The software could perform six main functions:

(1) Read in heat exchanger configurations.
(2) Control interfaces between various machine components.
(3) Generate text files to control the CNC.
(4) Control the stepper and winder motors during a scan sequence.
(5) Collect and analyse flaw image data from the HP54600 oscilloscope.
(6) Provide the user with information during the scan.

The heat exchanger configurations were entered in the same manner as with the robot model.

The two motors on the wrist mechanism were then manipulated via the software. The small winder motor was often adjusted to obtain the correct tension in the nylon string before starting a scan.

The co-ordinates of two pre-selected tube centres then had to be found and entered into the software. This was done to describe the orientation of the heat exchanger on the CNC's bed. The CNC's spindle was first moved to the centre of hole no. 1 (figure 2.15) and the CNC's co-ordinates registers zeroed. Then, the CNC's spindle was moved to hole no. 2 and the X and Y co-ordinate values shown by the CNC's registers were entered into the 386 PC's software. Using this information, the software then saved a textfile containing the co-ordinates of the tube ends onto a floppy disc on the A-drive.

The user was then required to enter the maximum number of flaw images to be captured during a scan. This affected the overall time taken to scan a hole. This information was also used in generating the textfile to control the CNC.

The user then placed the floppy disc into the A drive of the XT-PC and used the MIRROR(TM) software to download the textfile into the CNC's memory. Having completed this, the CNC was ready to proceed with a scan.

The edit button on the CNC was then pressed to initiate the SCAN. During the scan, the software displayed the following information on the screen:

- Tube end being inspected (shown by graphical picture).
- Number of flaws already identified up to present scan position.
- X,Y,Z position of probe.

Once the scan of the entire heat exchanger was complete, the user could then view the graphic images of the flaws detected.

- X,Y,Z position of probe.

Once the scan of the entire heat exchanger was complete, the user could then view the graphic images of the flaws detected.

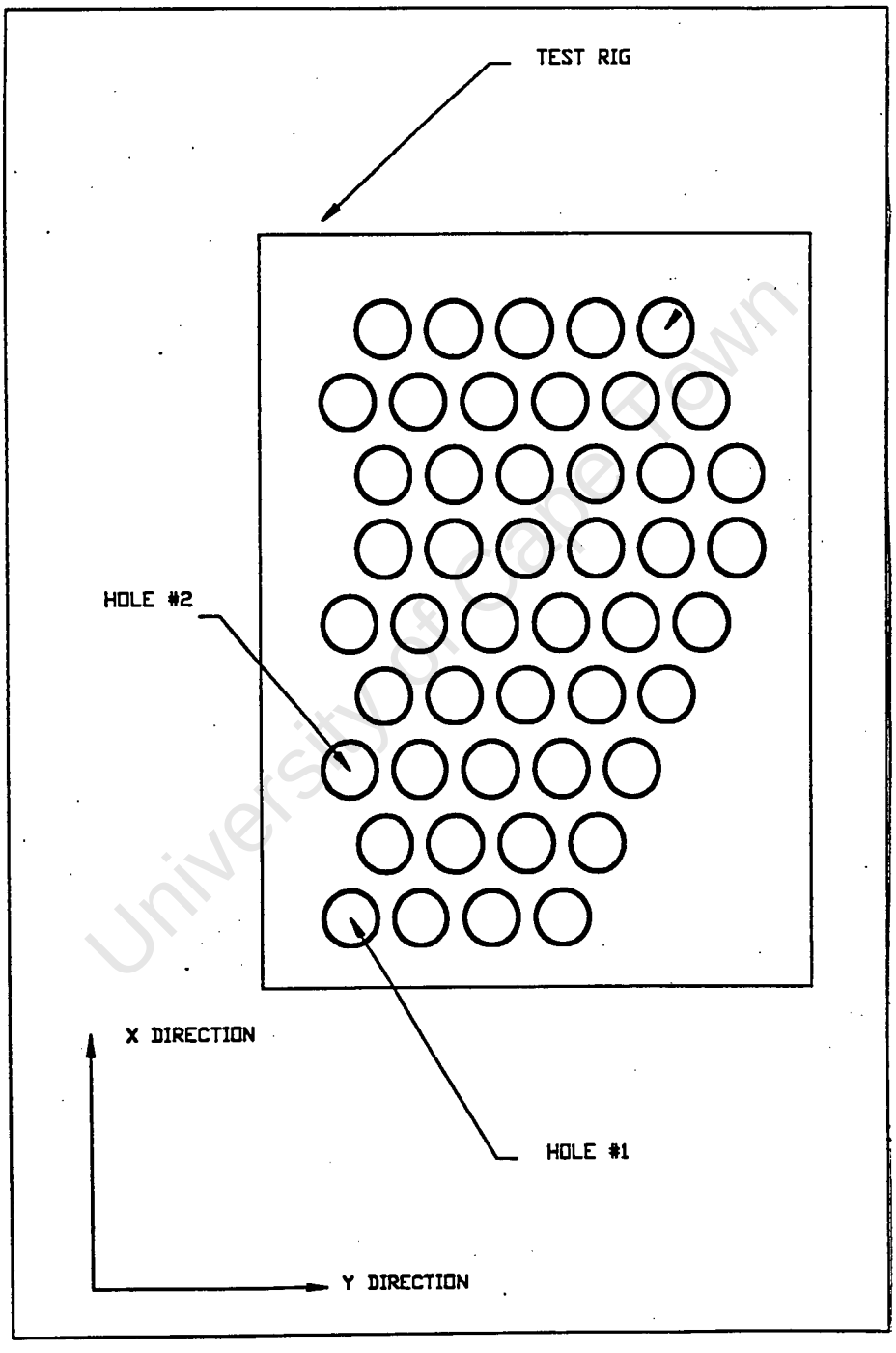

Figure 2.15: **Test rig configuration**

2.4. TEST PROCEDURES & RESULTS

The test procedures using both models can be divided up into two categories:

- Inter-tube positional accuracy tests
- Intra-tube positional accuracy tests

The accuracy of each category of movement was critical to the successful capturing of data from the tube's inspection surface.

2.4.1. Inter-tube positional accuracy tests

SCORBOT

Data provided by the manufacturers of SCORBOT estimated that the positional accuracy of SCORBOT's end effector was within 0.5 mm (i.e.: Length of vector between predicted position (x,y,z) and Actual position(x,y,z) was less than 1 mm for any movement of the arm). As initial tests had shown that this accuracy was not always achieved, thorough inter-positional tests were needed for SCORBOT.

The tests were divided into two stages; horizontal plane and vertical plane accuracy tests. The configuration of the test rig (section 2.3.1) was programmed into SCORBOT's software and the such that the end effector moved from hole opening to opening, pausing at each to allow positional measurements to be taken. Positional data gathered from both tests were compared to the theoretical coordinates in the programme, allowing a total "inaccuracy vector" to be calculated.

The position of the end effector in the horizontal (x,y) plane was determined with the use of a 50 mW Helium-Neon laser. This was mounted onto the gripper units, with the beam pointing vertically downwards. SCORBOT then performed the scanning movements with a piece of paper (A3 size, white) in being in place of the test rig. As SCORBOT's end effector paused at the position of each tube opening, the following was done:

- The end effector was checked to be vertical (i.e.: in line with the Z axis). This was done using a variable-angle spirit gauge (Accuracy: 1°).
- The point where the laser beam hit the paper was marked.

The initial results showed two trends:

- A ± 3 mm offset between identical positions from scan to scan.
- A cumulative x and y direction gain in deviation from the correct position as the scan progressed.

The offset from scan to scan was found to be a software error and was soon corrected.

The second trend, that of an increasing x and y positional gain throughout the scan, was eventually discovered to be caused by a faulty motor in SCORBOT. The fact that the same amount of deviation occurred for each scan suggested either a software or a hardware fault and not a random loss in position. A tachometer was used to measure the angular speed of each joint motor and it was found that motor five ran ± 50 rpm faster than motor 4. However, this error was found to be constant and a repeatability in positional accuracy from scan to scan was found to be ± 0.5. mm.

The second set of positional tests that were performed involved measuring the vertical height of the wrist joint at each tube position. Results showed that an error of up to 3 mm was experienced when the arm was fully extended due to the play in the toothed-belts controlling the arm (i.e: arm lower than predicted by software). Attempts to tighten these belts were not successful.

Thus, the total length of the inaccuracy vector was found to be, at worst, 3.05 mm. This was clearly beyond the manufacturers specifications and could be attributed to the play in the belt-drive system. Furthermore, the inaccuracy was not strictly related to the total distance the arm had extended and thus correction for the inaccuracy through the software was not feasible.

CNC model

It was known that the design of the CNC inherently gave it a greater degree of accuracy than SCORBOT. Inaccuracies in the end effector (CNC's chuck) would be immediately detected when the machine was used for cutting purposes. As accuracies within 0.01 mm were common when using the CNC for cutting purposes, it was assumed that this accuracy would pertain to the manipulation of the chuck during the scanning operation.

Thus, the only inter-tube tests performed on the CNC model were to verify the software co-ordinates. The test rig was fastened to the CNC's table and the initial co-ordinates were keyed in (as described, section 2.3.2). The software then executed the scanning motion, the end effector pausing at the opening of each tube for positional measurement. A vernier (accuracy 0.02mm) was used to measure the position of the end effector relative to the end of the tube wall.

The results of these tests yielded a total length of the "inaccuracy' vector to be 0.05mm. The majority of the inaccuracy could be attributed to the measurement technique used (i.e.: handling of the vernier).

2.4.2. Intra-tube positional tests

Intra-tube accuracy tests measured the manipulation accuracy of the probe face relative to the tube wall. The accuracy of this motion was dependent on two factors, namely:

- *The inter-tube accuracy. If the probe was not positioned in line with the axis of the tube to start with, subsequent motion would be inaccurate.*

- *The inaccuracy of the Probe Insertion Mechanism (P.I.M.).*

In the SCORBOT model, the probe holder mechanism could be thought of as the PIM, although the rotational motion of the probe was provided by SCORBOT's wrist joint. In the

CNC model, the wrist mechanism fitting in the CNC's chuck would represent the PIM.

SCORBOT

The measurement of intra-positional accuracy for SCORBOT was done by repeatedly performing the entire scanning motion on the test rig, but allowing pauses in the motion to gather positional measurements.

The results of these tests showed that the positional accuracy of the probe inside the tube was not within expected limits. The main reasons for this were:

- Inter-tube positional inaccuracies.
- The spiralling movement of the robots grippers when rotating the probe-holder around the tube's central axis.

The different speeds of the two motors driving the wrist's differential gear (motor #5 running at 50rpm faster) gave the gripper-unit not only a roll movement but also a pitch movement. This pitch movement caused the unit to rotate on an axis which increased in angular displacement from that of the tube's central axis.

The end result of this positional inaccuracy was that the probe was forced hard against some areas of the tube wall and lost contact in other areas. An attempt was made to use a larger spring on the probe holder mechanism to eliminate this problem but the erroneous motion also gave the probe an alignment error which could not be overcome by the spring. Furthermore, it was not possible to adjust for the erroneous motion using the software (ie: move the one motor in the wrist less than the other) as the motion commands would have had to be broken down into smaller segments, leading to an unacceptably jerky motion.

(Note: replacement of the faulty motor was not practical under the time constraints as it had to be imported from Israel.)

Another trend revealed by the Intra-tube tests was the sporadic loss of positional information

by SCORBOT. During a scanning procedure, SCORBOT would suddenly perform various movements that were not part of the programmed routine. These were totally random in time and place of occurrence and often led to the arm colliding with the table or itself. After finishing these random movements, SCORBOT would then continue with the programmed movements but from its new position in space.

CNC

The intra-tube accuracy of the CNC model was dependent on the inter-tube accuracy (provided by the CNC machine itself) as well as the motion provided by the CNC's wrist mechanism. Numerous 'dry-run' tests (ie: no ultrasonic signal interpretations) using the test rig were carried out to verify the intra-tube accuracy of the probe motion and the functionality of the manipulation software.

The most problematic stage of achieving accurate probe manipulation was synchronising the two control systems at various stages of the scan. As detailed in appendix E, the CNC movements were controlled independently from those of the wrist mechanism. The only time when the two systems could be reliably synchronised was at the beginning of a scan.

This initially resulted in the CNC movements occurring out of time with the wrist motion as the scan progressed and the system as an automated entity had no way of detecting or correcting for this error.

To counter this problem, the 386PC was made the 'master' time-keeper. The software run on the 386PC had the facility of referring to the computer's internal clock to keep track of when it was expected by the CNC to finish its movements and thus could make decisions as to whether to continue scanning or not. The CNC, however, had no such facility but its operations were simple enough to be predictable by the 386PC. The only place for error was estimating the time taken by the CNC to move between tube centres. An algorithm was developed that took account of the exact distance travelled by the CNC's tool end between the various tube centres and estimated speeds for each part of the movement were found. This narrowed the timing error down to less than 0.2 seconds for each tube inspected but as the

error was accumulative, the total time variance between the two control systems during the scanning of the last hole was as much as 5 seconds.

The end solution was to build a 'time buffer' into each of the control system's operations. If both of the systems were completely synchronised, there would have been no activity from either the CNC or the wrist mechanism in this stage of the scan. However, in practice, it allowed one of the two systems some leeway to complete its movements before the next scheduled stage of the scan started. Figure 2.16 shows the interaction between the two scanning procedures.

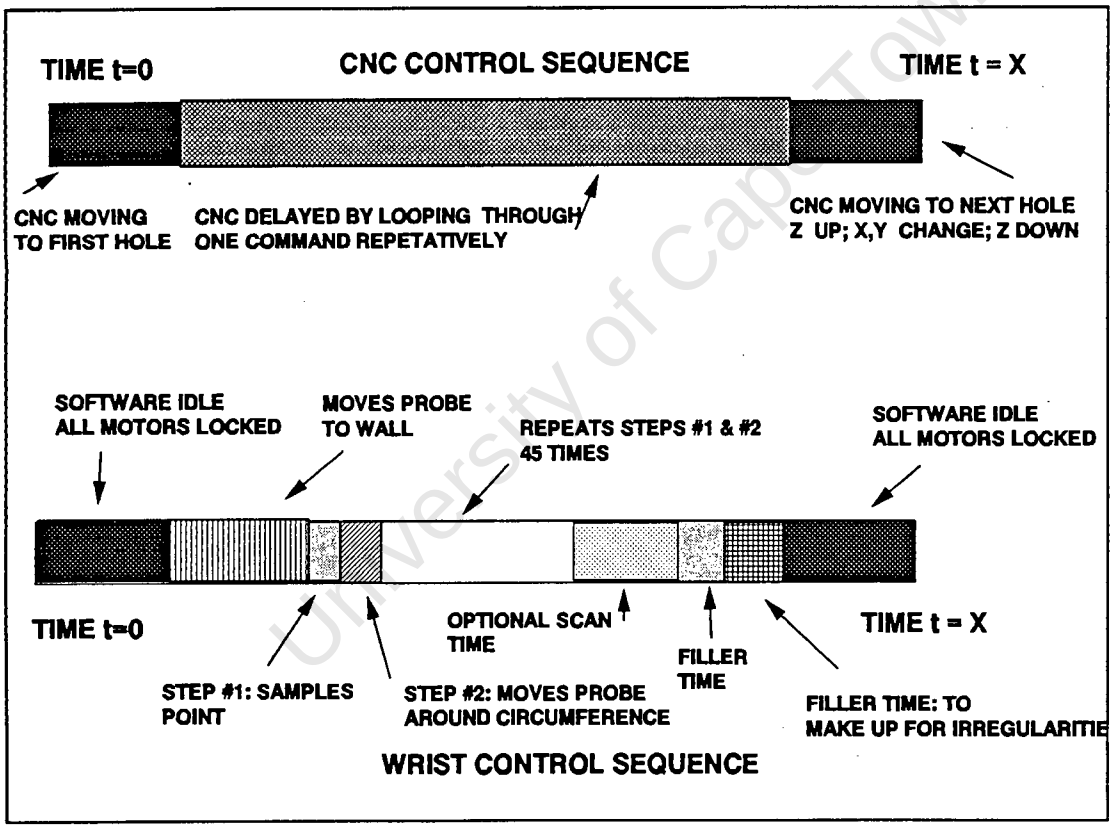

Figure 2.16: **Schematic diagram showing scanning procedure sequence**

Scanning the rig at any orientation on the CNC's bed, the probe manipulation around the inner circumference of the tubes was sufficiently accurate to give a maximum 10% deviation in the magnitude of the ultrasonic backwall echoes throughout the scanning of a tube.

2.5 CONCLUSIONS

2.5.1 Single position frames vs multiple position frames

Single position frames have only one advantage over multiple position frames: they only need to be attached to the tubesheet and positioned once during the entire scan.

However, single position frames have the following disadvantages:

- High inertial mass on moving arm. This meant that arm movements were low, accuracies were harder to obtain and drive motors had to be larger, thus increasing the scanner's mass.
- Restricted to certain orientations of the tubesheet.

The main disadvantage of using a multiple position frame was the time wasted re-locating the frame to cover a new area of the tubesheet. However, this can be overcome with the design of suitable quick-fastening mechanisms (ie: that attach the frame to the tubesheet).

Thus, multiple position frame type should be chosen for the final scanner model.

2.5.2 The mass of the frame should be less than 20 kg to allow easy placement of the frame on the tubesheet by a single operator.

2.5.3 the configuration of frame most suited to the scanning of the tubesheet is one consisting of three prismatic and one revolute joints (ie: Cartesian Plane frame).

The advantages of choosing this configuration were:

- *Simple motion control*: the scanning of the tubesheet requires the majority of the probe motion to be linear. The cartesian Plane frame only needs to move one 'joint' to provide linear motion. In contrast, a rotational arm has to move multiple joints to simulate linear motion in the required plane.

- *Rigidity of the frame:* The Cartesian Plane frame inherently provides rigidity in the same planes in which the forces on the probe act. Thus, the required rigidity can be achieved with a lighter frame.

CHAPTER 3

SIGNAL RECOGNITION

3.1. INTRODUCTION

One of the criteria for automated inspection of tubesheet welds was the automated interpretation of the ultrasonic inspection signals.

The present inspection methods used on the First Effects Steam Chest (Chapter 1) had disadvantages which included:

- No records of the integrity of the inspected welds were recorded for future comparisons.

- The quality of the assessment of welds was largely dependent on the skills of the operator. The results were thus subjective and had no standard to be compared against.

The automated interpretation and subsequent storage of the returned ultrasonic signals from a scan would eliminate both of these problems.

The difficulties to overcome in programming an algorithm to interpret ultrasonic signals were:

[1] The characteristics of returned signals from different flaw shapes and sizes varied considerably. The interpretation algorithm had to be able to recognise a wide band of signal shapes.

[2] The interpretation of incoming signals had to take into account variations of couplant flow, pressure on the probe lens and surface finish of the inspection surface.

[3] The speed of interpretation had to be sufficient to allow a scan to be completed in under 45 minutes.

The majority of testing used to develop the flaw recognition algorithms was done using the CNC model. This model offered accurate probe manipulation and high rigidity, two factors which ensured that recognition was not compromised by probe manipulation.

3.2 TEST PROCEDURE

The test rig (figure 2.12, Chapter 2) was mounted onto the CNC's bed. The exact location of the tubes of the test rig relative to the x and y axes of the CNC were determined using the routine described in section 2.3.2.

A tube was replaced in the test rig with another tube that had a number of artificial defects manufactured into its outer surface (figure 3.1). These defects were four flat-bottomed holes of 1mm, 2mm, 4 mm and 7 mm and a flattened area of 12mm in diameter. The range of defect size varied from 14% to 171% of the ultrasonic beam width, thus providing a wide range of signal responses.

The CNC model then was set up to scan the replaced tube repetitively. The incoming ultrasonic signals were recorded, along with the exact position of the ultrasonic probe on the inspection surface.

The signals returned from areas of the tube containing the artificial flaws were analysed in comparison to signals returned from acceptable tube surfaces. In total, fifty five unique signals from the five defect areas were analysed. The results of this analysis are summarised in appendix B.

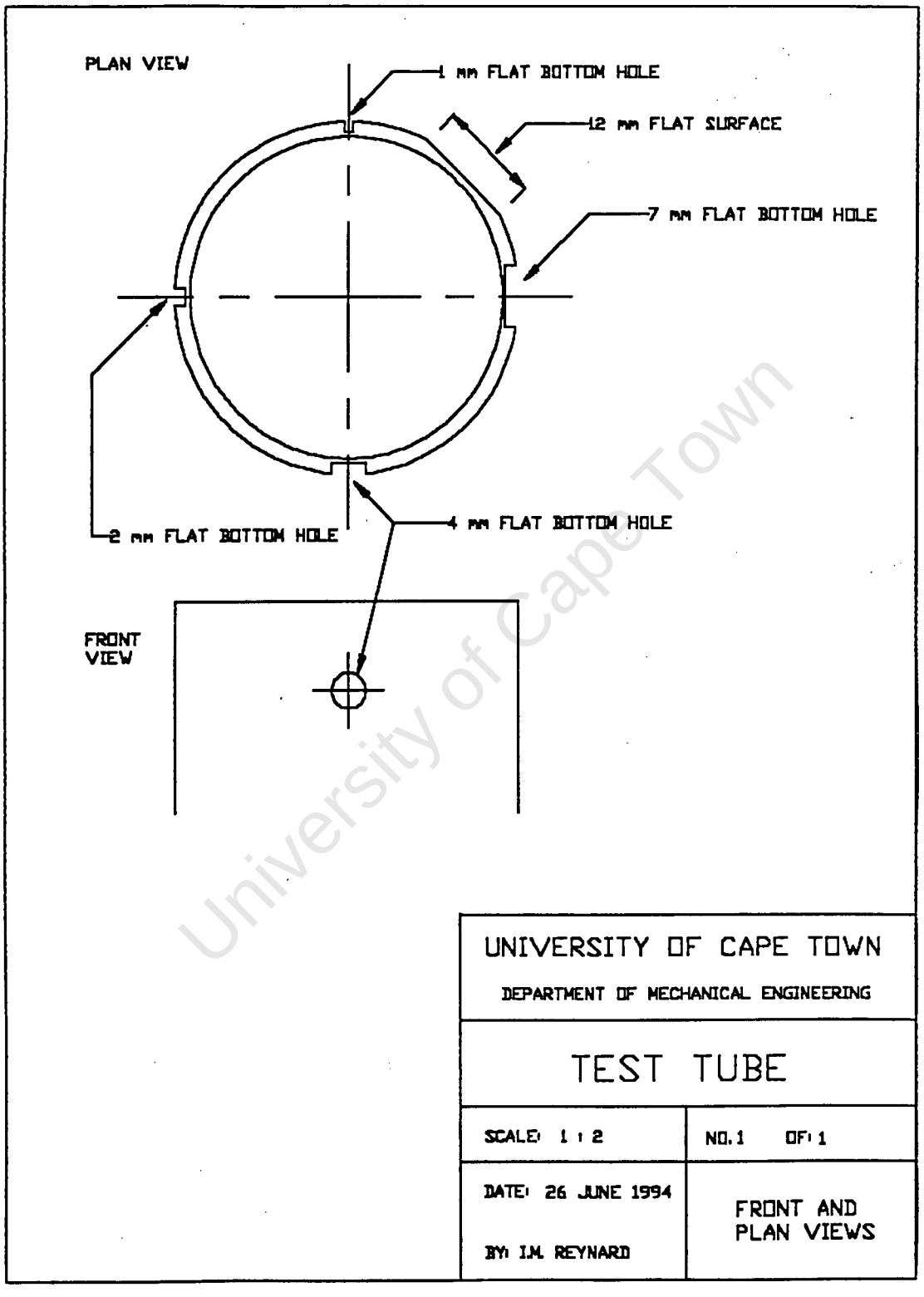

Figure 3.1: Test tube with artificial flaws in outer surface

3.3 FLAW RECOGNITION ALGORITHMS

The analysis of the fifty five returned signals from the defects formed the 'template' against which the flaw recognition algorithms were formed (ie: the algorithms had to be able to detect flaws that showed any one of the characteristics displayed by the fifty five signals). Two separate algorithms were developed, namely the primary and secondary flaw detection algorithms. These two algorithms had different functions, as explained below.

The fundamental purpose of the scanner was to locate flaws in the welds of the tubesheet. From the detection of the flaw, various follow-up action could take place, namely manual scanning or further automated inspection. Thus, the **primary** flaw detection algorithm was developed to distinguish between an acceptable area of the tube and that containing the smallest allowable flaw (1 mm).

Once the flaw had been detected and its position recorded, the scanning could continue or further data on the flaw could be collected. This detailed flaw information, such as size, shape and orientation, would be useful to the operator to determine how the flaw had formed. The **secondary** algorithm allowed this additional detailed information to be collected from the flaw. The choice of gathering further information on the flaw was made by the operator at the beginning of the scan, as it related to the total amount of time that would be needed to complete the entire scan.

Primary flaw recognition

Thus, the first algorithm developed looked for the presence of a flaw. (ie: and did not collect information concerning size, shape and orientation). This was done by detecting any returned signal that did not resemble that from a section of acceptable weld seam. From scans taken of the test tube, it was seen that the original first backwall echo amplitude (OFBEA) decreased in amplitude by atleast 25% when irradiating a flaw. Thus, the following condition was used to detect the presence of flaws:

Logic statement of primary algorithm: flaw ≡ (1)

CONDITION	QUERY	"TRUE VALUE"
(1)	:measure:tvolt? -20 +1	>1

Thus, when the query *:measure:tvolt? -20 +1 >1* was sent to the HP 54600 oscilloscope, it would check if the returned signal crossed over the -20V threshold - if not, it would return a value greater than 1, signalling the presence of a flaw.

Secondary flaw recognition:

It was determined that the shape and orientation definition of flaws was impractical using automated scanning methods. This was because the determination of the shape and orientation of a flaw is normally done by multiple scans using specialised techniques. One method of finding the shape of the flaw is by changing the angle of irradiation and monitoring the resultant changes in the echo pulse amplitude. An alternative method was proposed by Shcherbinschii et al[15], which involved using two angle probes in parallel and comparing the ratios of the returned signals. Both methods would involve either multiple scans of the flaw with specialised probes or a parallel probe set up. The orientation of a flaw relies on an initial sizing of the flaw and then additional irradiations of the flaw from different angles. Thus, definition of both shape and orientation of flaws is impracticable for automated scanning.

The size of a flaw can be estimated by the three methods mentioned in section 1.3.2. However, both DGS scales and spectrometry methods would prove too complicated for automated signal analysis. Thus, the remaining method of detecting the edges of the flaw was used. This allowed the area of the flaw in the irradiated plane to be calculated, giving a good estimate of the flaw size.

Thus, from the fifty five test scans, conditions were found that allowed for the detection of the edges of all five artificial flaws:

logic statement for the secondary algorithm: edge ≡ (1) OR (2)

where:

CONDITION	QUERY	"TRUE VALUE"
(1)	:measure:tvolt? -80 +3	>1
(2)	:measure:tvolt? -65 +1	< 9.2 E-6

Condition (1) checks whether the secondary backwall echoes have been reduced to below 40% of their original amplitude. Condition (2) identifies the presence of a peak which must have an amplitude larger than the original front wall echo and must be in a position corresponding to that of an echo from a surface inbetween the front and back surfaces.

Furthermore, when the secondary algorithm was chosen, the software automatically stored a complete digital picture of the traces received of the flaw. Thus, the operator could review the flaws after the scan was complete and gain additional information that might help with flaw shape and orientation identification. The position of that particular tube was also recorded, thus allowing the operator to manually inspect the flaw if needed.

3.4 RESULTS

Approximately twenty five scans were completed on all five of the artificial flaws. Tests using the primary algorithm were 100% effective in identifying all five artificial defects in the tube as flaws.

However, errors that were detected and rectified in the process of testing were:

[1] The returned signal was very sensitive to the lack of coupling fluid through the acoustic lens. Figure 3.2 shows this effect. This led to the software erroneously identifying parts of tube that were flaw-free. The solution was to ensure that more than sufficient coupling fluid was flowing through the lens at all times.

[2] The force needed to push the probe onto the inspection surface to give a consistent return signal was found to be in the range of 5 - 9 Newtons. A smaller force led to insufficient contact whereas a larger force led to increase in friction between the lens and the inspection surface, causing misalignment of the probe.

It was found that, under tension, motor #2 of the CNC's wrist mechanism allowed more cord to be wound out than when winding the cord in (ie: pulling the probe up against the tube wall). This was adjusted for in the software control of motor #2 and the correct forces between the probe and the inspection surface were obtained.

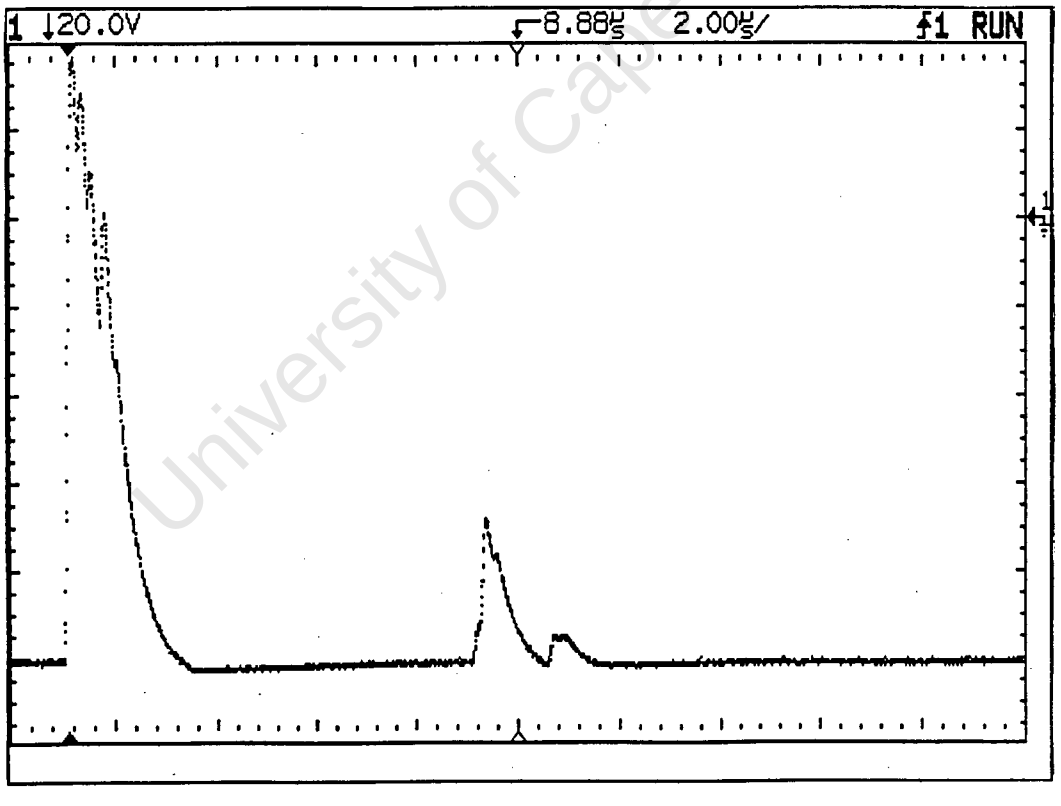

Figure 3.2: Trace received from inspection of normal surface (no flaws) but with insufficient couplant flow in the lens.

The results in using the secondary algorithm were not completely successful. The algorithm had a 100% success rate in detecting the edges of all five defects in the test scans. However, the distance of the probe from the edge of the flaw on detecting it varied from scan to scan and was dependent on the flaw size. The edge of the flaw was identified when the probe centre came within 5% to 25% of probe diameter from the edge of the defect. This variation limited accurate flaw sizing, especially with the smaller flaws. (ie < 2mm), which would show an error of up to 44% in determination of their size.

The capturing of the trace image of the flaws was initially problematic, mainly in the area of the storage of incoming data. Files were often found to either be 'unreadable' or to have been 'truncated' by the storage function. Secondly, commands given to the oscilloscope were sometimes ignored, thus causing all subsequent commands to be irrelevant.

These problems were solved in two ways:

[1] The baud rate of communication between the oscilloscope and the 386PC was reduced from 9600 to 1200 cpm.

[2] The storage technique used by the software was changed to give larger but simpler data files.

These modifications slowed down the image capturing process but made the process reliable. Approximately ten scans were captured onto disc and were able to be used for further flaw analysis.

3.5 CONCLUSIONS

In summary, it can be concluded that the two failings of the present system, mentioned in section 3.1, can be successfully overcome using the above automated signal interpretation algorithms.

The integrity of welds can be recorded for future inspections, as was shown with the capturing and storage of trace signals during the secondary algorithm implementation. The incoming signals are compared to a fixed set of criteria, thus eliminating the reliance on the operator's (subjective) interpretation.

Thus,

3.5.1 It was possible to detect the presence of a wide range of flaws using the primary algorithm and the equipment setup used in the CNC model. The detection success rate on the test tubes was 100% over the test period, suggesting that these algorithms will be very reliable.

3.5.2 The determination of the shape and orientation of flaws in the weld was deemed not to be practicable for an automated scanner. This was because most methods used to determine these characteristics of flaws rely on multiple scanning from different orientations, using specialised probes.

3.5.3. Flaw edge detection was possible but the deviation in results in determining the true position of the edge of the flaw led to large discrepancies in the calculation of the projected area of the flaw. It was concluded that, whilst the secondary algorithm was able to give an estimate as to the size of a flaw, further work in this area is possible. Algorithms for the recognition of both shape and size of flaws would have to be found for groups of flaws bearing the same characteristics.

3.5.4 Incorrect couplant flows and forces on the probe could lead to erroneous signals, thus causing the algorithms to falsely indicate flaws. The optimum couplant flow was when

the couplant pressure was sufficient to cause a slight flow of liquid out past the lens of the probe.

3.5.5 The force of the probe against the tube wall had to be kept within a range of 5 - 9 Newtons to ensure consistent scanning results.

CHAPTER 4

FINAL SCANNER DESIGN

4.1 INTRODUCTION

The results gained and the conclusions drawn from chapters 1, 2 and 3 gave sufficient information for the design of a final scanner. This chapter presents the proposed design, as well as an estimate of the performance characteristics of the scanner.

A working model of the final scanner was not constructed as the cost of construction did not justify the additional information that would be gained. The two models had allowed sufficient experimentation to take place to prove all aspects of the proposed hardware design of the final scanner. The major design decisions (ie: frame configuration, working ability of wrist mechanism) had been made during the SCORBOT model and had been tested in the CNC model. Furthermore, some of the equipment used in the CNC model was designed to undergo very minor adjustments before being adopted into the final scanning model. The software written for both of the models would have been 95% correct for the proposed scanner, just requiring minor configuration variables to be changed.

4.2 PROPOSED DESIGN

The scanner, shown in figures 4.1 to 4.7 was designed for inspecting the welds in the tubesheet of the First Effects Steam Chest, as described in section 1.4.3 of this report.

Frame:

The function of the frame was to position the Probe Insertion Mechanism (P.I.M) on the central axes of tube openings to be inspected. All square tubing material was aluminium for weight considerations. This gave the frame a mass of approximately 19.3 kg. The mass of

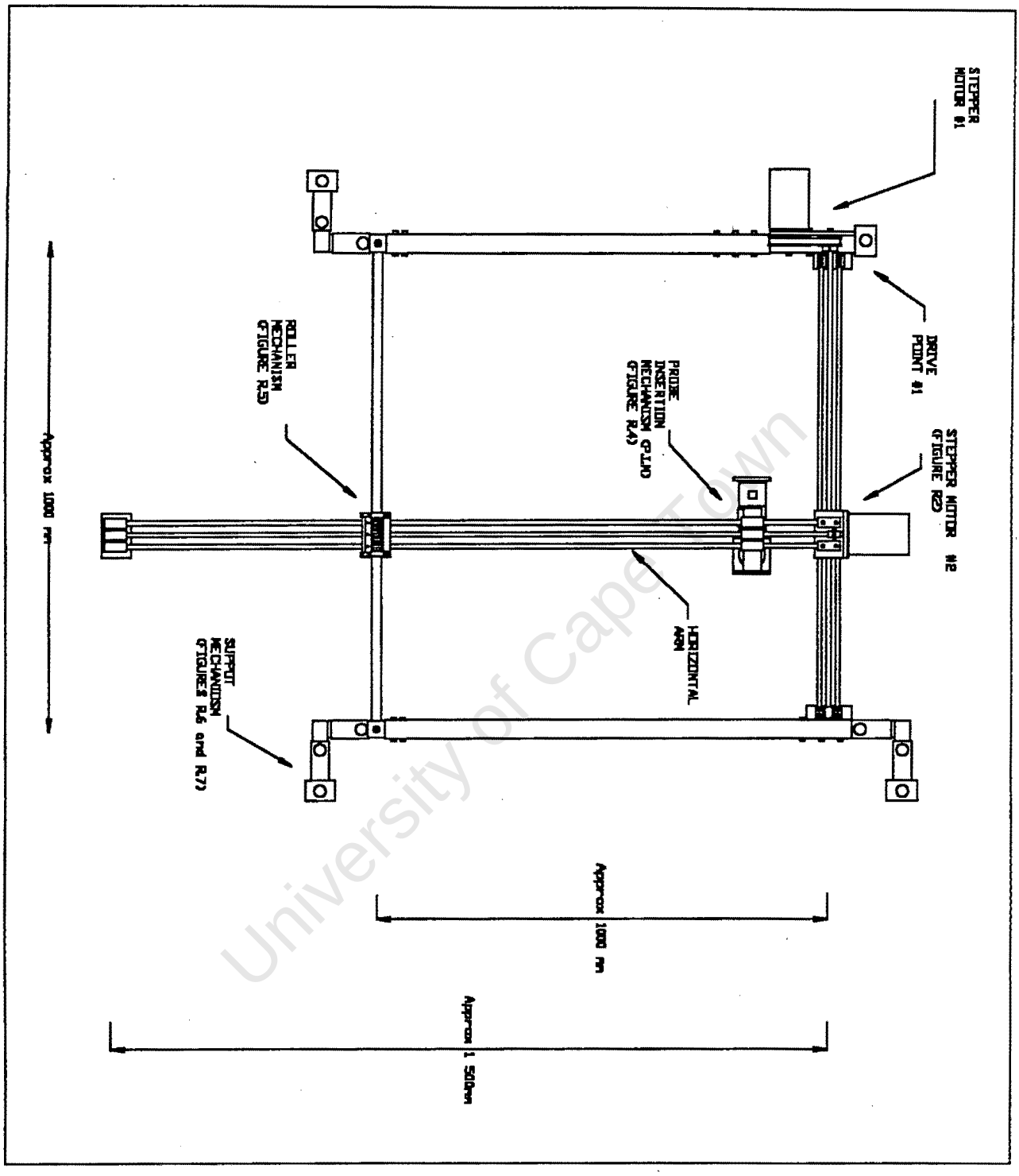

Figure 4.1: Scanner (plan view)

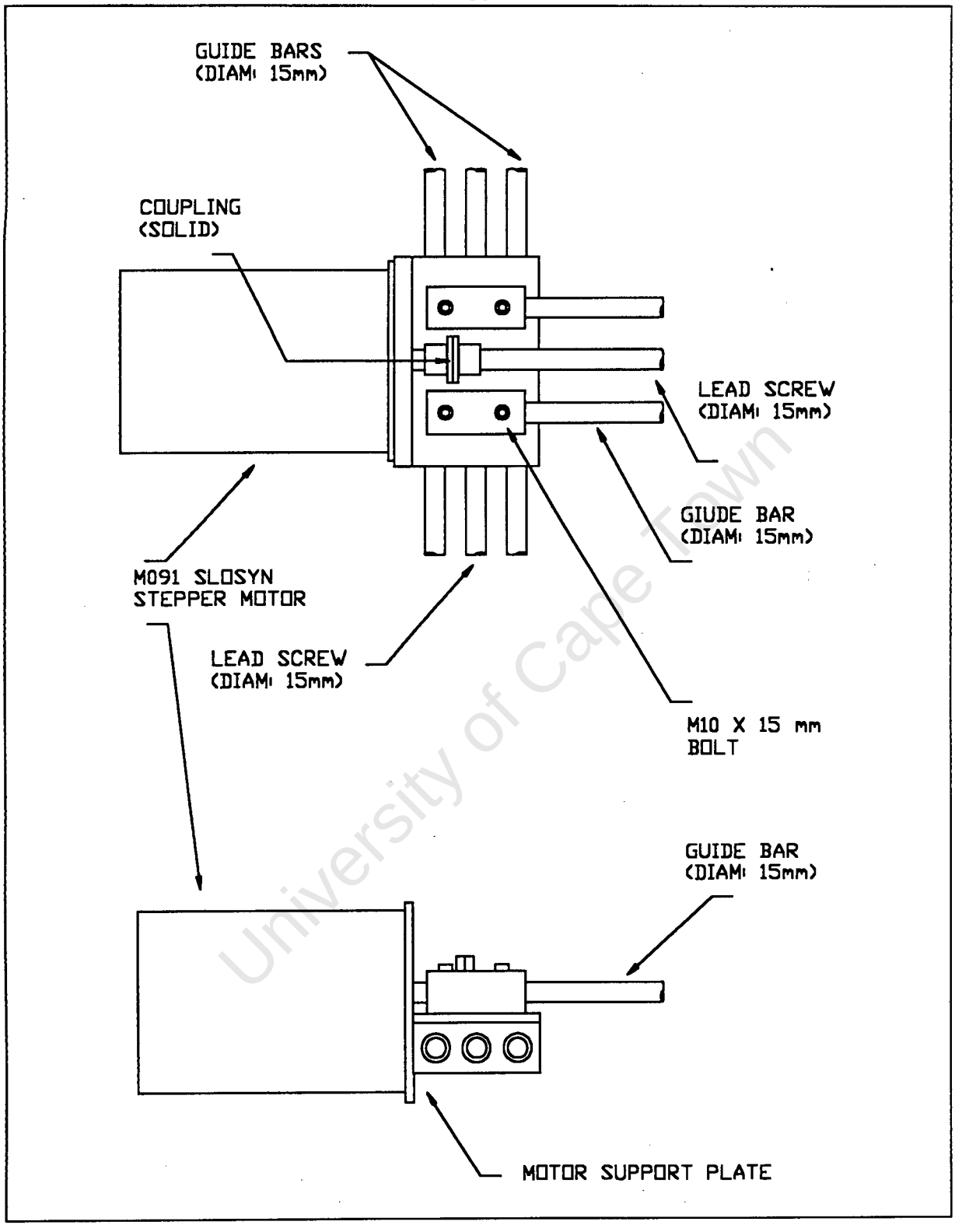

Figure 4.2: Horizontal Arm drive assembly

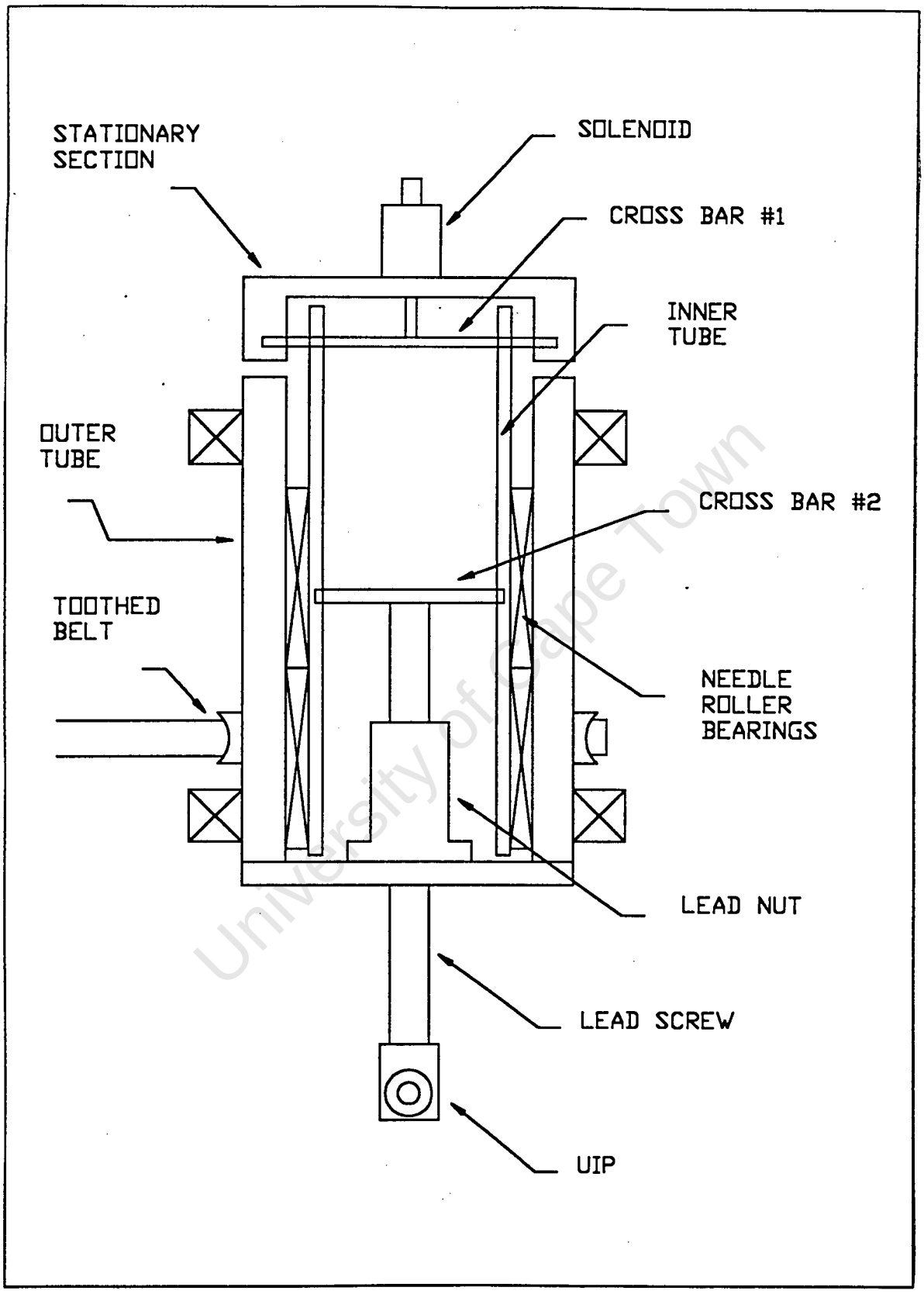

Figure 4.3: Probe Insertion Mechanism (sectional view)

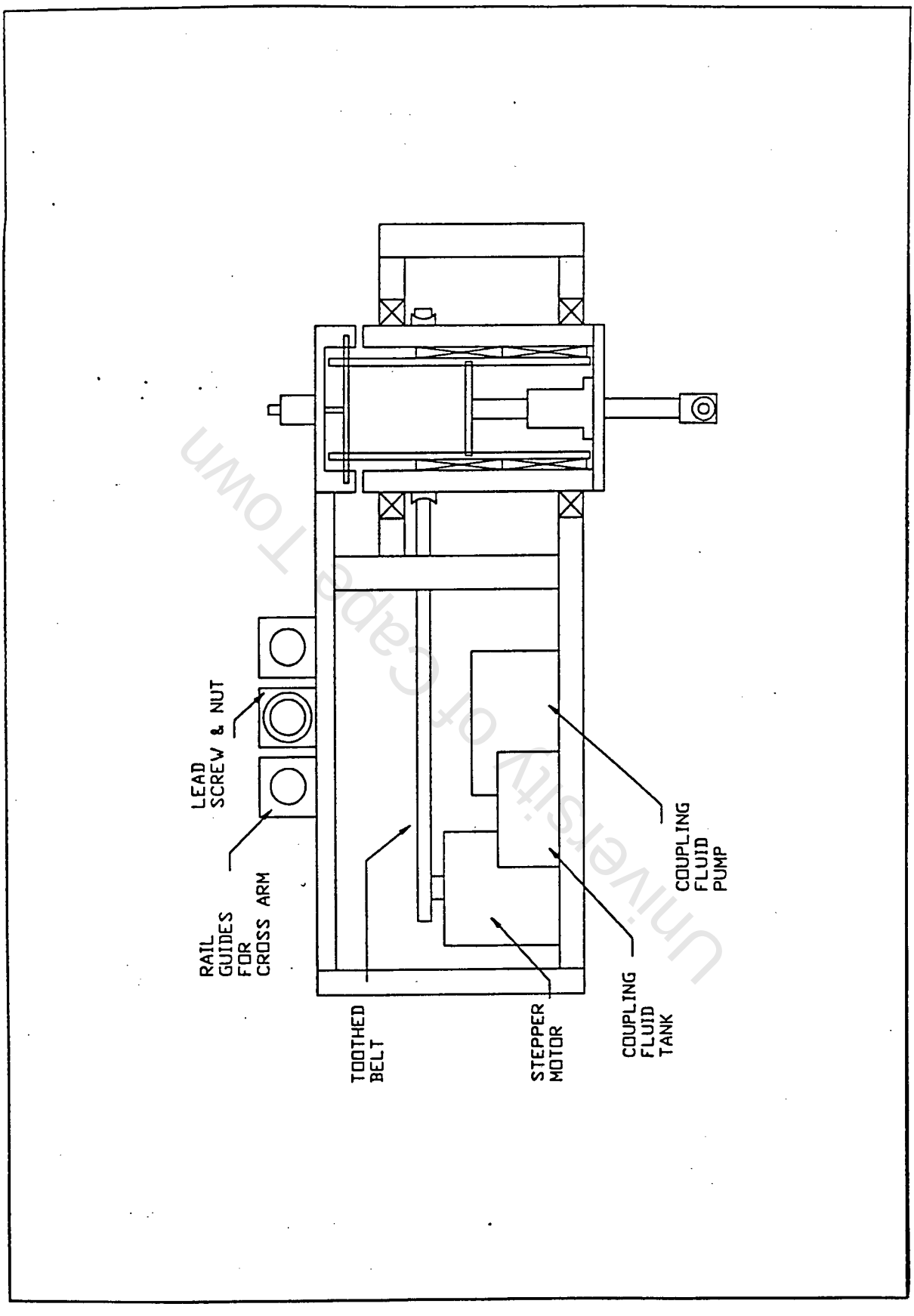

Figure 4.4: Probe Insertion mechanism (sectional view)

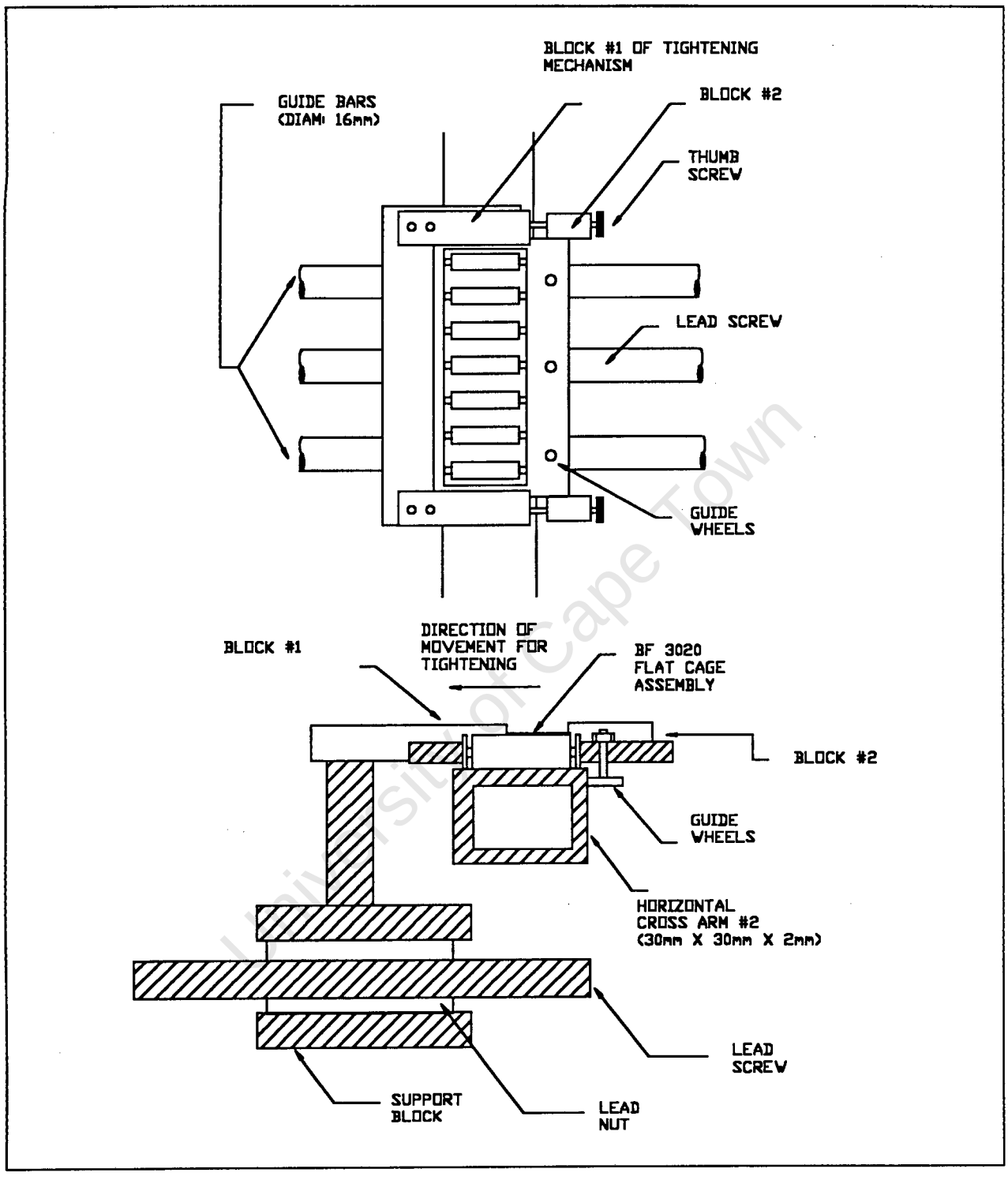

Figure 4.5: Roller mechanism

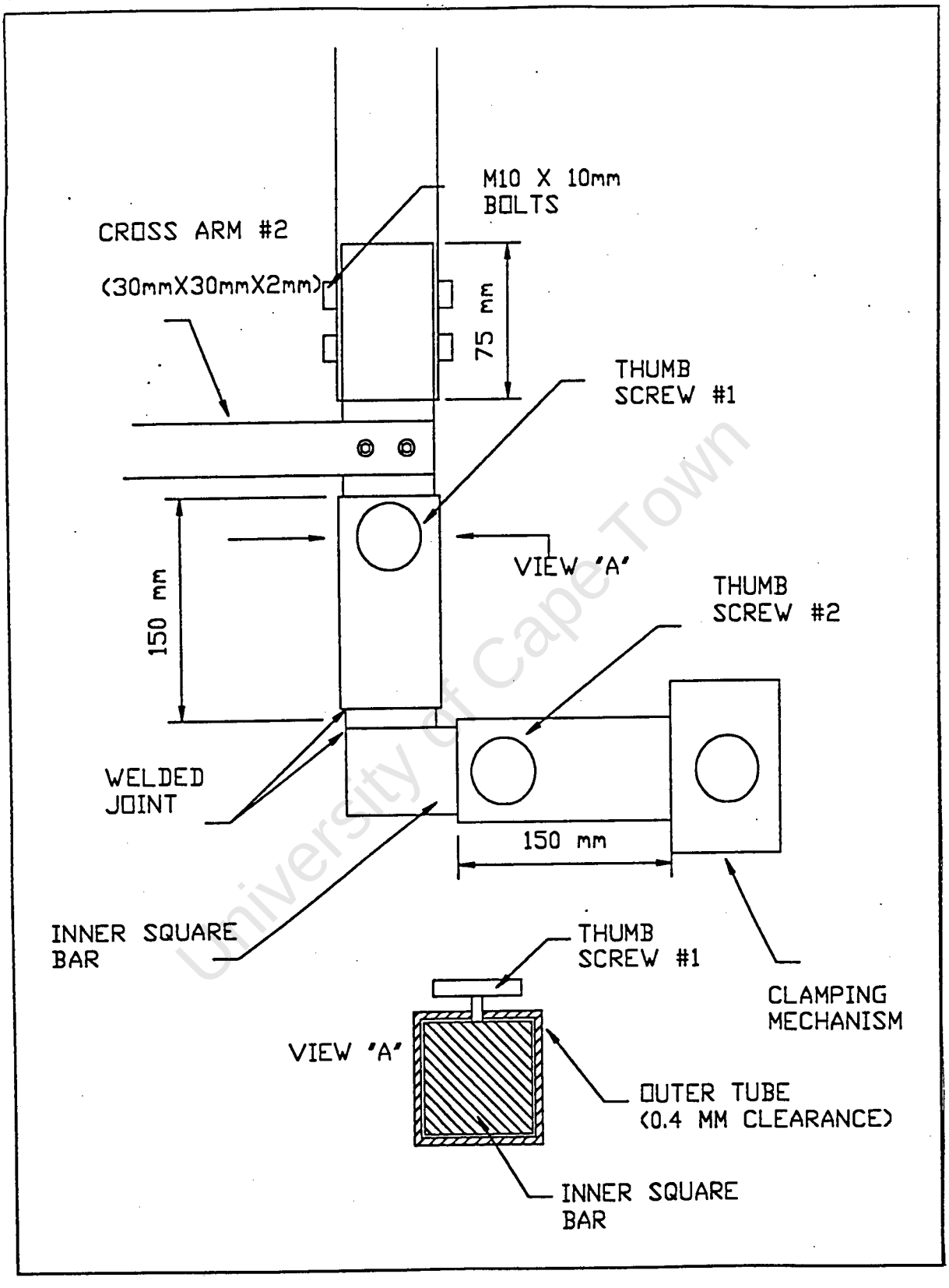

Figure 4.6: Foot mechanism

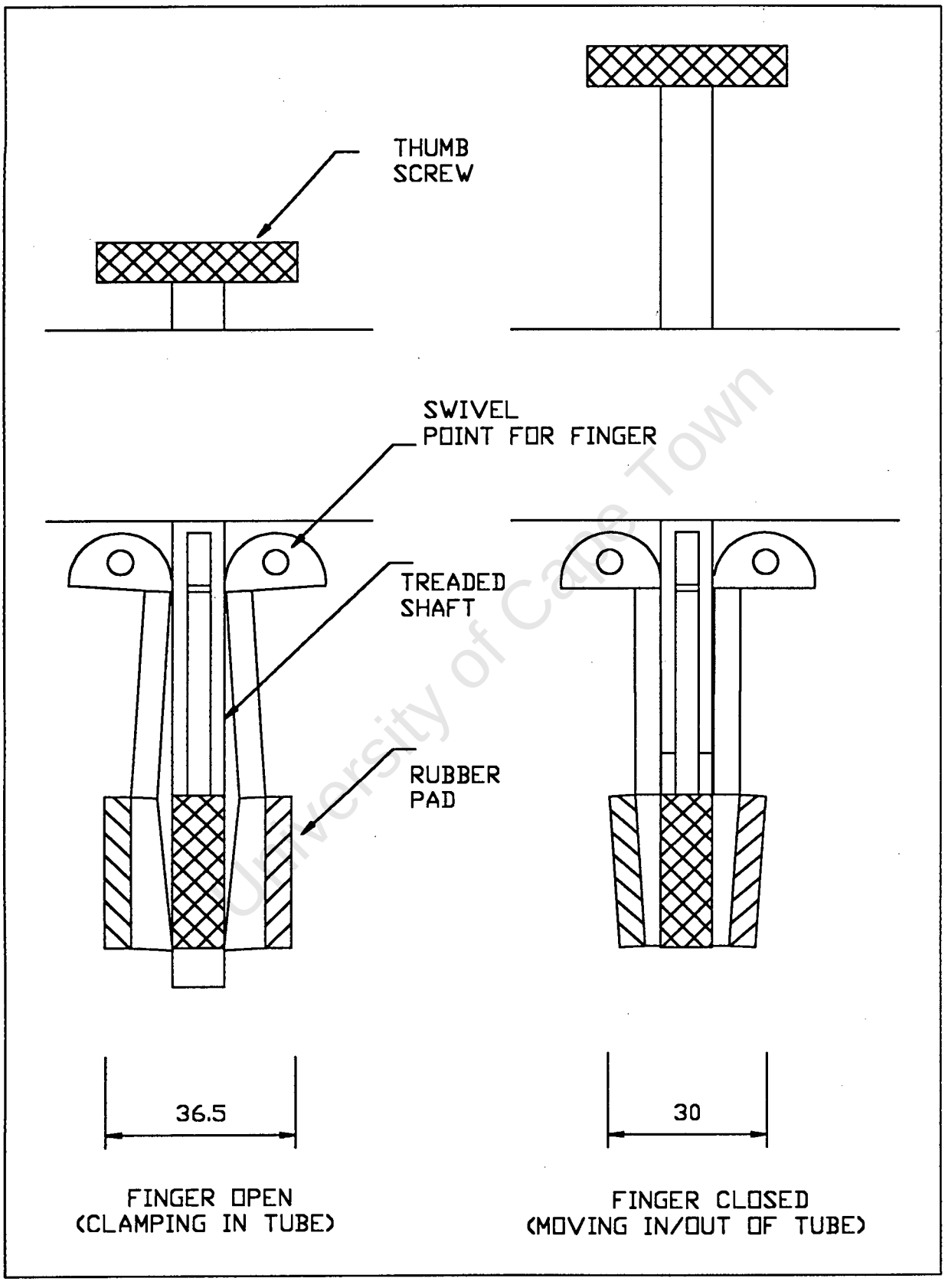

Figure 4.7: Clamping mechanism

the total assembly was calculated to be 23.3 kg.

It was decided to drive the X-axis (ie: entire horizontal arm) using a lead screw acting on only one side of the horizontal arm. the other end of the arm in contact with the frame is guided by a tensioned roller device but is not powered. Other options were to have the arm driven on both sides (ie: both contact points with the frame) using either two separate stepper motor and lead screw systems or by linking a second lead screw by chain to one stepper motor. The single-side drive was chosen for both weight and simplicity reasons.

Both X and Y axes for the scanner movement rely on a dual guide rail system to provide the rigidity as well as accuracy of motion required shown in figures 4.1 and 4.2). The lead screw used to power the horizontal arm and the Probe insertion Mechanism (P.I.M) runs inbetween the guide rails. Options as far as the choice of guide rails were concerned included using a rail and track mechanisms. Again, this was rejected for simplicity reasons. The guide rails are also standard items, supplied by most bearing companies.

The lead screw powering the horizontal arm is turned by stepper motor #1. One option was to mount the stepper motor on the horizontal arm and turn the nut instead, whilst holding the lead screw stationary. The advantages of this are that the nut has less rotational inertial mass than the lead screw. This had to be compared to the extra linear mass of mounting the motor on the object being moved (the horizontal arm). However, when the motor selection calculations were done, it was found that the SLOSYN MO61 stepper motor was able to overcome the lead screw's inertial mass whilst still accelerating according to specification. Thus, for stability reasons as well as reducing the number of cables to be dragged by the horizontal arm, stepper motor #1 was mounted on the frame as shown.

The same argument was applied to mounting stepper motor #2 on the horizontal arm and not on the P.I.M.

Probe Insertion Mechanism (P.I.M.)

The function of the P.I.M was to manipulate the ultrasonic inspection probe (UIP) within the tube opening. This involved the following:

(1) Lowering the UIP into the tube opening along the centre line
(2) Bringing the UIP up against the tube wall
(3) Rotating the UIP around the circumference of the tube wall
- Coupling fluid had to be applied between the tube wall and the UIP throughout this motion
- A constant force had to be applied to the UIP to obtain uniform inspection results
- The probe had to have an even contact interface with the tube wall, requiring an acoustic lens.

(4) Removing the UIP from the tube wall
(5) Raising the UIP out of the tube opening along the centre line.

A schematic diagram of the final PIM design is shown in figure 4.3 and 4.4. Stepper motor #3 is used to provide both the vertical motion of the UIP as well as turn the probe to the correct orientation to inspect the tube wall.

The stepper motors driving both the cross bar and the PIM on the cross bar could be controlled to give the P.I.M an X and Y motion that would trace the inner circumference of the tube. Stepper motor # 3 would merely align the probe face with the tube wall as the probe was moved around the circumference.

The dual function of stepper motor # 3 (ie: vertical motion as well as UIP alignment) is achieved with the use of a solenoid. Referring to figure 4.3., vertical motion was achieved as follows:

(1) The solenoid was de-activated. This caused the crossbar #1 to come up into a slot in the stationary section of the P.I.M. , thus locking the inner tube and the

stationary section together.

(2) Stepper motor # 3 then turned the outer tube via the toothed belt and pulley, thus also turning the lead nut.

(3) The lead screw, however, was restricted by a square bar mounted on top of it to vertical motion alone (cross bar #2 ran in slot in the inner tube). Thus, as the nut was turned, so the lead screw was forced vertically up or down.

Once the PIM, which was attached to the end of the lead screw, was lowered to the right depth into the tube opening, the motors driving the cross bar and the PIM on the cross bar (motors # 1 and # 2) provided the lateral movement to bring the UIP up against the tube wall. However, as motors # 1 and # 2 move the UIP around the tube wall, the UIP has to be continually orientated so that the probe face is in contact with the tube wall.

This orientation of the UIP is achieved with stepper motor # 3 as follows:

(1) The solenoid was activated. This causes cross bar #1 to come down and lock the inner tube to the outer tube (bar now located in slots in both inner and outer tubes).

(2) Stepper motor # 3 then turns the outer tube. As the nut was attached to the outer tube and the lead screw to the inner tube, there was not relative rotational motion between the two. Thus, the result was that the UIP remained at a constant depth in the tube opening whilst being rotated about the lead screw axis.

One feature of the design was that the change-over in motion of the UIP (vertically to rotationally) could only be done at certain points in the scanning of the tube. This was because cross bar #1 bar ran in slots in the inner, outer and stationary tubes. Thus, the bar could only move from the outer tube to the stationary tube when the slots in each tube were aligned. An advantage to come out of this was that any inaccuracy in the motion produced by motor # 3 would prevent the slots from aligning and thus an alarm signal could be raised.

The P.I.M. was designed such that it could travel underneath the one side of the frame. This was to allow the P.I.M. to reach tube openings around the edge of the tubesheet where the circular configuration of the tube spacings would not allow the frame to be secured near enough otherwise. Effectively, the horizontal arm was hung on the non-drive side of the frame. Thus, although the frame measured approximately 1000mm X 1000mm, the P.I.M. had a possible travel of 1500mm.

Acoustic lens and coupling fluid system

The design of lens and coupling fluid system as used in the CNC model, was adapted for the scanner.

The only modification to the design was the replacement of the hypodermic syringe with a coupling fluid tank (430 ml) and pump.

Roller tensioning mechanism

The roller tensioning mechanism, shown in figure 4.5, was designed similar to the guide mechanisms used on draughtmen's drawing boards. It consisted of a length of flat cage assembly that ran on top of the tube frame. To tension the horizontal arm onto the frame, two thumb screws were used to pull the flat cage assembly plus guide wheels closer to the lead nut (located on the horizontal arm) and thus bring the entire roller mechanism tighter up against the tube.

Adjustable feet and clamping mechanisms

One of the adjustable "feet" is shown in figure 4.6. It allowed for the positioning of the clamping mechanism in a linear fashion in both X and Y directions. Approximately 120mm of adjustment in each direction is possible. The square bar inserted in the square tubing will provide good joint rigidity as well as making the tightening devices (thumb screws) simple. These tightening thumb screws run in a threaded hole in the tubing and tighten up against the square bar to locate the foot in the required position.

The clamping mechanism, shown in figure 4.7, consists of a solid block of aluminium with a M12 X 175 mm thumb screw threaded through it. On the bottom side of the block, four 'fingers' are attached by swivel joints. The profile of the fingers are such that, as the screw is turned in through the block, they are forced outwards. In figure 4.7, the fingers were sized for a 36.4 mm inner tube diameter. Thus, when the thumb screw is fully turned in (approx. 50mm of travel), the outer edges of the fingers are parallel to the surface of the tube. These outer edges have a 1mm thick wedge of rubber to provide the necessary friction to locate the foot in the tube opening.

Signal interpretation equipment

The signal interpretation aspect of the inspection involved the following:

(1) Sending the outgoing pulse on the inspection probe (UIP).
(2) Receiving and filtering the incoming signal.
(3) Identifying the required sections of the signal and transferring them into the computer's memory.
(4) Analysis of the captured signal and storage of the final results for later viewing.

In selecting the methodology and, thus, the hardware for achieving the signal interpretation, a balance had to be found between the financial budget for building the scanner and the advantages of having a sophisticated equipment set up.

The deciding item of equipment when it came to a methodology of signal interpretation, was the transducer control unit (ie: that sends, receives and filters the ultrasonic signal). the sophistication of this unit would determine the equipment needed to do the end-processing of the signal.

Transducer control units are specialist equipment and would have to be purchased from inspection-related companies. The equipment presently on the market ranges from portable analogue units (eg: Krautkramer USK7s units) to the digitised, self-analyzing testing systems

(eg: Krautkramer IMPULS 1 unit).

A company presently involved in manual inspection of heat exchanger tube sheets would probably already have a portable, analogue unit. As this unit would not have any means of digitising and sending a signal to a computer terminal, additional equipment would be needed to transfer the signal to the processing computer.

Two options for this purpose were investigated. Firstly, an analogue to digital (AD) card could have been used to transfer the data straight from the transducer control units display circuits into the computers memory. The specifications for such a card would have been:

Total time for signal capture :		20micro seconds
No. of data points	:	250
Therefore,		
rate of capture	:	80 nano seconds
Frequency of card	:	12.5 MHz

A 20 MHz card with 8 Mbytes of RAM memory would cost approximately R14 250. The card could be activated by the computers's software. Once the required data had been collected, it could be transferred to the computer's memory for analysis.

Secondly, a digital oscilloscope could be used. It's function would be much the same as the digital AD card. However, it offered extra functions, such as querying signal peaks, before actual capturing of the signal. This made the hardware set up more "user-friendly" and also reduced the software requirements.

Thus, between the AD card and an oscilloscope, the latter would be selected.

If the company did not have an existing transducer control unit, then a more sophisticated unit (from the range of a Krautkramer USK7D to the IMPULS 1) could possibly be selected. Such a unit would be able to control the transducer signals, select the required signal envelope for

interpretation and digitally transmit the results to the processing computer. This would remove the necessity for a digital oscilloscope.

Thus, the selection of a transducer control unit would depend largely on the company's existing equipment and its budget for the scanner manufacture. The difference in set ups, as shown in figures 4.8 and 4.9, would not have any significant effect on the speed or quality of the final signal that was transferred to the scanner. The only consideration is that it would mean extra equipment to move if a digital oscilloscope was required.

Software for signal interpretation

The software developed for the CNC model had proved sufficient for the final scanner, given minor changes to allow for the driving of three SLOSYN motors (CNC model used one motor plus controlled the CNC's movements).

One modification would be made: a B-scan image could easily be produced and displayed from the information collected. An image of the tube surface could be graphically displayed. As the probe scanned the tube surface, irregularities could be marked on the graphical image, giving an indication of the size and extent of defects in the tube weld. A C-scan would not be reliably produced as the depth of the irregularities is hard to determine from the multiplicity of signal types received.

4.3 SUMMARY OF DESIGN SPECIFICATIONS FOR PROPOSED SCANNER

The following specifications were calculated for a scanner device constructed as in figures 4.1 to 4.7. These specifications are a summary of the theoretical checks done to ensure that the expected performance of the scanner would meet the criteria necessary to overcome the present problems as detailed in section 1.4.3.

4.3.1 Theoretical operational speed

The following are key indicators of the scanner's performance:

- Time taken to scan one tube opening
- Time taken to move probe between adjacent tube openings
- Time to scan entire tube sheet

Time taken to scan one tube

Assuming the following data:

*	Stroke distance of probe on Z axis on PIM (ie: distance to move probe vertically into tube opening	0.075 m
*	Inner diameter of tube opening	0.036 m
*	Rotational angle between scans (assuming a 25% overlap between consecutive scan sites)	9°
*	Pitch on lead screw on motor #3 (PIM)	100 revs/m

From the above data, the time taken to scan one hole was calculated as:

ACTIVITY	TIME FOR ACTIVITY (Sec)	NO. OF ACTIVITIES PER SCAN	TOTAL TIME (Sec)
Probe entering hole	1.00	1	1.00
Probe moving against wall	0.25	1	0.25
Receive scan info at scan site	0.18	40	7.20
Move to next scan site	0.07	40	2.80
Probe to centre of hole	0.25	1	0.25
Probe exiting hole	1.00	1	1.00
TOTAL TIME			**12.5**

Note that the time taken to receive information (ie: send ultrasonic pulse and interpret returned signal) was averaged from results obtained during scanning tests using CNC model.

Time taken to move probe between adjacent tube openings

The time taken for this activity can be expressed as :

(Time to accelerate PIM to maximum lateral speed) +
(Time to move PIM at max. speed) +
(Time to decelerate PIM)

Assuming a maximum speed of 1 500 steps/second by stepper motor #1 and #2, the maximum lateral speed of 0.075 m/s was calculated. Note that speeds beyond 1 500 steps/min compromise the reliability of the motor controls to receive all step commands from the output port of the 386PC.

To move the PIM between adjacent tube openings, either motor 1 or 2 will be used to move the horizontal arm and PIM respectively. As the horizontal arm had the larger inertial mass, the following data assumed that the horizontal arm alone moves the PIM between tube openings - assumed to be a lateral distance of 0.10 m.

It can be shown that the torque required from the motor will be:

$$T_{acceleration} = 1/g^* (J_{load}/e + J_{lead\ screw} + J_{motor\ rotor}) *w/t$$

where e = Efficiency of lead screw
J = Inertial mass (Nm^2)
w = Angular velocity of lead screw
t = Time taken to accelerate load from standstill to max. speed

For the horizontal arm defined in section 4.2, the following was calculated:

$J_{load} = W/ (2\Pi p) = 2.64 * 10^{-4}$ W = weight of load
p = pitch of lead screw

$J_{leadscrew} = (\Pi L d R^4)/2 = 5.82 * 10^{-5}$ L = Length of lead screw
d = Density of lead screw material
R = radius of lead screw

$J_{motor} = 1.18 * 10^{-4}$ (Given in Manufacturers specifications)

Thus, the time taken to accelerate (and decelerate) was found to be 1.14 ms. As the maximum lateral speed was 0.075 m/s, the total time for the probe to traverse between to tube openings (0.1 m apart) would be less than 1.35 seconds.

Time taken to scan entire tube sheet

From the above data, the total time to scan a tube surface and then move to the next tube opening was 13.85 seconds. Each tube sheet has 980 tube openings. Thus, the total time to scan a tube sheet was calculated to be:

Time to scan holes	12 250 (seconds)
Time to move between holes	1 323
Time to relocate scanner	2 400
Total time to scan tubesheet	**15 973 seconds** (4.1 hours)

Note: From analysis of the tubesheet configuration versus the size of the scanner proposed, it was estimated that a total of eight scanner relocations were necessary.

4.3.2 Theoretical mass of scanner

The mass of the scanner was estimated to be 18.7 kg. This is below the 20kg limit originally set as a criterion for easy relocation of the scanner.

Thus, it is concluded that the proposed scanner will fully overcome the problems being experienced with the present scanning methods, as described in section 1.4.3.

RECOMMENDATIONS

Based on the findings of the research and the conclusions made in this document, the following recommendations are made. Note that all recommendations pertain to future work that may be carried out to further define the operational ability of the proposed scanner.

R.1 Construction of the scanner

The scanner should be constructed according to the diagrams given in figures 4.1 to 4.7. The signal interpretation equipment used in the CNC scanning model can be applied, without modification, to the scanner. The software will have to be modified to accommodate the change in drives from the CNC wrist mechanism to the scanner. However, the software for signal interpretation can remain as is from the CNC model for preliminary tests.

From this, the exact operation of the scanner could be assessed. The scanning speed calculations could be verified. Furthermore, the PIM as described in chapter 4 could be tested. Lastly, the operational scan success rate could be tested with a greater number of scans that was possible in the CNC model.

R.2 Signal interpretation

The signal interpretation software used in the CNC model was found to be sufficient for locating flaws. However, the sizing of flaws was inaccurate and the identification of the shape and orientation was impossible with the limited information available.

An attempt could be made to improve upon the scanner's ability to detect the true edge of flaws. This, along with a suitable algorithm, could greatly increase the accuracy of the flaw size determination.

Furthermore, more diverse scanning techniques, involving different or multiple probe usage, could allow the shape and orientation of the flaws to be detected. This could aid the operating technician to determine the primary cause of the flaw.

R.3 Information Capturing

In an effort to increase the scanning speed of the setup, alternative ways of capturing the signal and transferring the information from the Ultrasonic Inspection Equipment could be investigated. The proposed equipment, as used in the CNC model, was based on readily available equipment on the market. These alternative equipment choices have been discussed in chapter 4 and mainly need justification from a financial point of view.

REFERENCES

[1] J. Krautkramer et al, *Ultrasonic testing of materials*, second ed. (Springer-Verlag, 1977).

[2] "Eddy Current Inspection", rev. by the ASM committee on Eddy current inspection, in *ASM Handbook*, pg 164-194.

[3] "Ultrasonic Inspection", rev. Y. Bar-Cohen et al, in *ASM Handbook*, pg 231-277.

[4] T.K. Locket, "Lamb and Torsional waves and their use in flaw detection in tubes", *Ultrasonics*, Jan, 1973, pg 31-37.

[5] T. F. Hueler and R.F. Bolt, *Sonics*, (New York: John Wiley & Sons Inc, 1955), citied by ref 6.

[6] R. C. McMaster ed, *Nondestructive testing handbook*, (Ronald Press Co, New York, 1959)

[7] H. kolsk, *Stress waves in solids*, (Oxford University Press, 1953), citied by ref.6.

[8] H. L. Whaley et al, "Ultrasonic Frequency Analysis", in *Oak Ridge National Laboritory Technical report ORNL-TM-2655*, citied by ref 5.

[9] G.A. Alders et al, "Ultrasonic techniques for measuring the strength of adhesive bonds", *Material Evaluation*, April, 1977, pg 77-84, citied by ref 5.

[10] E.A. Lloyd, "Nondestructive testing of Bonded Joints", *Nondestructive testing*, (London), Dec, 1974, pg 331-334, citied by ref 5.

[11] B. Harris-Maddox, "The identification of weld defects by ultrasonic methods", *Ultrasonics*, Oct-Dec, 1963, pg 189-193.

[12] "Weldements, Brazed assemblies, and soldered joints", in *ASM Handbook*, pg 582-605.

[13] V.G. Shcherbinskii and V.E. Belyi, "Identification of plane and volume defects in welds during ultrasonic flaw detection", *Russian Ultrasonics*, vol 5, no 1, 1975, pg 9-11.

[14] F. K. Lam and W. M. Tsang, "Flaw characterisation based on the diffraction of ultrasonic waves", *Ultrasonics*, Jan 1985, pg 14-20.

[15] V.F. Dianov, "Reproducibility of results from the ultrasonic monitoring of welds in boiler surface tubes", *Russian Ultrasonics*, vol 7, no 3, 1977, pg 111-116.

[16] P.A. Doyle and C.M Scala, "Crack depth measurement by ultrasonics - a review", *Ultrasonics*, July, 1978, pg 164-169.

[17] "Testing tubes from the bore", author unkown, *Ultrasonics*, Oct-Dec, 1964, pg 209-210.

[18] "Automated weld inspection", author unknown, *Ultrasonics*, July, 1978, pg 150.

[19] "Automated testing for dutch nuclear power plant", author unknown, *Ultrasonics*, Sept, 1976, pg 198.

[20] "Inspection system for nuclear power station", author unknown, *Ultrasonics*, Sept, 1978, pg 199.

[21] P. Woodborne, "Ultrasonic inspection of reator pressure valve", *The South African Mechanical Engineer*, vol43, July, 1993, pg 200-202.

[22] M.I. Maizenberg and S.V. Veremeenko, "Ultrasonic equipment for automated monitoring of tubes", *Russian Ultrasonics*, vol7, no 1, 1977, pg 53-55.

[23] S.V. Veremeenko et al, "Automated ultrasonic equipment, ATLAT-1, for comprehensive testing of especially thin-walled small diameter tubes", *Russian Ultrasonics*, vol 14, no 1, 1984, pg 43-50.

[24] V. G. Brandorf et al, "Automatic system for ultrasonic flaw inspection of large articles", *Russian Ultrasonics*, vol 16, no 3, 1986, pg 58-59.

[25] K.J Michaels et al, *Computerised shear wave technique for detecting and characterising welding defects*, in Proceedings of the sixteenth Symposium on NDE, April 21-23, 1987. Printed by NTIAC, Southwest Research Inst., San Antonio, Texas

[26] N. A. Cambell et al, *Short's robotic ultrasonic scanning system*, Shorts Brothers, presented in "U.K. Robotics Research 1984", IMech Conference Publications 1984\15

[27] D. Dobbeni and C. Van Melsen, "Inspecting steam with a fully automated polar manipulator", *Nuclear Engineering International*, June, 1984, pg 43-45.

[28] "Rosa's strong arm approach to dose reduction", author unknown, in *Nuclear Engineering International*, April, 1985, pg 29.

[29] Roger: a no-jump manipulator for steam generators", author unknown, in *Nuclear Engineering International*, April, 1985, pg 30.

[30] B.W Nuclear Services Company, Brochure on Cobra manipulator

[31] "Five years experience with the Vermaat manipulator", author unknown, in *Nuclear Engineering International*, April, 1985, pg 31.

[32] Intercontrôle Ltd, Brochure on Bikinic manipulator.

[33] Intercontrôle Ltd, Brochure on Ritmic manipulator.

[34] Paul, R, "Robot Manipulators, Mathematics, Programming and Control, 1981, pg 37-86.

BIBLIOGRAPHY

[1] John D Wood, ed, *Guide to Nodestructive Evaluation techniques*, (Lehigh University), ASM handbook, volume 17, pg 49-52, printed by ASM international, May 1992.

[2] N. A. Cambell et al, *Short's robotic ultrasonic scanning system*, Shorts Brothers, presented in "U.K. Robotics Research 1984", IMech Conference Publications 1984\15

[3] K.J Michaels et al, *Computerised shear wave technique for detecting and characterising welding defects*, in Proceedings of the sixteenth Symposium on NDE, April 21-23, 1987. Printed by NTIAC, Southwest Research Inst., San Antonio, Texas

[4] J. A. Brunk, *Performance comparisons of dry coupling with conventional contact ultrasonic transducers, 0.5 Mhz - 20 Mhz*, Ultran Laboritories, in Proceedings of the sixteenth Symposium on NDE, April 21-23, 1987. Printed by NTIAC, Southwest Research Inst., San Antonio, Texas

[5] D. W. Fitting et al, *Ultrasonic Spectral Analysis for NDE*", (Plenium Press, New York, 1981)

[6] R. C. McMaster ed, *Nondestructive testing handbook*, (Ronald Press Co, New York, 1959)

[7] Troitskii V. A. and Bondarenko Yu. K., "Ultrasonic flaw detection testing of welded joints - a review", *Russian Ultrasonics*, vol13, no 4, 1983, pg 151-158

[8] *De Road, Automatic ultrasonic examination of welds*, in Seventh Intern. Conf. on NDT, Warsaw, 1973, pg 49-53, cited by ref 7.

[9] H. I. Meyer, "Ultraschallprufung von Schweissnahten und Wandugen in Druck behaltezbau in Hisieht auf Mechanierung und Automatisierung des Prufublaufes", *Materialprufung*, Vol 12, 1970, pg 330-336, citied by ref 7.

[10] L. F. Lovelace and L. A. Luini, "Theory applied to the automatic inspection of welds", *Material Evaluation*, Vol 26, 1968, pg 204-211, citied by ref 7.

[11] G. Zossengeiner, "Organisation of research and development in the field of welding in the FRG", *Automat. Svarka*, no 5, 1981, pg 47-51, citied through ref 7.

[12] V. L. Koryachenko, I.I. Fak and A. A. Tkachenko, "Increasing the reliability of results for automated ultrasonic testing of welds in large-diameter tubes", *Russian Ultrasonics*, 1981, pg 115-118.

[13] M. Shkarlet, *Remote method of ultrasonic testing* (in russian), Yu. Mashinostroenie, Moscow, pg 56, 1974, citied by ref 7.

[14] V. G. Brandorf et al, "Automatic system for ultrasonic flaw inspection of large articles", *Russian Ultrasonics*, vol 16, no 3, 1986, pg 58-59.

[15] Yu. K. Bondarenko and L. N. Vasil'er, "Distinguishing defects in the ultrasonic monitoring of the quality of welded seams", *Russian Ultrasonics*, vol 7, no3, 1977, pg 100-103.

[16] I. G. Babkin et al, "Automation of ultrasonic testing of welded joints", *Russian Ultrasonics*, vol 5, no3, 1975, pg 98-102.

[17] M.I. Maizenberg and S.V. Veremeenko, "Ultrasonic equipment for automated monitoring of tubes", *Russian Ultrasonics*, vol7, no 1, 1977, pg 53-55.

[18] S.V. Veremeenko et al, "Automated ultrasonic equipment, ATLAT-1, for comprehensive testing of especially thin-walled small diameter tubes", *Russian Ultrasonics*, vol 14, no 1, 1984, pg 43-50.

[19] "Testing tubes from the bore", author unkown, *Ultrasonics*, Oct-Dec, 1964, pg 209-210.

[20] "Automated testing for dutch nuclear power plant", author unknown, *Ultrasonics*, Sept, 1976, pg 198.

[21] "Linear actuators in automated NDT sustem", author unknown, *Ultrasonics*, vol 26, Nov, 1988, pg 359.

[22] "Software-based scanner", author unknown, *Ultrasonics*, July, 1982, pg 149.

[23] P. Woodborne, "Ultrasonic inspection of reator pressure valve", *The South African Mechanical Engineer*, vol43, July, 1993, pg 200-202.

[24] "Automated weld inspection", author unknown, *Ultrasonics*, July, 1978, pg 150.

[25] "Computer-controlled flaw detection", author unknown, *Ultrasonics*, Jan, 1980, pg 5-6.

[26] "Inspection system for nuclear power station", author unknown, *Ultrasonics*, May, 1980, pg 105-106.

[27] "Inspection system for nuclear power station", author unknown, *Ultrasonics*, Sept, 1978, pg 199.

[28] P.L. Primrose and R. Leonard, "Incorporating the 'intangible' benefits of robots within a comprehensive financial evaluation", in *UK Robotics Research 1984 report no C478/84* , pg 115-119, presented at IMech Conf. held in London, Dec 1984.

[29] W.D.H. Blackman, "Economic consiferations applied to ATE", in *Report on the Automation of testing*, pg 176-185, IEE Conf. publication no 91.

[30] L.T. Michaels and L.A. Quintrell, "Cost/ Benefit", in *Robotics Encyclopaedia*, vol 1, pg 288-293.

[31] "Tubular Products", author unknown, in *ASM Handbook*, pg 561-581.

[32] "Ultrasonic Inspection", rev. Y. Bar-Cohen et al, in *ASM Handbook*, pg 231-277.

[33] W.C. Harmon and T.W. Judd, "Ultrasonic test system for longitudinal fusion welds in pipe", *Material Evaluation*, March 1974, pg 45-49, citied by ref 31.

[34] "Inspection, Radiographic", Military Standard 453A, May, 1962, citied by ref 31.

[35] N.P. Aleskin et al, "Ultrasonic testing of welds in boiler tubes", *Russian Ultrasonics*, vol 7, no 3, 1977, pg 106-110.

[36] V.F. Dianov, "Reproducibility of results from the ultrasonic monitoring of welds in boiler surface tubes", *Russian Ultrasonics*, vol 7, no 3, 1977, pg 111-116.

[37] Hegean Kwun et al, "Ultrasonic transducers, performance variability, design and manufacturing procedures", Southwest Research Institute Technical Report, Texas, August 1984.

[38] J.R. Brewster and K.H.G Ashbee, "Further insight into the potential role of shear wave caustics in NDE of rods and pipes", *Ultrasonics*, vol 29, May, 1991, pg 252-256.

[41] "Weldements, Brazed assemblies, and soldered joints", in *ASM Handbook*, pg 582-605.

[42] J. Krautkramer et al, *Ultrasonic testing of materials*, second ed. (Springer-Verlag, 1977).

[43] "Liquid Penetration Inspection", rev. J.S. Borucki et al, in *ASM Handbook*, pg 71-89.

[44] "Magnetic Particle Inspection", Rev. Art Lindgen, in *ASM Handbook*, 89-122.

[45] "Leak Testing", rev G.L. Anderson, in *ASM Handbook*, pg 57-71.

[46] "Eddy Current Inspection", rev. by the ASM committee on Eddy current inspection, in *ASM Handbook*, pg 164-194.

[47] H. Houserman, "Multifrequency techniques", citied by ref 46.

[48] "Remote-field eddy current inspection", J.L. Fisher, in *ASM Handbook*, pg 195-202.

[49] T.K. Locket, "Lamb and Torsional waves and their use in flaw detection in tubes", *Ultrasonics*, Jan, 1973, pg 31-37.

[50] H. Kolksk, *Stress waves in solids*, (Oxford Unersity Press, 1953), citied by ref 6.

[51] T. F. Hueler and R.F. Bolt, *Sonics*, (New York: John Wiley & Sons Inc, 1955), citied by ref 6.

[52] M.G. Silk, *Ultrasonic transducers for nondestructive testing*, (Bristol, Adam Hilger Ltd, 1984).

[54] J.A. Ogilvy, "Model for the ultrasonic inspection of rough defects", *Ultrasonics*, vol 27, March, 1989, pg 69-77.

[55] J. Moysan et al, "Crack-like defect detection and sizing from image segmentation through co-occurence matrix analysis", *Ultrasonics*, vol 30, no 6, 1992, pg 359-363.

[56] R.S. Sharp ed, *Research Techniques in NDT,* vol III, Chap 1, (Academic Press, New York, 1977), citied by ref 58.

[57] G.S. Mills, "Time Domain Analysis of Ultrasonic pulse diffraction for defect characterisation", *Material Evaluation*, no 34, 1974, pg 256-258.

[58] F. K. Lam and W. M. Tsang, "Flaw characterisation based on the diffraction of ultrasonic waves", *Ultrasonics*, Jan 1985, pg 14-20.

[59] O.R. Gericke, "Spectrum and Contour analysis of Ultrasonic Pulses for Improved NDT", in *Watertown Arsenal Laboritories Technical report WAL TR 830.5/1*, 1960, citied by ref 5.

[60] G.A. Alders et al, "Ultrasonic techniques for measuring the strength of adhesive bonds", *Material Evaluation*, April, 1977, pg 77-84, citied by ref 5.

[61] H. L. Whaley et al, "Ultrasonic Frequency Analysis", in *Oak Ridge National Laboritory Technical report ORNL-TM-2655*, citied by ref 5.

[62] E.A. Lloyd, "Nondestructive testing of Bonded Joints", *Nondestructive testing*, (London), Dec, 1974, pg 331-334, citied by ref 5.

[63] B. Harris-Maddox, "The identification of weld defects by ultrasonic methods", *Ultrasonics*, Oct-Dec, 1963, pg 189-193.

[64] J.A. Ogilvy, "Ultrasonic reflection properties of planar defects within austenitic welds", *Ultrasonics*, vol 26, Nov, 1988, pg 318-327.

[65] V.V. Gor'skii et al, "Increasing the information obtained from ultrasonic monitoring of butt welds with a perminent backing ring", *Russian Ultrasonics*, vol 12, no 4, 1982, pg 122-125.

[66] V.A. KozLov and Damilov A.I.,"Ultrasonic monitoring of cutting tool welds", *Russian Ultrasonics*, vol 9, no 3, 1979, pg 166-168.

[67] Shraiber D.S., "Ultrasonic Flaw detection (in Russian)", *Metallurgiya*, Moscow, 1965, citied by ref 66.

[68] V.F. Dianov, "Slide rule for ultrasonic flaw measurements", *Russian Ultrasonics*, vol 5, no4, 1975, pg 167-169.

[69] D. K. Mak, "Ultrasonic methods of measuring crack location, crack height and crack angle", *Ultrasonics*, Sept, 1986, pg 223-226.

[70] P.A. Doyle and C.M Scala, "Crack depth measurement by ultrasonics - a review", *Ultrasonics*, July, 1978, pg 164-169.

[71] V.G. Shcherbinskii and V.E. Belyi, "Identification of plane and volume defects in welds during ultrasonic flaw detection", *Russian Ultrasonics*, vol 5, no 1, 1975, pg 9-11.

[72] Y.K. Bondarenko, "Distinguishing defects in the ultrasonic monitoring of the quality of welded seams", *Russian Ultrasonics*, vol 7, no 3, 1977, pg 100-103.

[73] "Replication Microscoyp Techniques for NDE", rev. A.R.Marder, in *ASM Handbook*, pg 52-56.

[74] "Microwave inspection", rev. W.L. Rollwitz, in *ASM Handbook*, pg 202-229.

[75] M.P. Groover, "Automation", in *Dictionary of Industrial robots*, pg 136-151.

[76] "Radiographic Inspection", rev. ASM Committee on Radiographic inspection, in *ASM Handbook*, pg 295-326.

[77] D. Dobbeni and C. Van Melsen, "Inspecting steam with a fully automated polar manipulator", *Nuclear Engineering International*, June, 1984, pg 43-45.

[78] "Rosa's strong arm approach to dose reduction", author unknown, in *Nuclear Engineering International*, April, 1985, pg 29.

[79] Roger: a no-jump manipulator for steam generators", author unknown, in *Nuclear Engineering International*, April, 1985, pg 30.

[80] "Five years experience with the Vermaat manipulator", author unknown, in *Nuclear Engineering International*, April, 1985, pg 31.

[81] B.W Nuclear Services Company, Brochure on Cobra manipulator

[81] Intercontrôle Ltd, Brochure on Bikinic manipulator.

[83] Intercontrôle Ltd, Brochure on Ritmic manipulator.

[84] "Magabsorption NDE", rev W.L. Rollwitz, in *ASM Handbook*, pg 143-159.

APPENDIX A1

SPECIFICATIONS OF THE SCORBOT-ER III

Model:	-ER III
Power requirements:	110/220 V.A.C. 60/50 Hz
No. of axes	
-mechanical arm:	5 plus gripper
-controller:	7 plus gripper
Controlled axes:	8 (7 plus gripper)
Construction:	Articulated arm
Load capacity:	1 kg (2.2 lbs.)
Repeatability:	0.5 mm (0.02 ins.)
Speed:	Fast and slow speeds
Maximum speed:	330 mms. per second (13.2 ins. per second)
Actuators:	6 D.C. Servo motors with closed loop control
Feedback:	Optical encoders on all axes
Working envelope:	Body joint - 340° Shoulder joint - ± 85° Elbow joint - ± 150° Pitch joint - ± 150° Roll joint - unlimited Maximum radius of operation - 610 mms.(24.4 ins.)
Inputs/Outputs:	8 inputs (2 didactic) 8 outputs (4 with relays)
Gripper opening:	75 mm (3 ins.) (excluding rubber pads) 65 mm (2.5 ins.) (with rubber pads)
Sensors:	Gripper can measure object's size
Transmission:	Gears, timing belts and leadscrew.
Communication interface:	RS - 232C

Programming language:	SCORBASE (interactive menu in 3 levels)
No. of programming lines:	400
Hard home:	Fixed reference positions on all ~~axes~~
Self diagnostics:	Internal diagnostics test on all motors
Weight:	16 Kgs (35 lbs.)
Accessories:	Teach pendant, motor kit, conveyor, rotary table, laboratory experiment set
Safety features:	Motors stop automatically should robot arm strike obstacle without loss of data from memory. Immediate brake - user can stop robot immediately without any loss of data from memory. Encoders and all 'live' components are totally enclosed.

APPENDIX A2

SPECIFICATIONS FOR DA 312 ULTRASONIC PROBE

Manufacturer:	Krautkramer
Test frequency (fe):	10 ± 1 MHz
Focal distance (F):	3 ± 1 mm (steel)
Focal width (FB_6):	0.8 ± 0.2 mm
Focal length (FL_6):	1.3 ± 0.3 mm
Max. allowable wear (Mz):	1.5 mm
Working temperature range (Ta)	-20 + 60 °C

APPENDIX A.3

SPECIFICATIONS OF THE USM2 FLAW DETECTOR

Depth range:	0.5 - 12 MHz by wide-band amplifier continually variable from 10 mm to 5 m (steel).
Gain:	With stepped-switch, in 2 dB steps, adjustable from 0 - 80 dB (40 Db can be switched to 0 -40, 20 -60 or 40 - 80 dB.)
Instrument sensitivity:	maximum 140 ± 3 dB
Monitor response accuracy:	± 0.5 dB
Test method:	ultrasonic-pulse-echo.
Test modes:	single-probe, double-probe and TR-operation.

APPENDIX B1

RESULTS FROM SCANS (CNC MODEL)

1mm hole inspection

- When probe centre was between 2.0 mm and 0.5 mm from edge of defect:
  - 26% drop-off in first backwall echo amplitude (figure B.1)
  - 70% drop-off in secondary backwall echo amplitudes

- When beam centre was directly in line with defect centre:
  - 48% reduction in first backwall echo amplitude with almost complete elimination of secondary backwall echoes (figure B2).
  - 100% increase in amplitude of front wall echo amplitude with slight widening of echo base. (figure B.3)

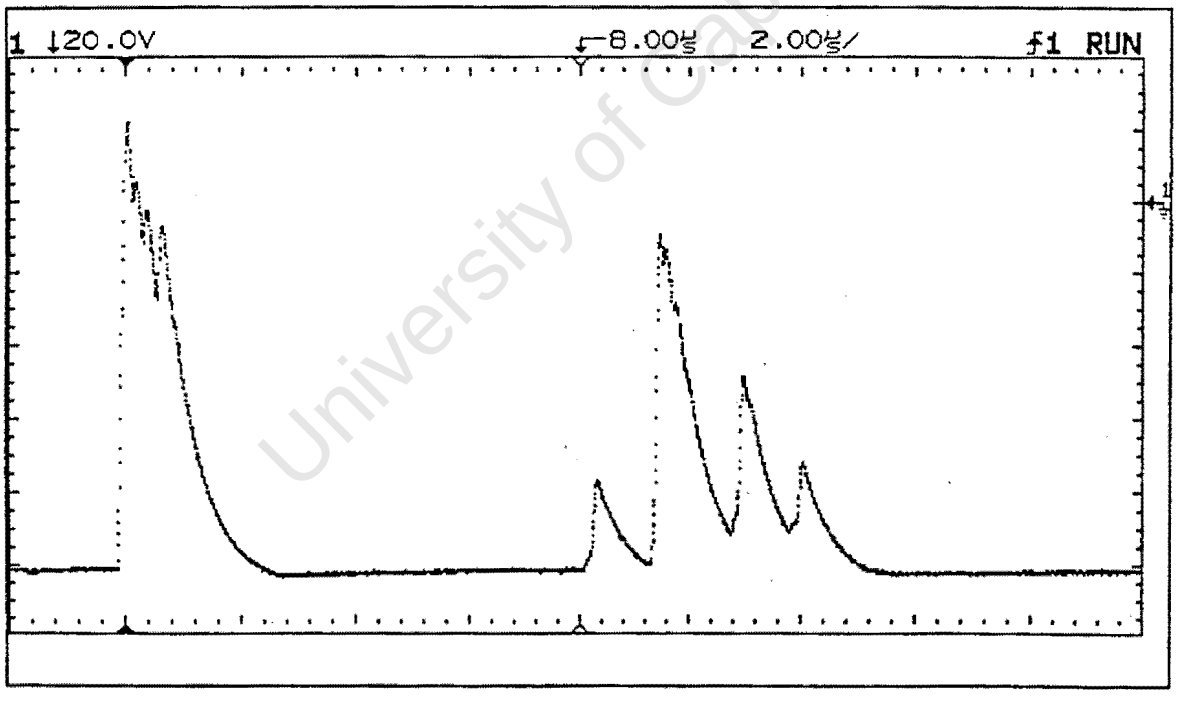

Figure B.1: Ultrasonic return signal from probe; probe off defect completely.

The reduction in the first backwall echo amplitude and the apparent increase in the front wall echo amplitude was due to the sound energy being reflected from the defect surface, approximately 0.4 mm from the front wall surface.

The failure of the trace to show the sound energy reflected by the defect as a separate echo (at a position between that of the front and first backwall echoes on the time base) could have been due the possibility of the non-planar shape of the defect bottom. This would have led to a scattering of the reflected sound energy, shown as the widening of the front wall echo base.

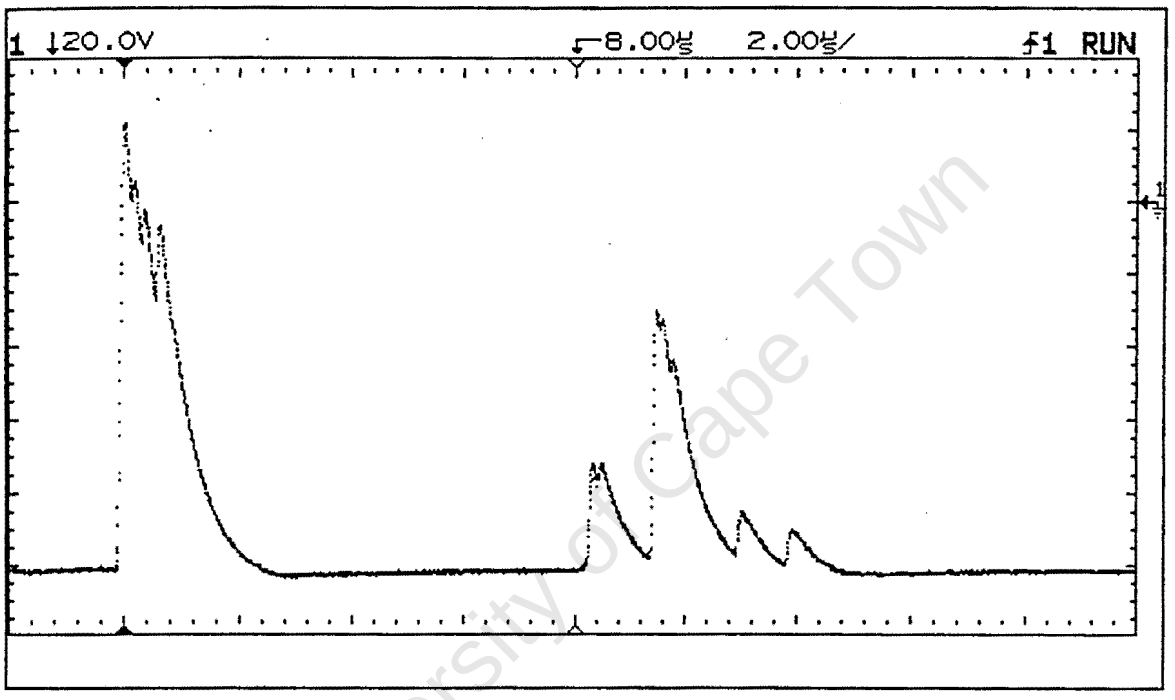

Figure B.2: Ultrasonic return signal from probe; probe centre 1.0 mm from defect centre.

2mm hole inspection

- When beam centre was 0.3mm from defect edge:
  - ☼ 50% drop in first backwall echo amplitude
  - ☼ Elimination of secondary backwall echoes
  - ☼ Formation of intermediate peak of 50% Original First Backwall Echo Amplitude (**OFBEA**). (figure B.4)

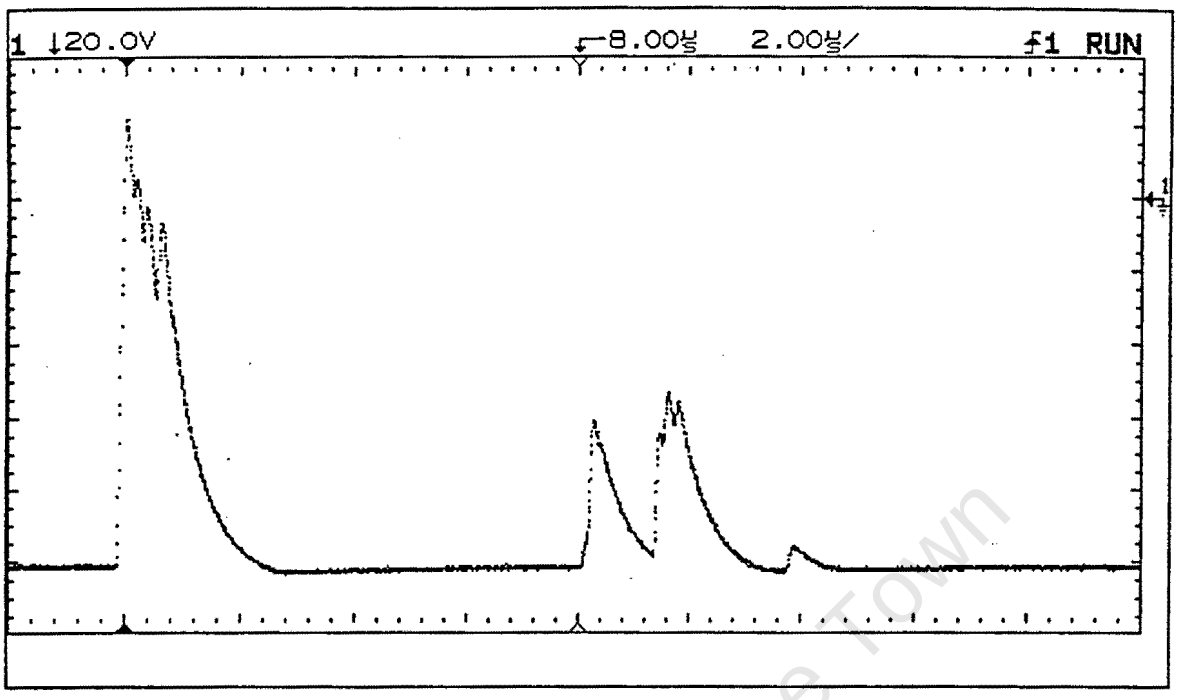

Figure B.3: Ultrasonic return signal from probe; probe centre directly in line with defect centre.

- When beam centre was directly in line with defect centre:
  - ☼ 100% drop-off in first backwall echo amplitude
  - ☼ Intermediate echo amplitude rises to 65% of OFBEA as well as slight widening of base of echo. (figure D.5)

The intermediate echo (figure B.4) is due to the reflected energy from both the front wall and the defect surfaces. The time difference between the intermediate and the first backwall echoes was 800ns. This corresponds to 1.6mm of sound travel in the PVC tube material (vel. of longitudinal sound wave: 2000 m/s) which would indicate that the defect surface was 0.8 mm from the inspection surface (total tube thickness was 1.8mm, thus defect depth was 1.0mm).

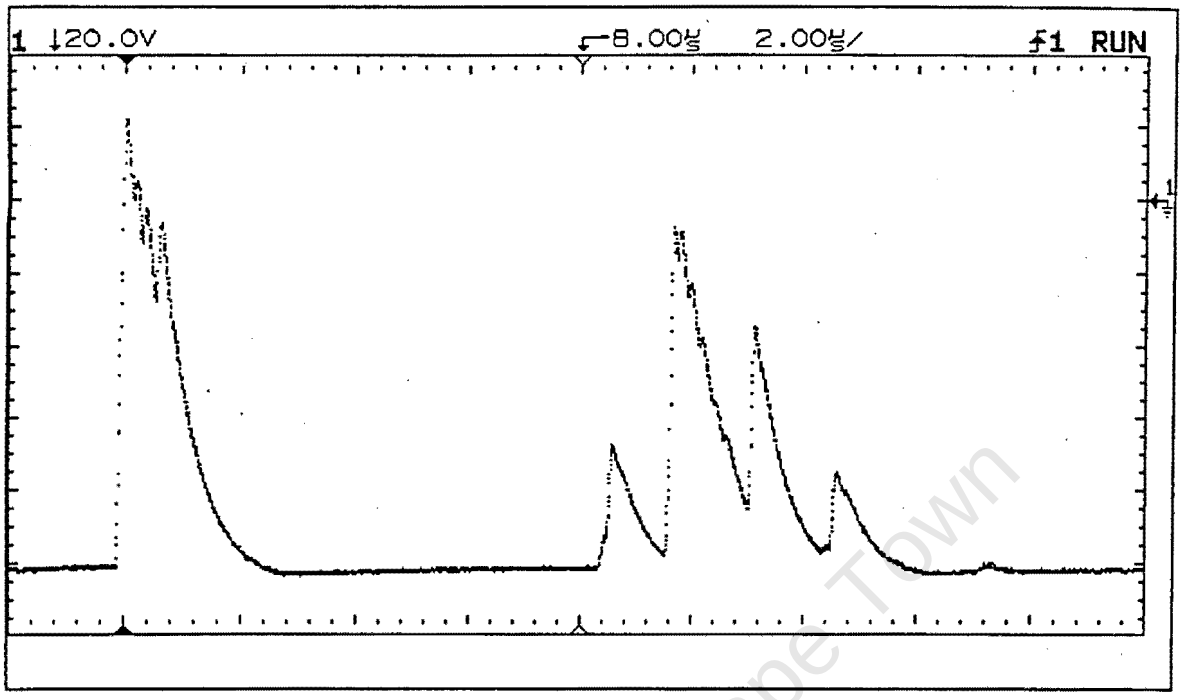

Figure B.4 Ultrasonic return signal from probe; off defect completely.

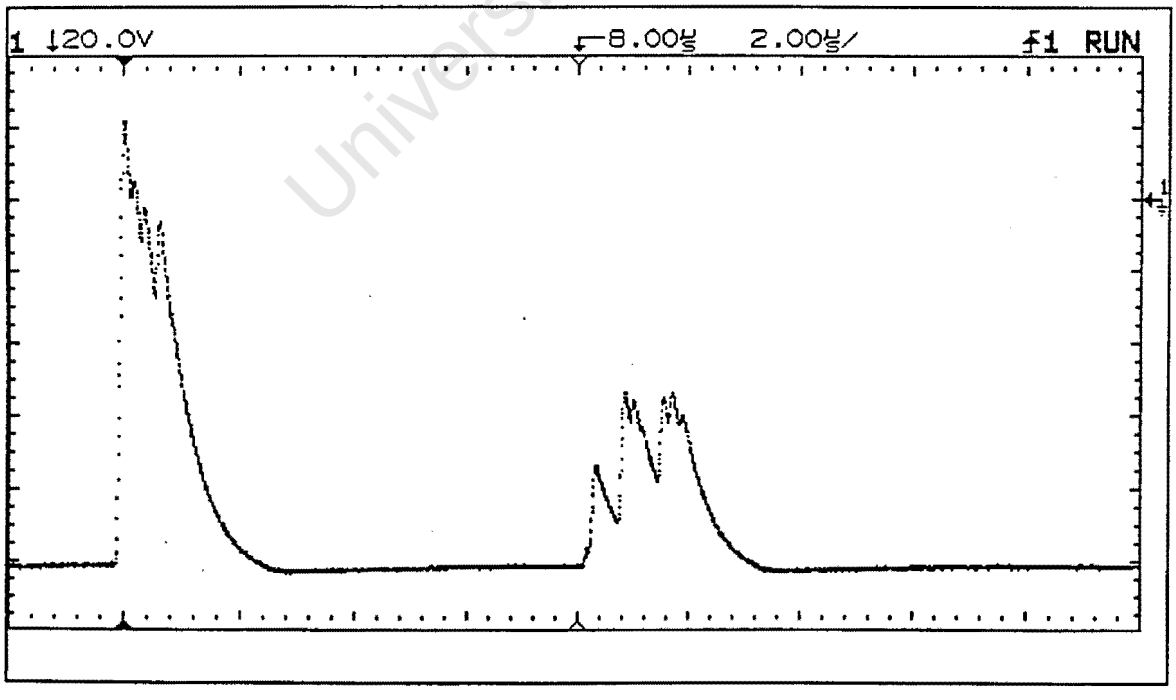

Figure B.5: Ultrasonic return signal from probe; probe centre 1.3 mm from defect centre.

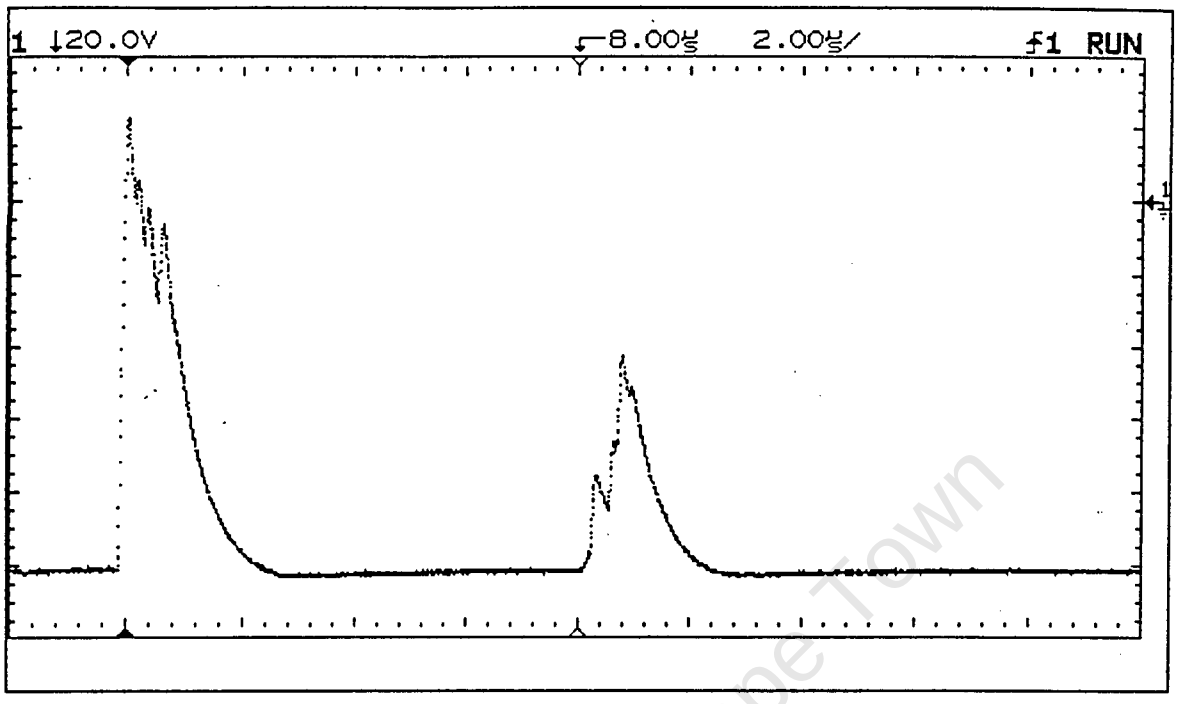

Figure B.6: Ultrasonic return signal from probe; probe centre directly in line with defect centre.

<u>4mm hole inspection</u>

- When probe centre was between 1.8 mm and 0.5 mm from edge of defect: (Fig. B.8)
  - ☼ 20% drop-off in first backwall echo amplitude
  - ☼ Merging of secondary backwall echoes into first backwall echo.
  - ☼ Formation of intermediate echo with a 40% OFBEA at a time position 800ns in front of the first backwall echo.

- When beam centre was directly in line with defect centre: (Fig. B.9)
  - ☼ Merging of front wall, intermediate and all backwall echoes into one single wide-based echo. The echo amplitude was between 60% and 78% of OFBEA.

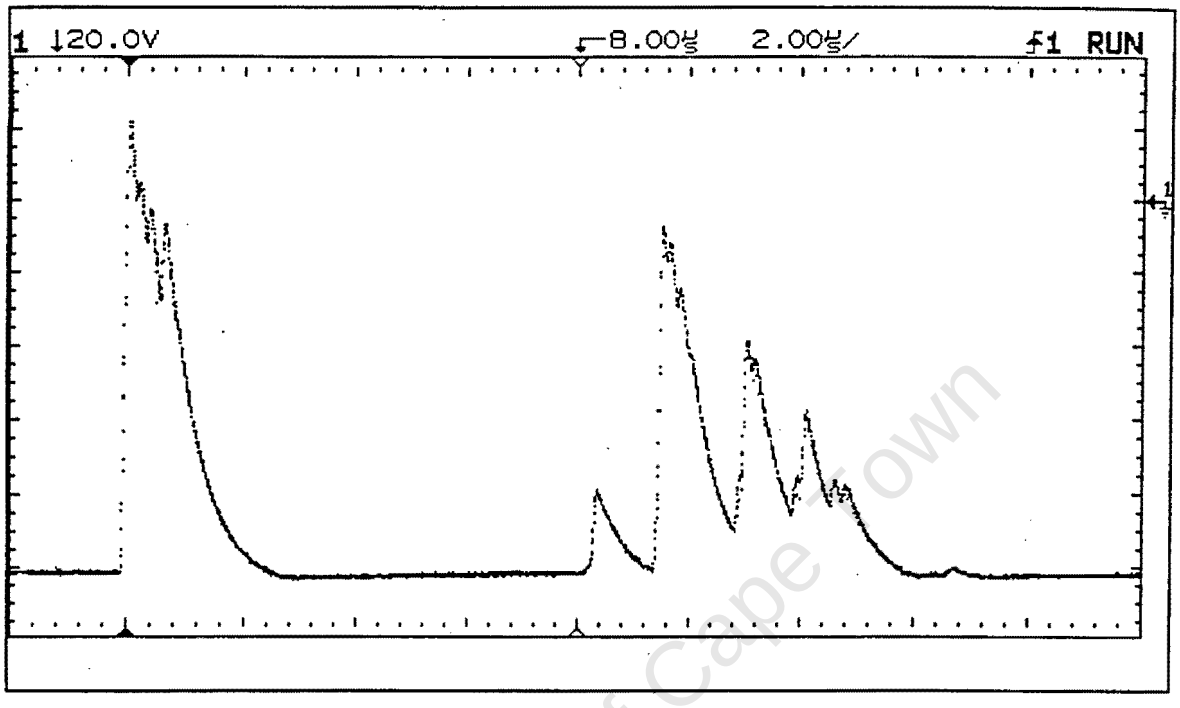

Figure B.7: Ultrasonic return signal from probe; off defect completely.

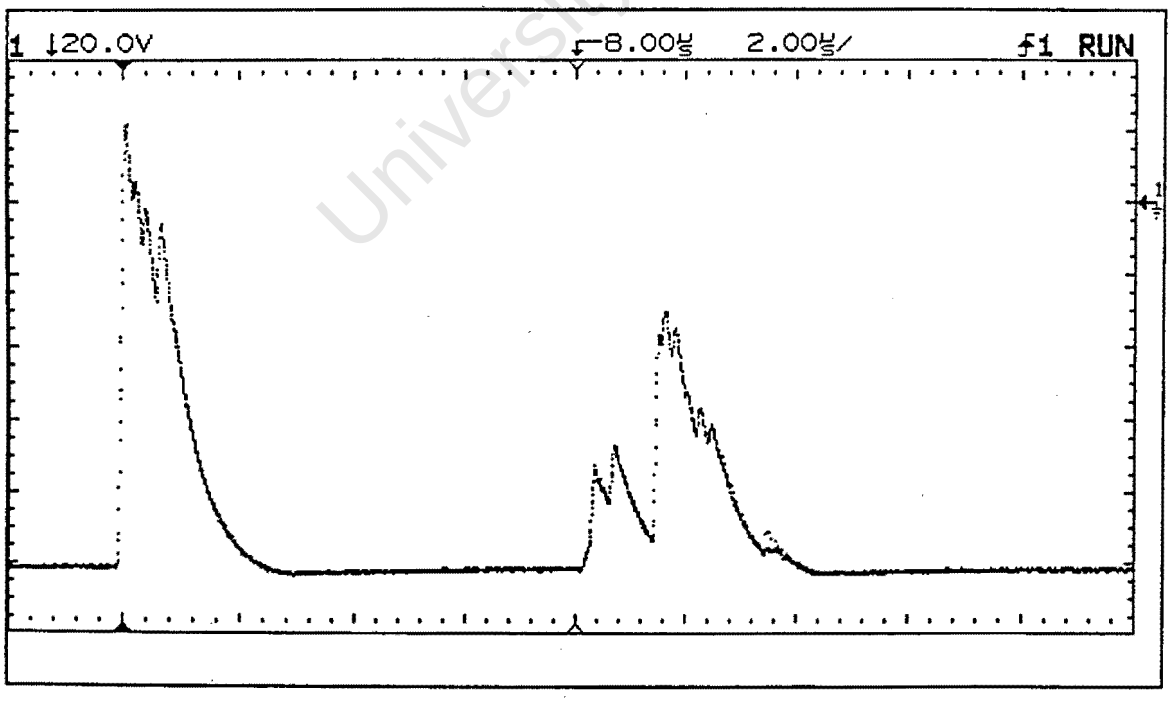

Figure B.8: Ultrasonic return signal from probe; probe centre 1.0 mm from defect centre.

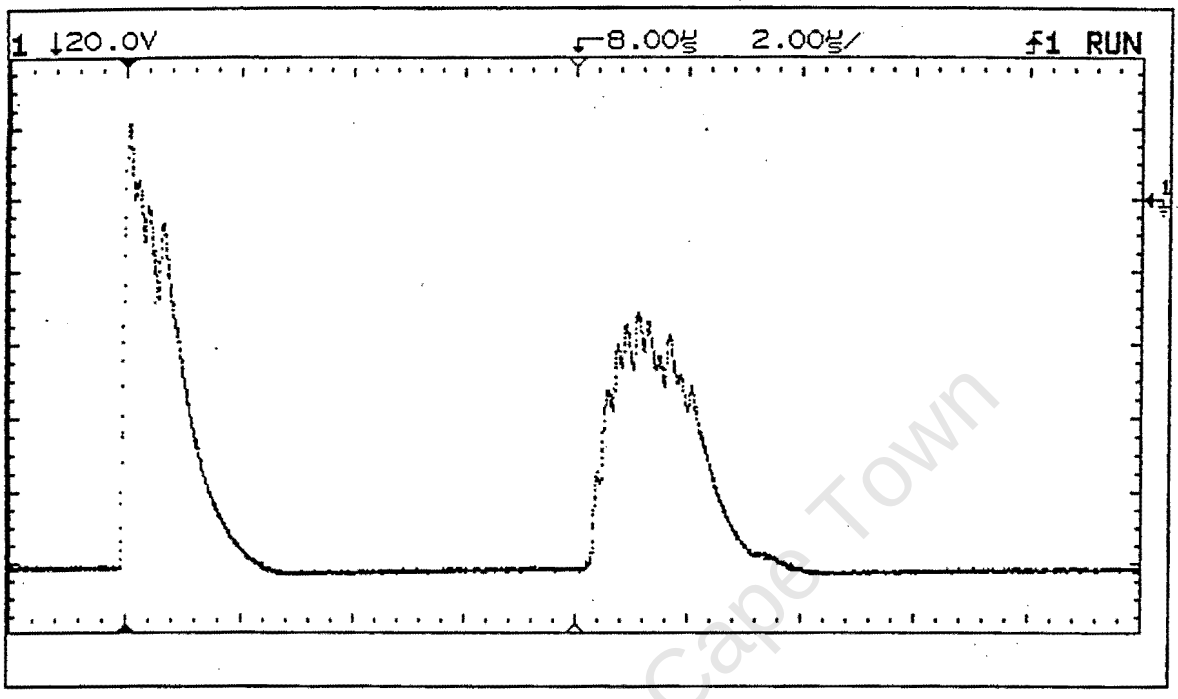

Figure B.9: Ultrasonic return signal from probe; probe centre directly in line with defect centre.

<u>7mm hole inspection</u>

- When probe centre was between 1.5 mm and 0.3 mm from edge of defect:
  - ☼ 40% to 50% drop-off in first backwall echo amplitude and formation of intermediate echo. (figure B.11)
  - ☼ Elimination of secondary backwall echoes
  - ☼ In some instances, merging of front wall, intermediate and first backwall echoes into a single, multi-peaked echo. (figure B.11)

- When beam centre was directly in line with defect centre:
  - ☼ Single, narrow-based echo at a time position of that of the intermediate echo. The echo amplitude was 80% of OFBEA. (Fig. B.12)

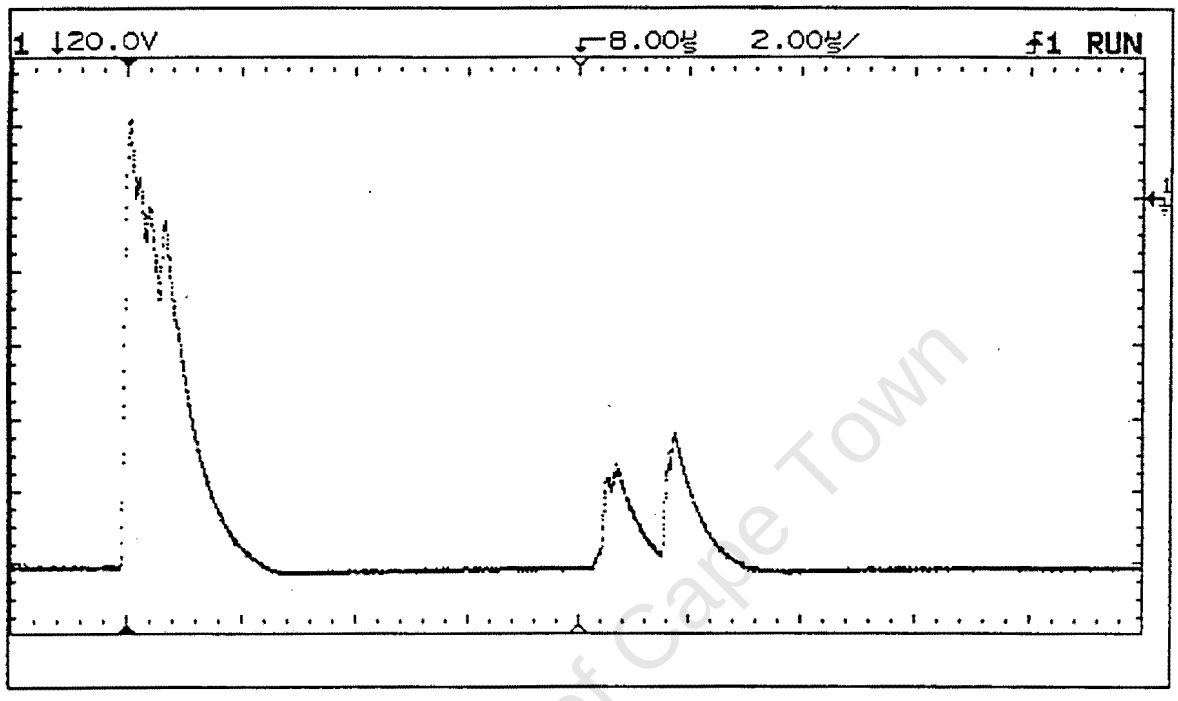

Figure B.10: Ultrasonic return signal from probe; off defect completely.

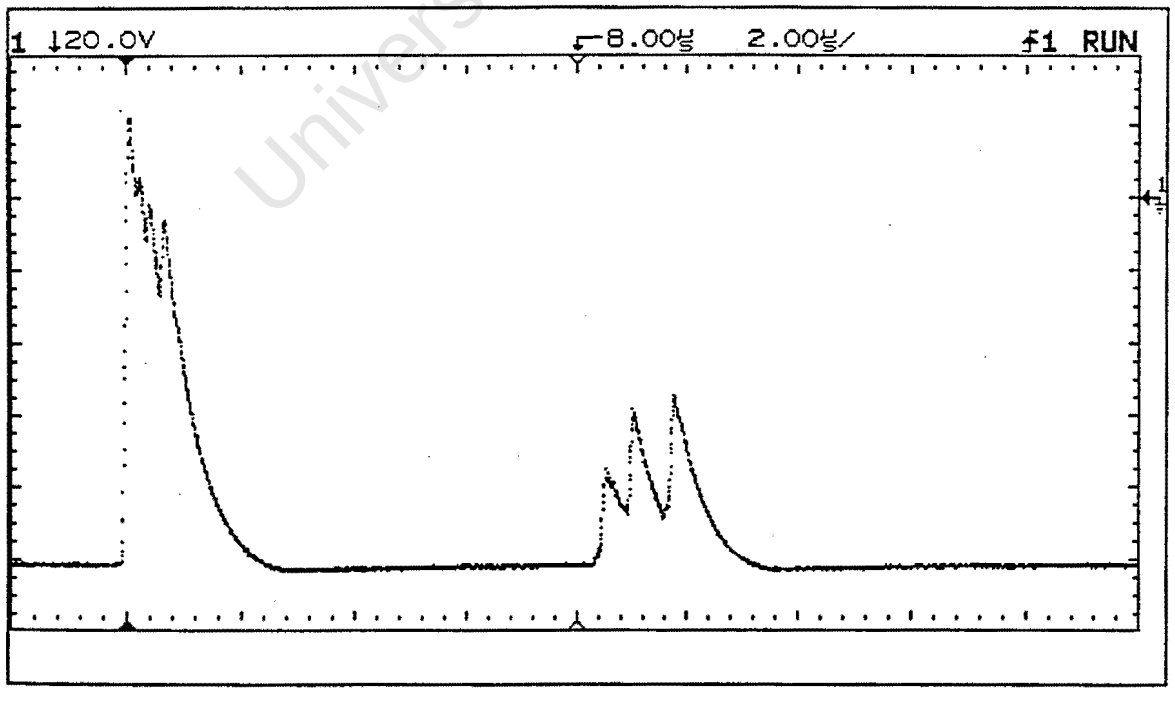

Figure B.11: Ultrasonic return signal from probe; probe centre 1.0 mm from defect centre.

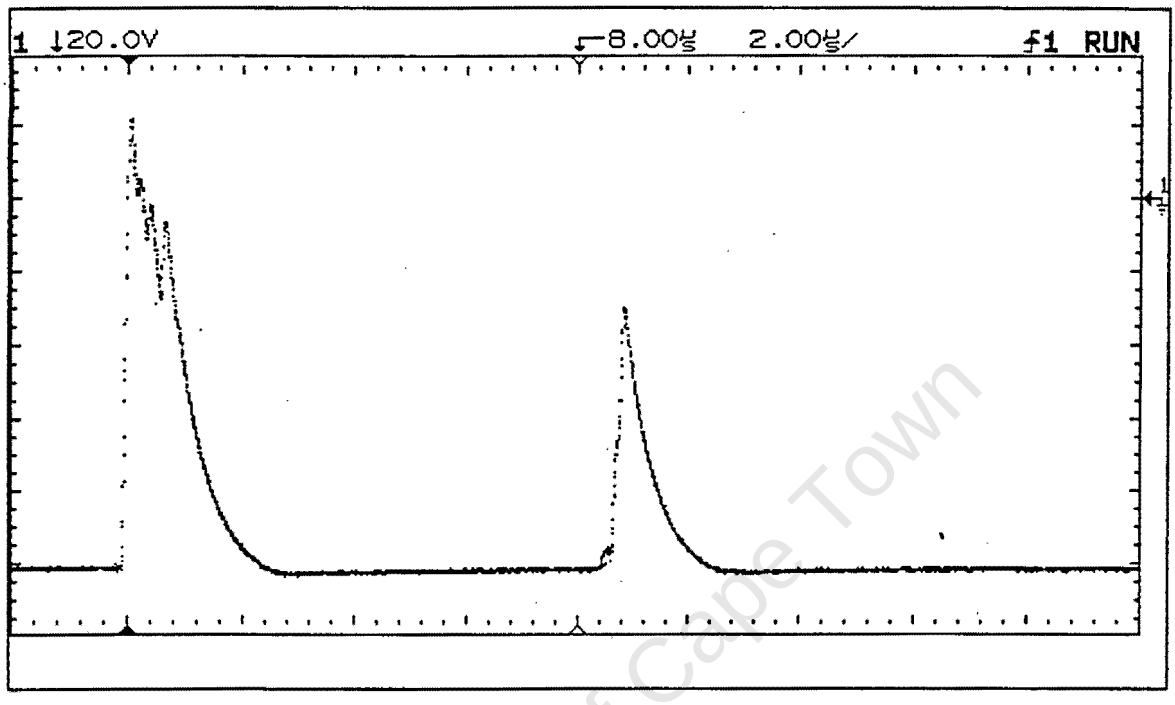

Figure B.12: Ultrasonic return signal from probe; probe centre directly in line with defect centre.

The variation in signal response near to the edge of the defect occurred when approaching it from different sides. This highlights the differences in signals that can occur even from a supposedly uniform defect.

Flattened area inspection

- When probe centre was between 1.3 mm and 0 mm from edge of defect:
  - 18% and 100% drop-off in first and secondary backwall echoes respectively. (figure B.14)
  - Gradual movement of first backwall echo from its original time position to that 800ns forward. (figure B.14)
- When beam centre was directly in line with defect centre:
  - Merging of front wall and first backwall echoes into single, multi-peaked echo. (figure B.15)

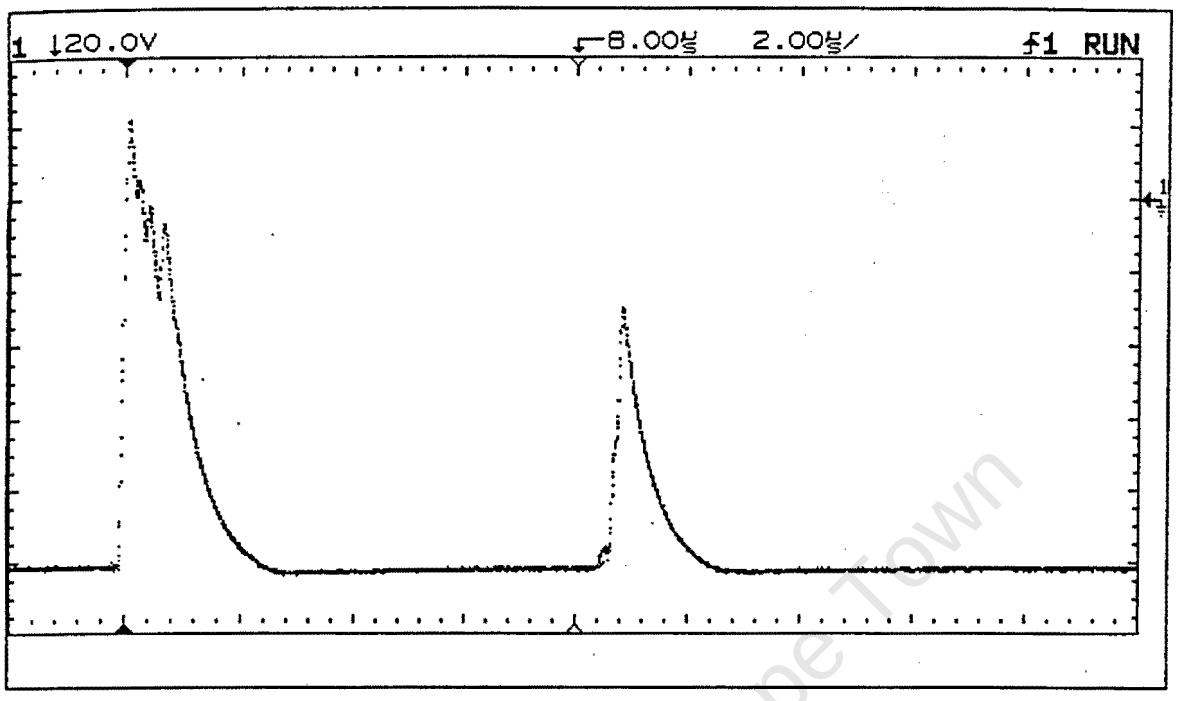

Figure B.13: Ultrasonic return signal from probe; off defect completely.

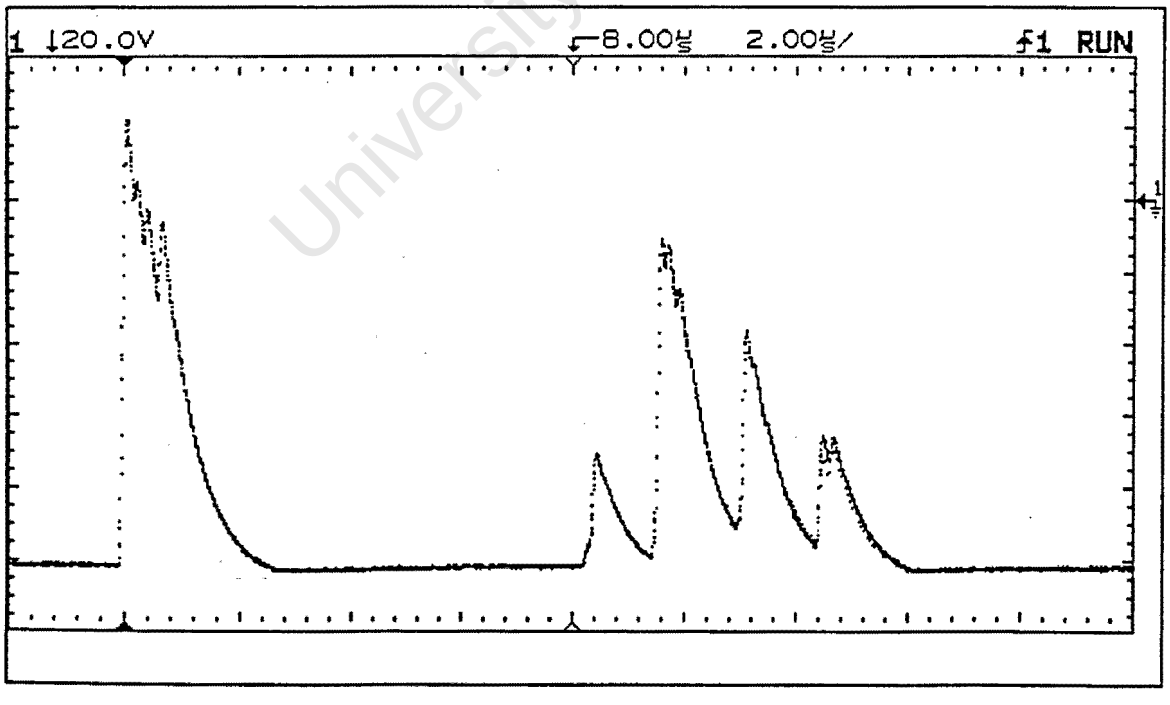

Figure B.14: Ultrasonic return signal from probe; probe centre 1.0 mm from defect centre.

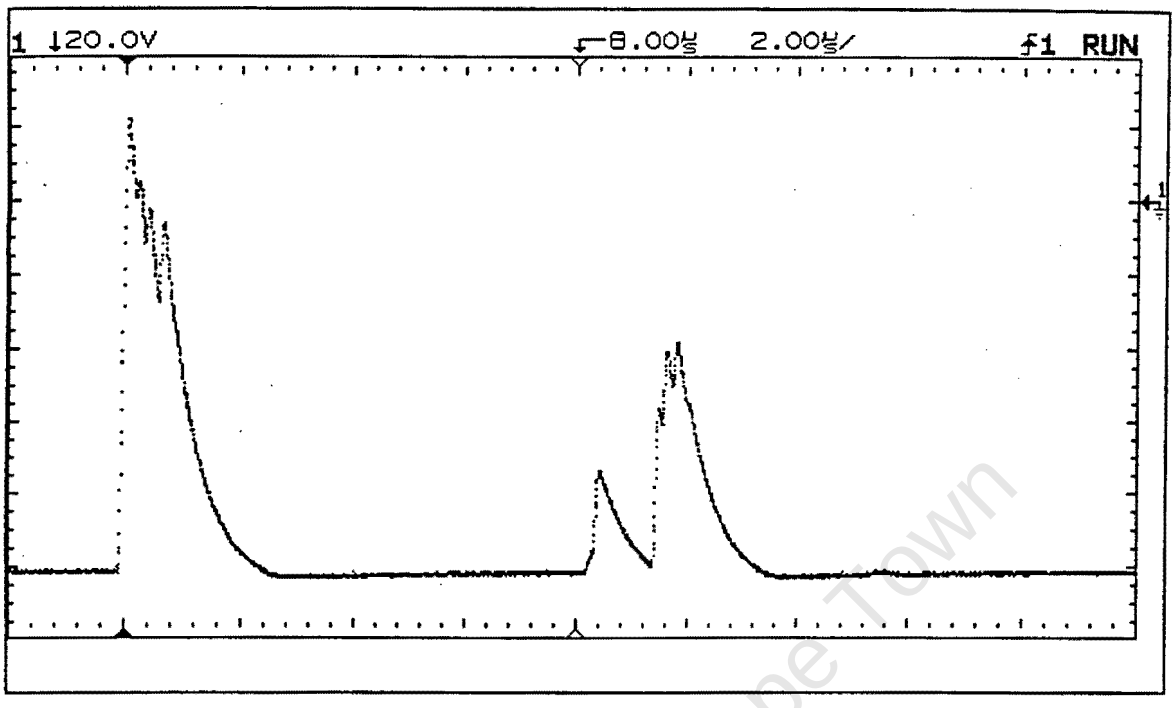

Figure B.15: Ultrasonic return signal from probe; probe centre directly in line with defect centre.

The wide-based, multi-peaked echo returned at the centre of the defect occurred as a result of the varying material thickness across the width of the sound beam. (ie: the flattened surface on the one side versus the rounded inner surface of the tube.)

APPENDIX C.1

WIRE UP DIAGRAM OF CONTROLLER/386 PC INTERFACE

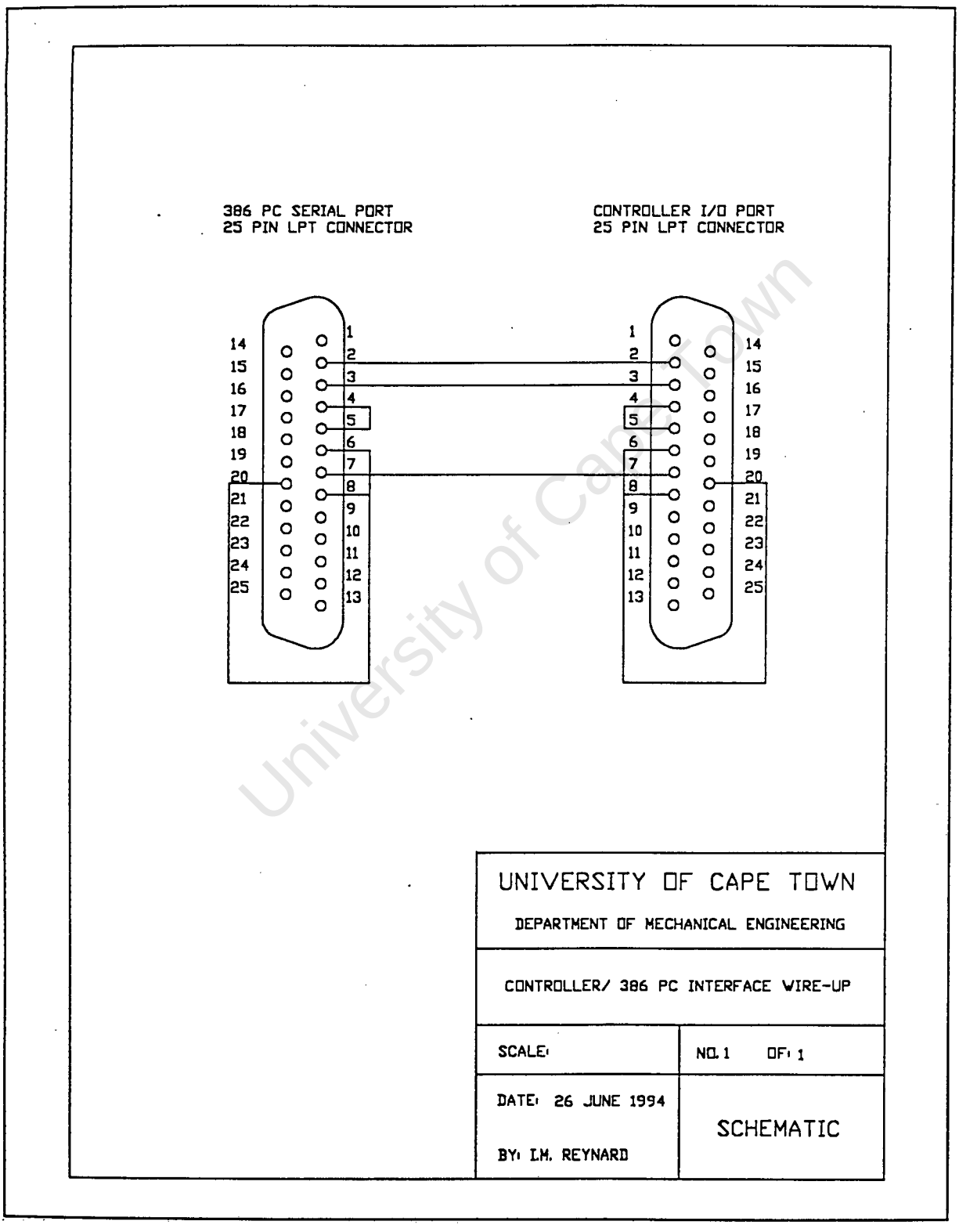

APPENDIX C.2

WIRE UP DIAGRAM OF USM2/HP54600 INTERFACE

DIAGRAM - AMPLIFIER CIRCUIT, USM2 FLAW DETECTOR

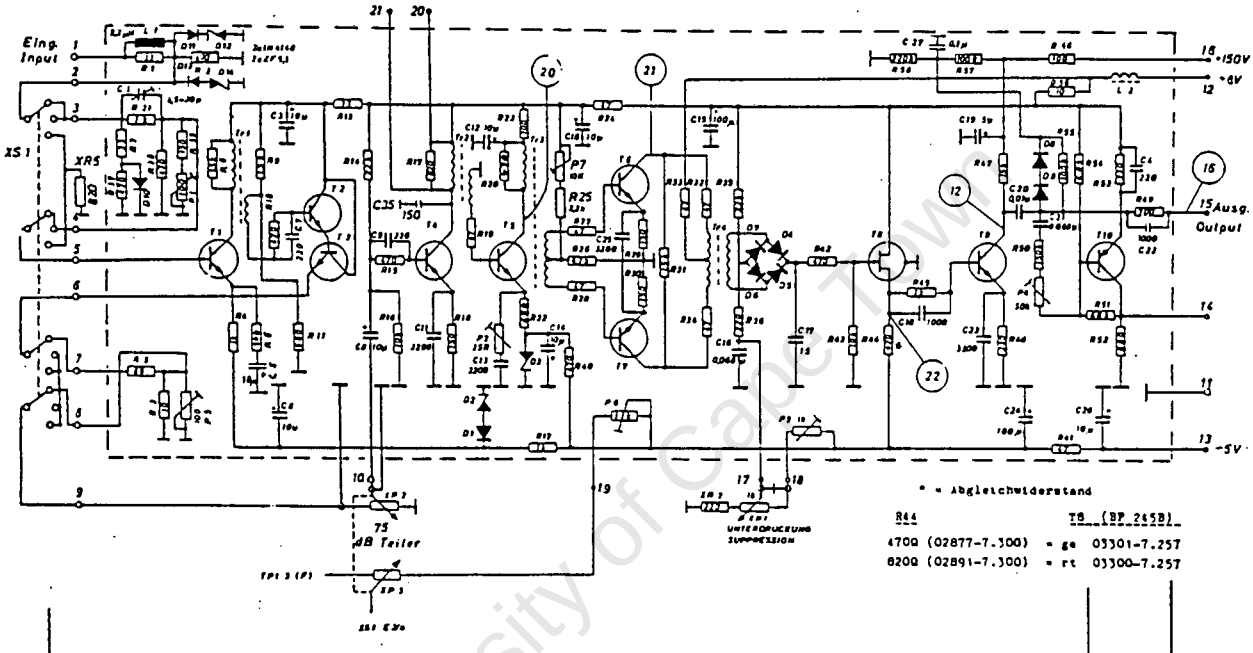

HP 54600 OSCILLOSCOPE

PIN 16
AMPLIFIER CIRCUIT -
USM2 FLAW DETECTOR
(DIAGRAM ABOVE)

UNIVERSITY OF CAPE TOWN DEPARTMENT OF MECHANICAL ENGINEERING	
USM2 / HP 54600 WIRE-UP	
SCALE:	NO. 1 OF: 1
DATE: 26 JUNE 1994 BY: I.M. REYNARD	SCHEMATIC

APPENDIX C.3

WIRE UP DIAGRAM OF HP54600/386 PC INTERFACE

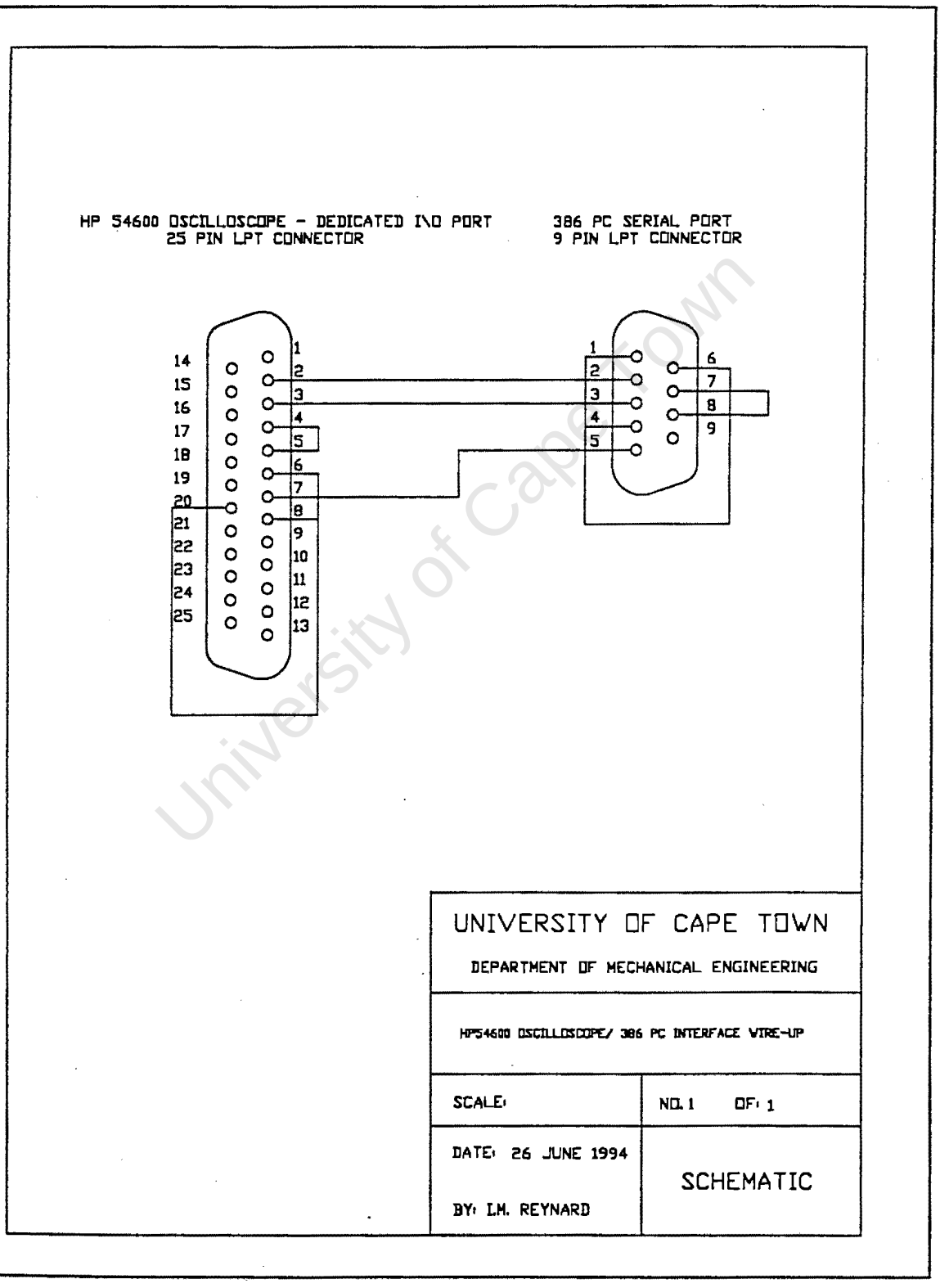

APPENDIX C.4

WIRE-UP DIAGRAM OF CNC/386PC CONTROL BOARD

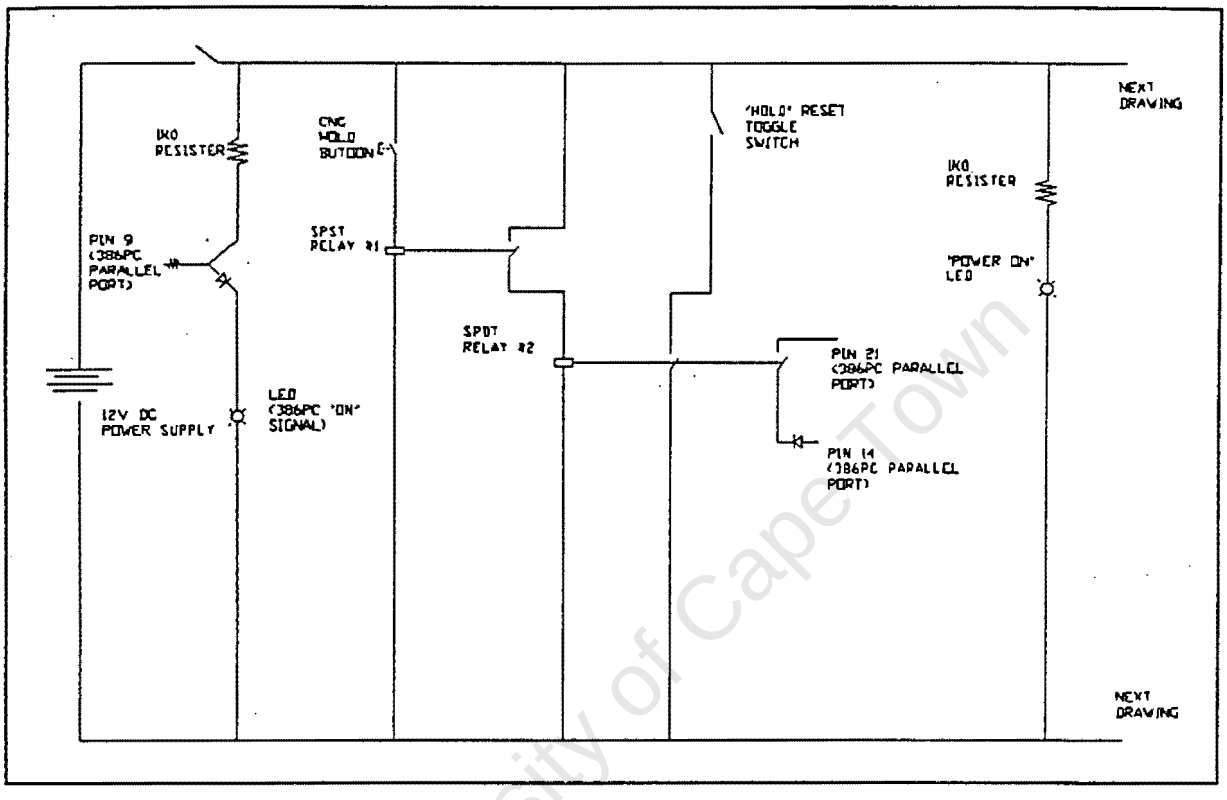

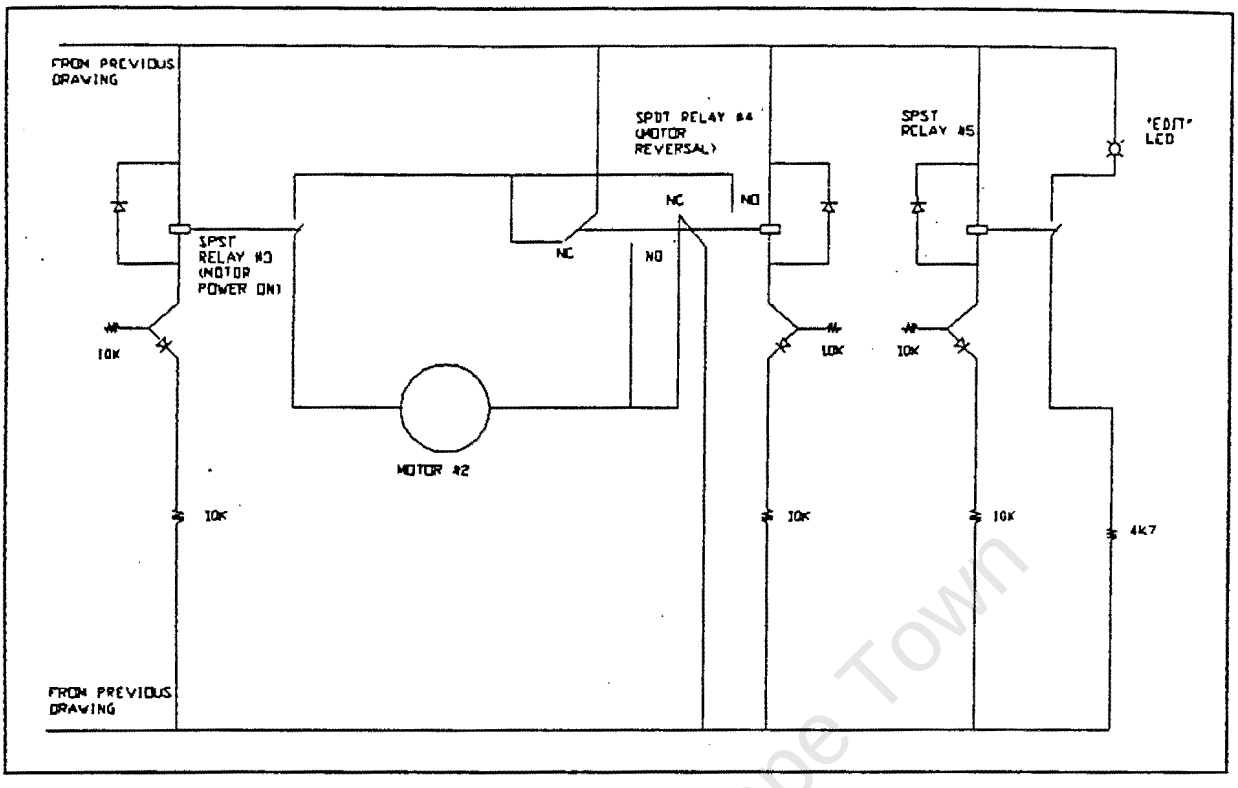

APPENDIX D.1

INITIAL DESIGN FACTORS FOR SCORBOT PROBEHOLDER

The initial design concepts of the probeholder were developed to overcome the inaccuracies of the end effector of SCORBOT.

It was perceived that the two most critical inaccuracies of the end effector on the positioning of the probe would be with respect to:

- the central axis of the tube end
- the parallism of the probe to the tube wall or inspection surface

If the probe entered the tube on a axis of rotation other than that of the tube centre, the probe holder mechanism had to ensure that the probe remained in contact with the tube wall when rotated around inside the tube. Furthermore, the probe holder mechanism was to ensure that any error in the angle with which the face of the probe came into contact with the inspection surface was corrected.

The two separate design concepts that were investigated to overcome these inaccuracies were:

(a) Electronic sensing of the tube end and subsequent software correction

(b) Mechanical correction of the positional inaccuracies by the probe holder mechanism alone.

The first concept relied on electrical (or other) components to detect the inaccuracies of the end effector, whereafter the feedback from the sensors would enable the software controlling SCORBOT to make the necessary motor motion adjustments.

Designs investigated to overcome the parallism inaccuracy between the probe face and the tube wall, used the following equipment:

- Linear differential variable transducers (LVDT's)
- Transmitting and receiving LEDS
- Mercury-filled electronic level indicators.

A design incorporating a group of four vertical LVDT's relied on the LVDT's to come in contact with the endplate of the heat exchanger as the probe holder entered a tube. Any orientation inaccuracies could thus be detected by the difference in displacements of the cores of the LVDT's.

A similar design used transmitting and receiving LED's to detect the edge of tube wall as the probe holder was lowered into the tube. Thus, using two sets of LED's orientated at right angles to each other in the horizontal plane, feedback on the probe holder's orientation could again be obtained.

A pneumatic hole alignment sensor, described in the literature[D1.1], was the only device found capable of giving feedback on the position of the end effector relative to the central axis of the tube.

However, all of the above designs were found to be complicated, potentially unreliable and slow to provide inaccuracy correction. It was thus decided that the mechanism, for reliability reasons alone, had to rely on mechanical techniques.

Two different types of mechanical probe holder mechanisms were investigated, namely:

- Linear motion mechanisms
- Lever manipulated mechanisms

The linear motion mechanisms typically consisted of a spring forcing the probe forward in a guided horizontal groove. The probe entered the hole by having the grippers of SCORBOT compress the spring, and thus retracting the probe towards the central axis of the tube. Once inside the hole, the spring would be partially released, forcing the probe face against the tube wall. Most designs included the use of stabilising rollers to ensure that the probe was held parallel to the inspection surface.

Lever manipulated mechanisms consisted of a set of struts arranged in a scissor-like arrangement. The top of these struts were designed to attach onto the grippers of SCORBOT whilst the probe was mounted on the bottom of one set of struts. To enter the hole, SCORBOT's grippers would close, bringing the struts together in the centre of the tube. Once inside, the grippers would open, thus forcing the probe against the inspection surface.

The advantages of a lever manipulated mechanism over that of a linear motion mechanism were:

- less space required
- greater force could be applied to probe
- simpler operating mechanism

APPENDIX D.2.

LENS DESIGN ANALYSIS

Two separate stages in the lens design were:

(1) selection of the lens face curvature
(2) optimisation of the lens thickness

The first analysis was done into finding the optimal curvature of the lens so as to minimise the effects of the gap existing between the probe and the tube wall. In order to achieve this, the varying thickness of the lens and coupling fluid would have to add up to a constant acoustical pathlength across the diameter of the probe. Furthermore, in choosing a suitable curvature, additional focusing of the sound beam was to be avoided as the TR probe had already an ideal focal length of 3 mm from the face of the probe.

However, it was realised that the only shape of lens capable of averaging out the pathlength for the entire signal as well as keeping the focal distance constant was a concave-shaped lens. The reason for this was twofold. Firstly, the sound beam leaving the DA312 was angled towards the axis of the probe (a concave lens would ensure the incident wave would be normal to the lens/ coupling fluid interface). Secondly, the fact that the acoustical impedance of most coupling fluids was less than that of perspex (the lens material) means that, geometrically, a concave lens is the only option for providing a constant acoustical pathlength across the face of the probe.

However, a concave lens was considered impractical as it meant that there was only a line contact between the lens and tube wall. This would lead to unacceptable shear forces on the

Thus, it was decided that the curvature of the lens would be identical to that of the tube. This minimised the effects of the

unequal acoustical pathlength whilst providing the most stability when the lens was pressed up against the tube wall.

The second stage of the lens design was to optimise the lens thickness in order to maximise the acoustic energy passing through the lens/coupling fluid interface.

The thickness of the lens, assuming the aforementioned curvature, could then be characterised by one dimension, namely the distance from the apex of the lens curvatue to the back of the lens.

The transmission coefficient (ie: giving the percentage energy transmitted across a perspex/border material interface) for perspex can be found by:

$$T_p = \frac{W_t}{W_i} = \frac{1}{1 + \frac{1}{4}(r + 1/r)^2 \sin^2 \frac{2\pi t r}{L}}$$

where W_t = energy transmitted

W_i = energy incident on interface

$r = \frac{Z_2}{Z_1}$ Z_1 = acoustic impedance of coupling fluid

Z_2 = acoustic impedance of perspex

t_r = thickness of perspex through which a particular ray travels

$L = v_2 / f$ (wavelength of acoustic energy)

Figure D.2.1. (next page) shows this transmission coefficient as a function of the thickness of perspex.

As it can be seen, by choosing a value of t = 0.00105 a 'maximum' value of T_p (T_p = 1) would occur at the front of the lens. However, as the lens curved away from the front tip, the thickness of perspex would decrease and the value of T_p would vary.

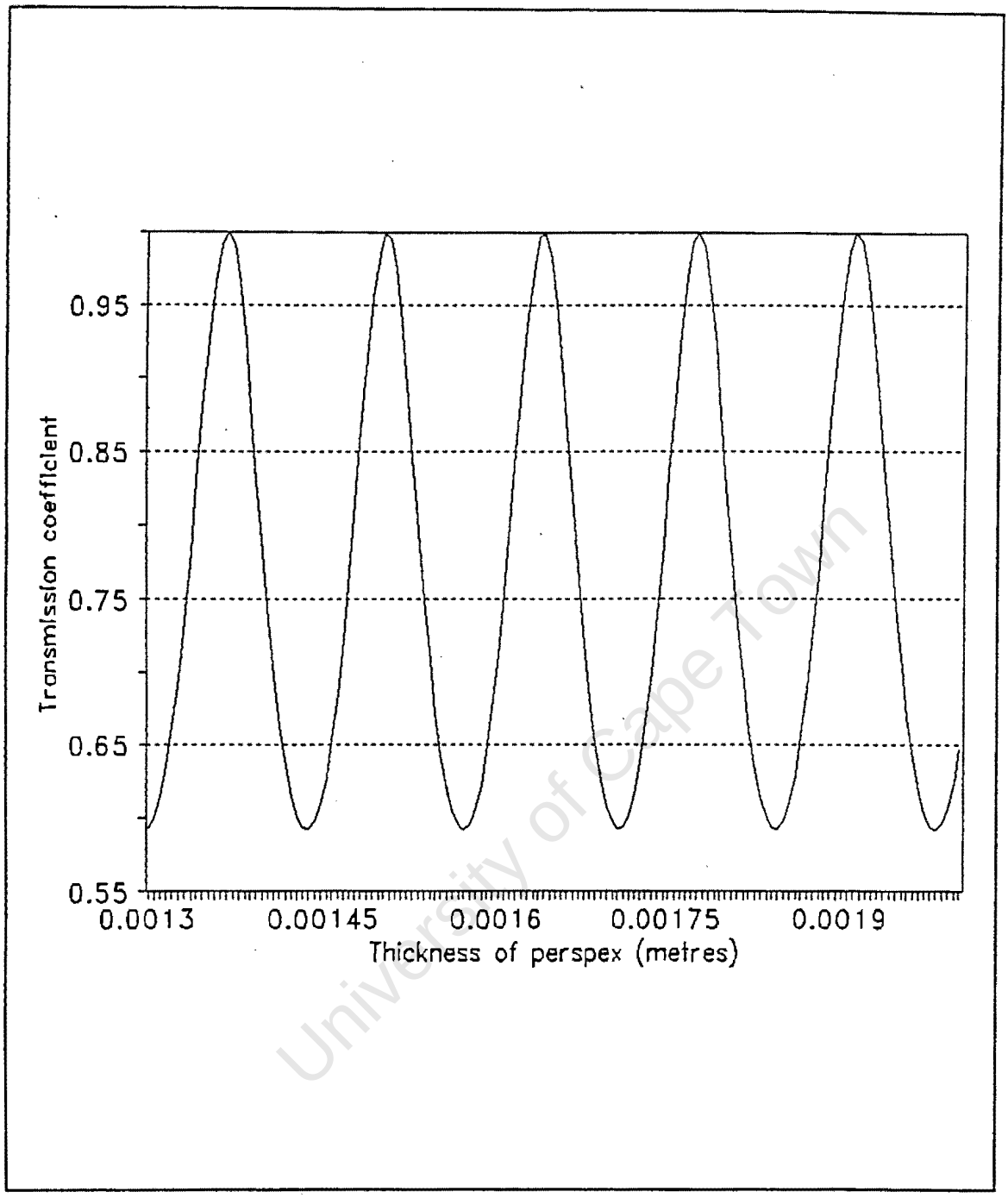

Figure F.2.3. Transmission coefficient for various thicknesses of perspex.

Furthermore, the intensity of the sound energy varies both laterally and longitudinally across acoustic beam. Thus, a more accurate method of optimising 't' would be to take into consideration the energy arriving at each point on the lens face and the corresponding value of T_p at this point.

In other words, the following summation should be maximised:

$$\text{Energy transmitted} = \Sigma\ E_i\ T_{i,t}$$

where E_i = energy incident on small area of lens face
$T_{i,t}$ = transmission coefficient for the thickness of the lens corresponding to the area of lens face selected.

The energy at any point in the acoustical beam can be calculated using Zemenek's equations[D2.1]. This involves a complex evaluation of a Bessel function whereby the energy contribution of every section of the transducer's face to a particular point in the sound beam is summated.

The calculation of the energy field for the DA312 Probe was complicated by the facts that:

(a) The a/l ratio was high (12.5) - thus producing a field with many peaks.

(b) The effect of the sidelobes on the overall sound field would not be the same as calculated by Zemeneck, as the acoustic barrier in the DA 312 probe would have a dampening effect on these waves.

Now, the energy variations on the central acoustic axis are dominant over the other off-axis variations. Thus, in light of the above complications, it was decided that the lens thickness, 't', would be optimised with regard to the central acoustic energy variations.

The positioning of these axial energy maxima can be calculated using:

$$Y_{+m} = \frac{4R^2 - L^2(2m + 1)}{4L(2m + 1)} \qquad (m = 0,\ 1,\ 2\ldots)$$

APPENDIX E: DESCRIPTION OF SOFTWARE USED ON CNC MODEL

The controlling software for the CNC scanning model was written entirely in Turbo C++, version 3.0.

E.1 Software user interface

The software was programmed to perform six main functions:

(1) Read in heat exchanger configurations.
(2) Control interfaces between various machine components.
(3) Generate text files to control the CNC.
(4) Control the stepper and winder motors during a scan sequence.
(5) Collect and analyse flaw image data from the HP54600 oscilloscope.
(6) Provide the user with information during the scan.

The heat exchanger configurations were entered in the same manner as with the robot model.

The two motors on the wrist mechanism were then manipulated via the software. The small winder motor was often adjusted to obtain the correct tension in the nylon string before starting a scan.

The co-ordinates of two pre-selected tube centres then had to be found and entered into the software. This was done to describe the orientation of the heat exchanger on the CNC's bed. The CNC's spindle was first moved to the centre of hole no. 1 (figure E1) and the CNC's co-ordinates registers zeroed. Then, the CNC's spindle was moved to hole no. 2 and the X and Y co-ordinate values shown by the CNC's registers were entered into the 386 PC's software. Using this information, the software then saved a textile containing the co-ordinates of the tube ends onto a floppy disc on the A-drive.

The user was then required to enter the maximum number of flaw images to be captured during a scan. This affected the overall time taken to scan a hole. This information was also

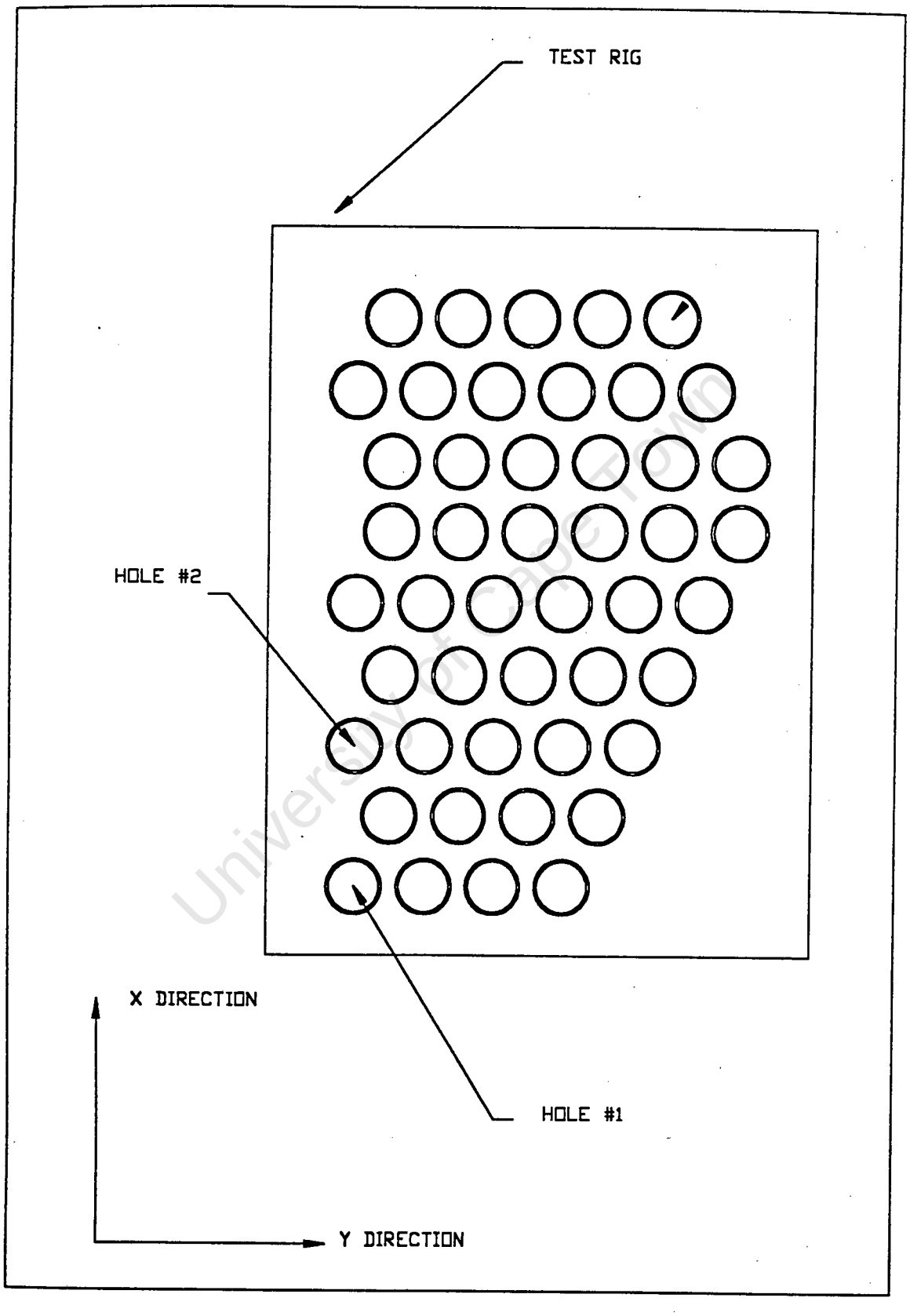

Figure E1: Schematic diagram of test rig

used in generating the textfile to control the CNC.

The user then placed the floppy disc into the A drive of the XT-PC and used the MIRROR(TM) software to download the textfile into the CNC's memory. Having completed this, the CNC was ready to proceed with a scan.

The edit button on the CNC was then pressed to initiate the SCAN. During the scan, the software displayed the following information on the screen:

- Tube end being inspected (shown by graphical picture).
- Number of flaws already identified up to present scan position.
- X,Y,Z position of probe.

Once the scan of the entire heat exchanger was complete, the user could then view the graphic images of the flaws detected.

E2. Overall project layout

The project file, *CNC1.prg*, consisted of 32 files. Of these files, only 28 were actively used for the software controlling the CNC model. The remaining 4 files (ie: *robinter.cpp*) were left in the project file to make the software compatible with both the CNC and SCORBOT model. The majority of files that were re-used from the SCORBOT model were functionally unchanged.

Sections E.3 to E.6 below describe the important sections of the software.

E3. Calculating orientation of test rig on CNC bed.

One feature of system was that it had to be able to scan the test rig in any position in the horizontal plane. Thus, the software had to calculate the overall orientation of the test rig with respect to the x any y axes of the CNC.

To do this, the user had to identify the position of two pre-selected holes. Once these co-ordinates were entered (described in section 3.2.3.1), the function *cncfilecreate.* in module *cal-cnc1.cpp* generated the co-ordinates of the centres of each tube opening according to the CNC's reference frame.

Referring to figure E.2, the following can be written:

$$\theta_1 = \text{TAN}\ (y_1 / x_1)$$

$$\alpha_2 = \text{TAN}\ (y_2 / x_2)$$

$$\gamma = \theta_1 - \alpha_2$$

Thus, the transformation was used to translate the co-ordinates of the original heat exchanger configuration to those used by the CNC's frame of reference:

$$\{x_1 , y_1\}_{\text{NEW ORIENTATION}} = \{ R\ \text{COS}\ \gamma,\ R\ \ \text{SIN}\ \gamma \}\ \{x_1 , y_1\}_{\text{OLD ORIENTATION}}$$

E.4. CNC textfile generation

The CNC received its positional instructions from the controlling software in the form of a textfile.

The contents of this textfile were:

[1] Initial settings (specifying units, coordinate systems etc.)

[2] All x, y, z positional information (as given by absolute coordinates rather than relative vectors).

[3] The time allocated to pause in the centre of each tube opening.

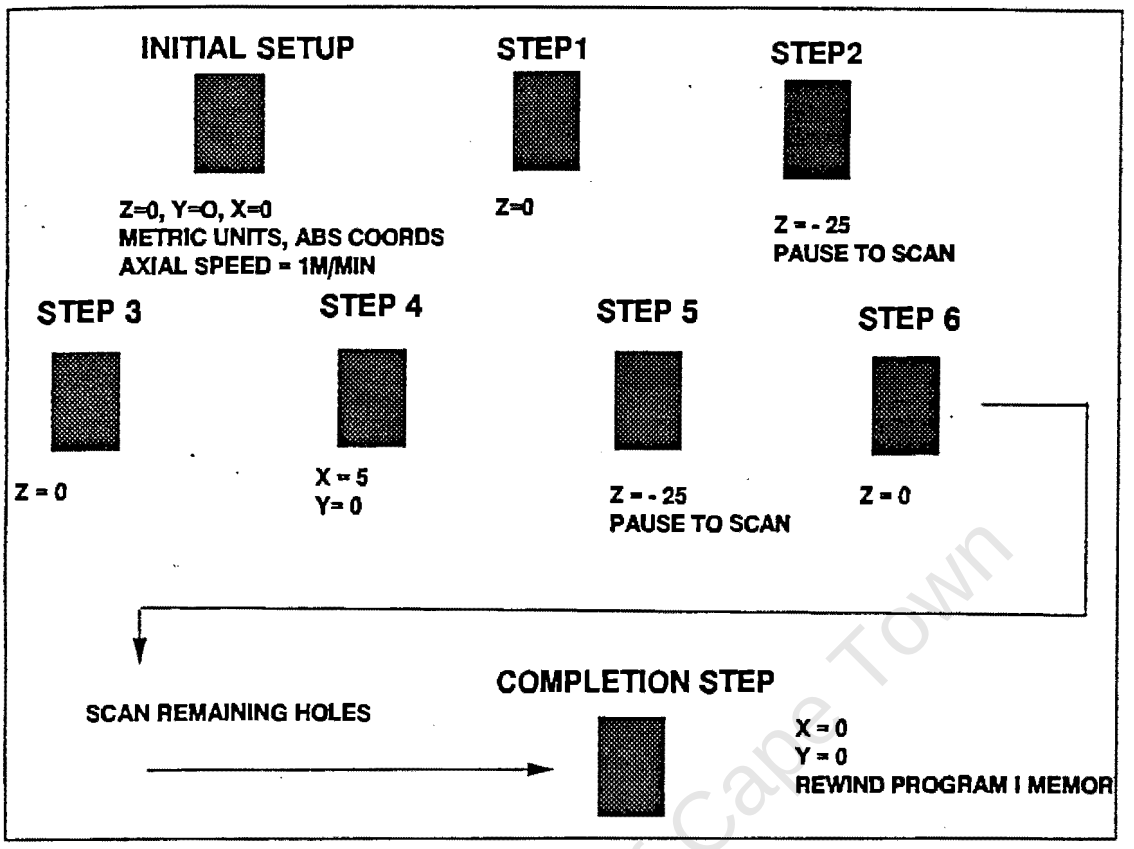

Figure E3: Schematic representation of movement commands issued to CNC.

Figure E.3 shows a schematic representation of the commands issued to the CNC for the required movements.

The x, y, z coordinates were generated for the heat exchanger configuration, as explained in section 3.2.3.3.

E.5. CNC textfile transfer

This textfile was transferred from the 386 to CNC before the start of the scan as on-line communication between the two machines during the scan was impossible due to the nature of the CNC's memory format.

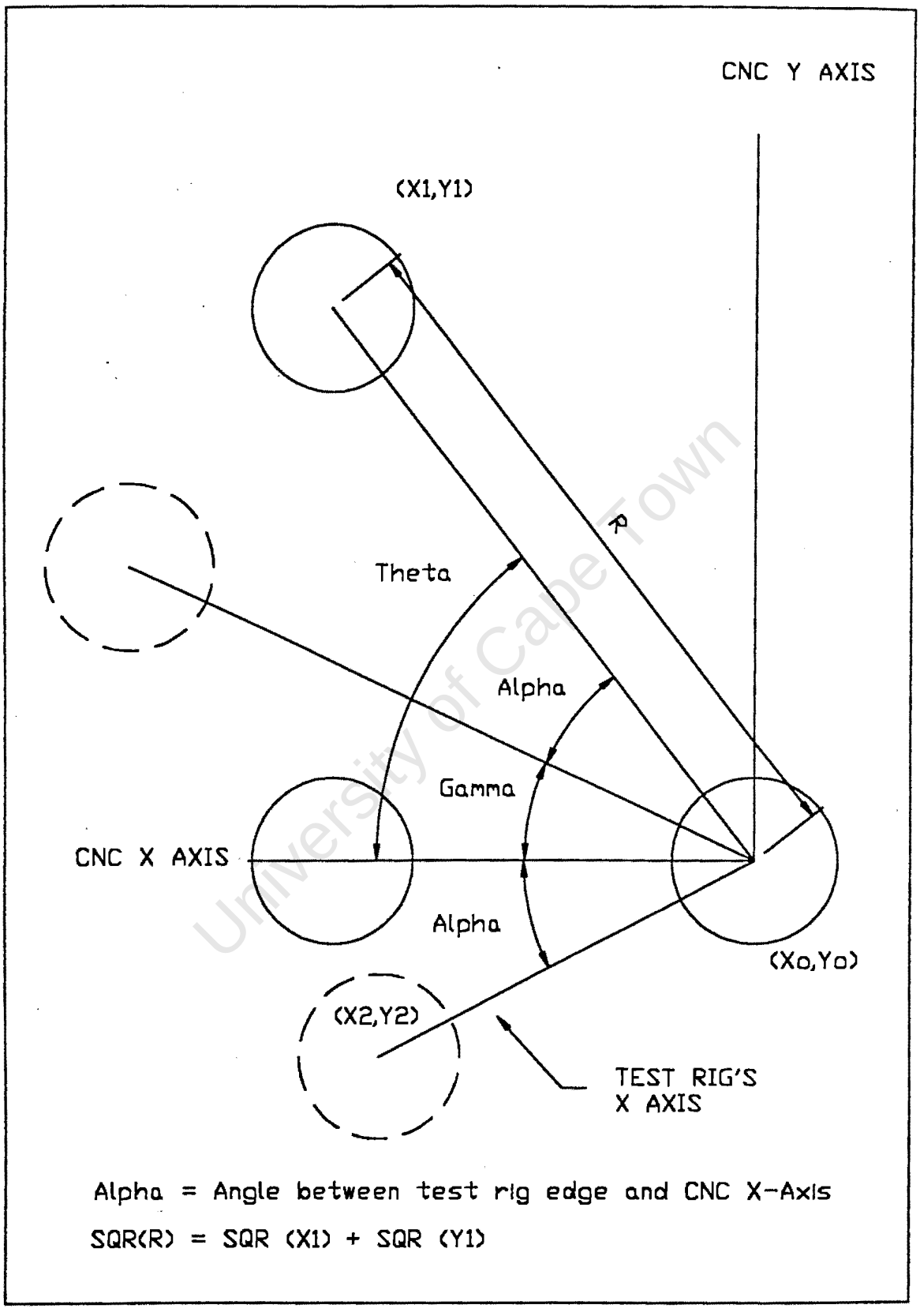

Figure E2: Diagrammatic representation of test rig orientation

Initial design plans had the 386 PC transfer the textfile directly to the CNC. Transfer of the information into the CNC's memory had to be done at an extremely slow band rate (200 characters per minute), thus requiring the use of dedicated communication software. An attempt was made to incorporate the communications software package, MIRROR version 4.01, into the turbo C++ controlling software. However, it was found that the turbo C++ command which allowed separate software to be run as part of the overall program was unreliable and thus the communication software had to be run on a separate entity.

Thus, in the final model set-up, the 386 PC controlling software generated the textfile and saved it to a floppy disc. The XT then transferred the data from the floppy disc to the CNC, leaving the controlling software free to continue other pre-scan procedures.

The pause of the CNC was obtained by making the program loop through a command which continually reset the Z position of the CNC spindle. It was found that 100 loops of the program delayed the CNC by exactly 1 second. Thus, the commands

```
= N1040/6700
N1040 Z - 25.00
```

repetitively set the Z position of the spindle to Z = - 25 for 67 seconds.

E..6. Scanning procedure

The scanning of the tube surfaces was achieved by two separate control systems working in parallel: the CNC movement system and the wrist mechanism / ultrasonic scanning system. This was not an ideal situation as far as control philosophers are concerned but was a pyridine set by the nature of the CNC's communication abilities.

Figure E4 shows a schematic representation of the two control systems during a typical scan:

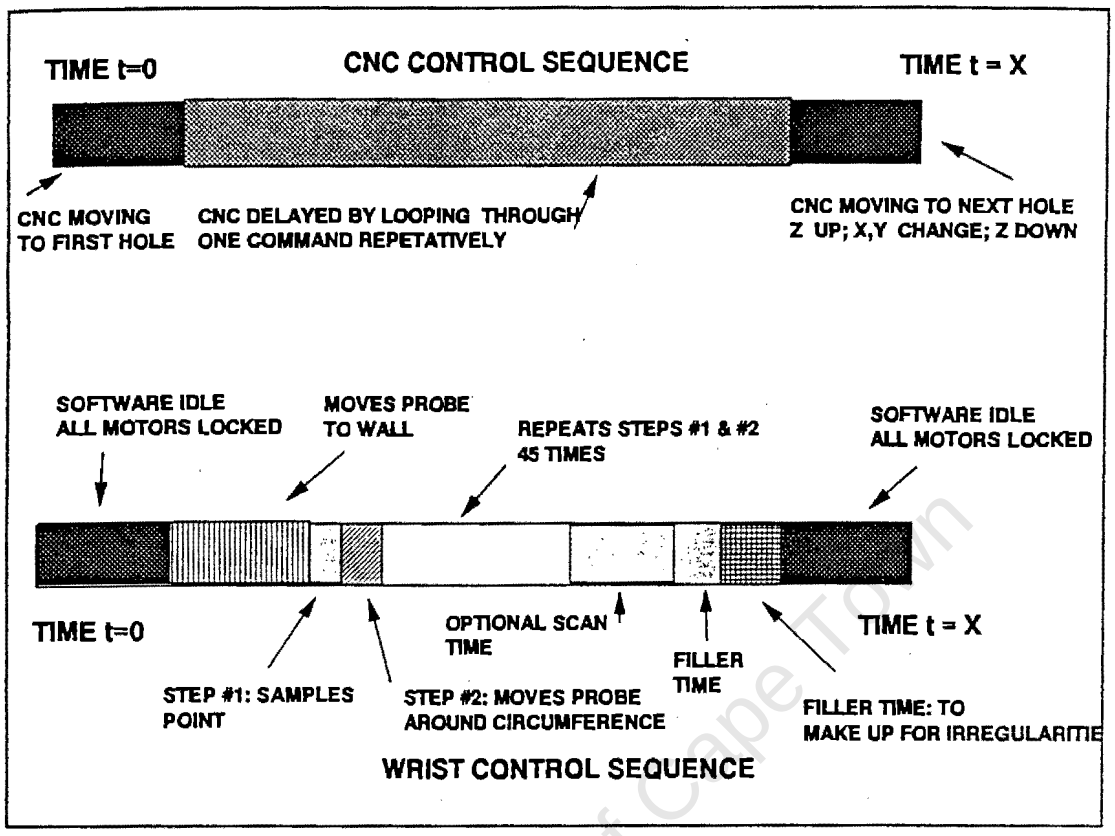

Figure E4: Schematic representation of the two control systems during scan.

The two systems are initially synchronised at the start of a scan by the 386 PC's software receiving a signal that the `edit' button on the CNC has been pressed.

The first stage of the scan is taken up by the CNC moving to the starting point. This ideally should only involve the spindle moving down into the first hole as this is a measurable time and thus can be predicted by the 386 PC's software. The next stage of the scan involves the 386 PC controlling the wrist mechanism during a scan of the tube. The probe is moved up against the tube wall by the winder motor. The ultrasonic scanning of the wall the proceeds, with the probe being moved round 75% of its frontal area after every inspection.

If one of the inspections reveals an irregularity which may be a flaw, the graphical image shown by the ultrasonic detection equipment may be captured and stored for later analysis. A maximum no. of flaw images to be captured during each scanning of a tube is set prior to

the scan and thus the required time for this capturing is built into the overall time allowed for a tube scan.

After the inner circumference of the tube has been completely scanned, the probe is moved back into the centre of the tube again.

At this point, the CNC moves the wrist mechanism to the next tube centre, whilst the 386 PC's software remains idle. The amount of time allowed for the CNC to move to the next tube varied according to the distance between the two tubes. This delay time was calculated by the 386 PC's software for each individual tube movement.

To remain in perfect synchronisation, the times taken for each of the control systems to perform their tasks must be pre-defined and known by each system. Table 3.1 shows the time estimations of tasks categorised into determinable and statistical sections.

	Task	**Time estimation method**
1.	CNC moving to hole	statistical
2.	Probe moved to wall	determinable
3.	Ultrasonic sampling of point	determinable
4.	Moving probe around circumference	determinable
5.	Move probe from wall	determinable
6.	CNC moving to next hole	statistical

Table E.1. Categorisation of time estimations to perform scanning tasks.

Statistical time estimations were calculated by taking an average of the time taken for the task to be done over a number of observations. For example, the time taken for the CNC's spindle to lower was found to be, on average, 1.1 seconds.